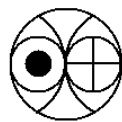


Studies on time dependent and stationary classically chaotic quantum systems

A Thesis submitted to
Gujarat University

for the degree of
Doctor of Philosophy in Physics

by
R. SANKARANARAYANAN



Physical Research Laboratory
Ahmedabad
INDIA

November 2001

Certificate

I hereby declare that the work presented in this thesis is original and has not formed the basis for the award of any degree or diploma by any University or Institution.

R. Sankaranarayanan
(Author)

Certified by:

Prof. V.B. Sheorey
(Thesis Supervisor)
Physical Research Laboratory
Ahmedabad
INDIA

dedicated to
my parents

◇ Acknowledgements ◇

I take this opportunity to express my sincere gratitude to my thesis supervisor Prof. V.B. Sheorey. His constant encouragement was very helpful in all these years. I have dearth of words to express my thanks to Dr. Arul Lakshminarayan with whom I have been associating through out the thesis. I enormously learned from his wide and deep insight in the subject. I consider myself very fortunate to have been able to work with him. I considerably benefited from my interactions with Dr. M.S. Santhanam (IBM, Delhi) in the initial years. I am thankful to the staff members of computer centre and library of PRL who have been highly supportive at all times. I thank Prof. M.G. Raizen (University of Texas, Austin) who gave me permission to present an experimental result (Fig. 1.1) in this thesis.

R. Sankaranarayanan
PRL, Ahmedabad.

Contents

1	Introduction	1
1.1	Chaos in Hamiltonian systems	2
1.1.1	Integrable systems	3
1.1.2	Nonintegrable systems	4
1.1.3	Few examples	5
1.2	Quantum chaos	6
1.2.1	Eigenvalues	7
1.2.2	Eigenstates	8
1.2.3	Statistics	9
1.3	Kicked rotor: a paradigm	11
1.3.1	Dynamical localization	11
1.4	Motivation for the thesis	14
1.4.1	An illustration	15
1.4.2	Outline of the thesis	18
2	Classical map	19
2.1	Introduction	19
2.2	Generalized standard map	20
2.3	Transition to chaos	21
2.4	Stability analysis: new approach	24
2.5	Hyperbolic regime	30
2.6	Diffusion	31
2.7	Summary	36
3	Quantum map	39
3.1	Introduction	39
3.2	Matrix form of quantum propagator	40
3.3	Special case: kicked rotor	43
3.4	Quantum resonance	44
3.5	Results	46
3.5.1	Localization and length scales	46
3.5.2	Localization and classical diffusion	49
3.5.3	Measure of quantum chaos	52

3.5.4	Eigenvalues and eigenstates	54
3.6	Summary	60
4	Accelerator modes	62
4.1	Introduction	62
4.2	Classical modes	63
4.3	Quantum modes	67
4.3.1	Gaussian wave packet	68
4.3.2	Quantum effects and correspondence	69
4.4	Summary	73
5	Quantized torus	74
5.1	Introduction	74
5.2	Quantized GSM	75
5.3	Quasienergies	77
5.4	Quasienergy states and phase space	80
5.4.1	Information entropy	80
5.4.2	Coherent-state representation	82
5.5	Level dynamics	85
5.5.1	Level velocities and RMT predictions	86
5.5.2	Correlation of level velocities	91
5.6	Summary	93
	Epilogue	95
	Bibliography	97
	List of Publications	104

1. Introduction

Sir Isaac Newton is considered as the founder of modern science. His great perception gave birth to what is regarded as Newtonian mechanics, the “physical laws” of nature. His mechanics presents us the picture of deterministic universe provided all the physical laws and initial conditions are given. French mathematician Laplace (1749-1827) fantasized the deterministic world and wrote [1]:

“Let us imagine an Intelligence who would know at a given instant of time all forces acting in nature and the position of all things of which the world consists; let us assume, further, that this Intelligence would be capable of subjecting all these data to mathematical analysis. Then it could derive a result that would embrace in one and the same formula the motion of the largest bodies in the universe and of the lightest atoms. Nothing would be uncertain for this Intelligence. The past and the future would be present to its eyes.”

Laplace’s view point stands by “cause and effect” of a system. The initial condition is the cause and subsequent behaviour is the effect. The cause and effect are connected to each other by the physical laws, expressed as differential equations. Towards the end of 19th century, French mathematician Henri Poincaré realized that small error in initial condition can be catastrophic and remarked [2]

“A very small cause which escapes our notice determines a considerable effect that we cannot fail to see, and then we say that the effect is due to chance. If we knew exactly the laws of nature and the situation of the universe at the initial moment, we could predict exactly the situation of that same universe at a succeeding moment. But even if it were the case that the natural laws had no longer any secret for us, we could still know the situation approximately. If that enabled us to predict the succeeding situation with the same approximation, that is all we require, and we should say that the phenomenon has been predicted, that it is governed by the laws. But it is not always so; it may happen that small difference in the initial condition produce very great ones in the final phenomena. A small error in the former will produce an enormous error in the latter. Prediction becomes impossible ...”

Systems which are sensitive to initial conditions exhibit chaos, even though they are deterministic by the physical laws. Studies on chaotic systems were not given much importance for quite a long time since Poincaré had foreseen the possibility of chaos in physical systems.

Differential equations, by which physical systems are described, are generally not solvable. Or in other words, solutions of the equations can not always be represented by known mathematical functions. Even if the solutions exist in the form of infinite series of known functions,

such solutions will not bring out any qualitative features of the system. Limitation to solve the insurmountable differential equations is the prime reason in ignoring the studies on chaos through out the first half of 20th century.

Emergence of chaos from deterministic systems has been much appreciated only after an “accidental discovery” made by the meteorologist Lorenz who attempted weather predictions in 1960’s. His model, derived on the basis of fluid dynamical flow, consisting of twelve differential equations were solved numerically by computers. His simulated results were found to be aperiodic and highly sensitive to initial conditions. He observed such chaotic behaviour even in his much simpler version [3], recognized latter on as Lorenz equations, that retained mainly the nonlinear force terms. The bitter fact of this discovery is the impossibility of long-time weather forecasting.

However, Lorenz’s discovery evoked enormous interest to study simplified models of many real life systems *viz.* biological, economic and social systems. In particular, the detailed investigations by the biologist Robert May in 1970’s on a one-dimensional difference equation are of significance. He chose [4] to study the so called logistic difference equation:

$$x_{n+1} = \alpha x_n(1 - x_n). \quad (1.1)$$

This is a crude yet somewhat reasonable model developed by ecologists in 1950’s for the seasonal population growth of a species. In this equation, α is a parameter and x is a variable which can take any value between 0 and 1. The system behaviour was found to be highly sensitive to parameter as well as to the initial conditions. A graph of his data had shown the coexistence of regular and chaotic behaviour at all scales. The latter peculiarity had been supported with a mathematical proof [5]. The underlying message is that even simplest models of the seething real world possess variety of complex features.

In the past couple of decades, rapid developments in computers have fueled numerical explorations of numerous simple physical models to unravel very many fascinating new phenomena of chaotic dynamics.

1.1 Chaos in Hamiltonian systems

Deterministic dynamical systems are completely described by the equation $\dot{\mathbf{x}} = \mathbf{F}(\mathbf{x}, t)$ where \mathbf{x} is a finite dimensional vector in state space. This equation always has *unique* solution $\mathbf{x} = \mathbf{x}(\mathbf{x}_0, t)$ where $\mathbf{x}_0 = \mathbf{x}(0)$ is the initial condition of the system under consideration. A trajectory formed by $\mathbf{x}(t)$ describes dynamics of the system in the state space. If two trajectories, which differ in their initial conditions by an infinitesimal amount, exponentially diverge from each other in the tangent space then the system is locally unstable. This local instability is

characterized by positive Lyapunov exponent defined as

$$\Lambda = \lim_{\substack{t \rightarrow \infty \\ d(0) \rightarrow 0}} \left(\frac{1}{t}\right) \ln \left(\frac{d(t)}{d(0)}\right) \quad (1.2)$$

where $d(t)$ is the Euclidean distance between the two trajectories. The exponent measures the mean rate of divergence. Local instability is the characteristic feature of a chaotic system. Reader may refer to [6] and the subsequent work [7] for more mathematical definition of chaos.

In classical physics, an important class of dynamical systems are the Hamiltonian systems. They are defined by Hamiltonian equations of motion

$$\dot{\mathbf{q}} = \frac{\partial H}{\partial \mathbf{p}} \quad ; \quad \dot{\mathbf{p}} = -\frac{\partial H}{\partial \mathbf{q}} \quad (1.3)$$

where the Hamiltonian function $H(\mathbf{q}, \mathbf{p}, t)$ describes the dynamical flow and \mathbf{q}, \mathbf{p} are the N -component vectors: $\mathbf{q} = (q_1, q_2, \dots, q_N)$, $\mathbf{p} = (p_1, p_2, \dots, p_N)$ with N being the number of degrees of freedom. In this description, state space (here it is called phase space) is spanned by the $2N$ components of position vector \mathbf{q} and momentum vector \mathbf{p} . A fundamental property of the Hamiltonian flow is that it possesses *Poincaré-Cartan integral invariant* [8], and consequently the flow in phase space is a canonical transformation. It implies that the flow has hierarchy of N quantities, preserved by the canonical transformation, called *Poincaré invariants*. Volume of the phase space that is preserved under Hamiltonian flow (Liouville's theorem) is in fact one of the family of invariants. For the simplest case of one degree of freedom system, the flow in phase space $(q, p) \rightarrow (Q, P)$ is *area-preserving* i.e., $\partial(Q, P)/\partial(q, p) = 1$.

1.1.1 Integrable systems

Let us consider time independent Hamiltonian system in which case the energy $H(\mathbf{q}, \mathbf{p}) = E$ is a constant of motion. Constant energy confines the dynamics on $2N - 1$ dimensional subspace of the $2N$ dimensional phase space. Liouville proved that the system with N degrees of freedom is *integrable* by quadratures, if N independent first integrals (constants of motion) in involution are known. This implies that one degree of freedom systems are integrable (for eg. harmonic oscillator, simple pendulum). Existence of N independent constants restricts the dynamics on N dimensional *invariant* tori each of them characterized by N frequencies. For nonlinear systems, the frequencies vary from torus to torus. It is worth remarking that stable confinement of motion on the torus leads the integrable system to be regular and predictable. The dynamics on N dimensional tori embedded in $2N - 1$ dimensional energy shell is beyond our ability to visualize. However, many features of the Hamiltonian systems can be understood with just two degrees of freedom.

For two degrees of freedom ($N = 2$) system, the energy shell is three dimensional. To further simplify the visualization of the dynamics on this shell, Poincaré devised a powerful technique of projecting the 3D-space onto a 2D plane. This plane (say q_1p_1 -plane, with fixed q_2), called *Poincaré section*, transversally intersects the 2D tori that are embedded in the 3D energy shell. The trajectory beginning in that plane returns to it after making a circuit around the tori. Thus we have a mapping of the plane on to itself. Since the Hamiltonian flow is a canonical transformation, mapping on the plane is area-preserving. On characterizing every torus with frequencies ω_1 and ω_2 , the ratio of them $\alpha = \omega_1/\omega_2$, called *winding number*, classifies the tori into two types: resonant (rational α) and non-resonant (irrational α). The motion is periodic on the resonant tori and quasiperiodic on the non-resonant tori. Since α is real and recollecting that in real axis rationals form a set of measure zero as they are infinitely outnumbered by the irrationals, for an integrable system ‘almost all’ the tori are non-resonant. In the Poincaré section, a resonant torus appears as finite number of points and a non-resonant one as smooth closed curve. This is equivalent to mapping on a circle, called *twist map*

$$\begin{aligned}\theta_{n+1} &= \theta_n + 2\pi\alpha(r_n) \\ r_{n+1} &= r_n\end{aligned}\tag{1.4}$$

where r identifies the torus. We note that the equivalence arises from the fact that the twist map is also area-preserving.

1.1.2 Nonintegrable systems

The integrable systems are very rare and exceptional. In general, the Hamiltonian systems are *nonintegrable* i.e., the system will not have as many constants of motion as degrees of freedom, or in other words there will be some non-trivial perturbation to the integrable system. In 19th and 20th century, it was considered to be a fundamental issue in mechanics to understand the dynamics of nonintegrable systems. The issue was concerned with the fate of unperturbed tori under perturbation. This problem was resolved in 1960’s by two celebrated theorems namely *Kolmogorov-Arnold-Moser (KAM) theorem* and *Poincaré-Birkhoff (PB) theorem*. While the former concerned with the non-resonant tori, latter concerned with the resonant tori. KAM theorem assures the presence of non-resonant tori with little deformation (KAM tori) provided the perturbation is sufficiently small and smooth. We may note that the resonant tori with $\alpha = m/n$ appears as n periodic points on the projected plane. According to PB theorem, under perturbation these points become $2n$ periodic points of which n points are stable (elliptic) and n points are unstable (hyperbolic). The chain of $2n$ points are also arranged such that both types are located alternatively. Thus successive applications of both the theorems provide self-similar structure at all scales as the scenario of *nearly integrable* systems. However, the vicinity

of emerging unstable points from the resonant tori is the beginning of new phenomenological transition to complex behaviour of the nonintegrable systems.

For very small perturbation, the KAM tori are strong barriers for the development of chaos in the phase space. On increasing the perturbation, the KAM tori are gradually destroyed resulting to ‘smooth transition to chaos’. In the absence of KAM tori, a chaotic orbit wanders all possible regions of the energy shell. This can be seen as scatter of points in the Poincaré section. The rich range of transition to chaos in nonintegrable systems can be efficiently studied using the *perturbed twist map*

$$\begin{aligned}\theta_{n+1} &= \theta_n + 2\pi\alpha(r_n) + \epsilon f(r_n, \theta_n) \\ r_{n+1} &= r_n + \epsilon g(r_n, \theta_n)\end{aligned}\tag{1.5}$$

where the functions f and g are chosen such that the area-preserving property still holds. This map exhibits all generic features of the chaotic Hamiltonian systems. The iterative map of this kind is very easy to compute and also convenient for analytical treatments, unlike the Hamiltonian equations of motion.

1.1.3 Few examples

Investigations on chaotic dynamics of two degrees of freedom systems, using the Poincaré section construction, became possible only after the use of computers in physics. It is worth briefing few systems in the development of Hamiltonian chaos.

- The first and most enduring effort is the exploration by Hénon and Heiles. They chose a simple Hamiltonian system to model the motion of a star in cylindrically symmetric gravitational potential of a galaxy [9]. Their model potential is bounded only upto a critical energy and hence the energy is crucial in dictating the dynamical features. For very small energy, with respect to the critical energy, they observed that the Poincaré section is predominantly regular where there were many smooth close loops. As the energy is increased the system displays a transition to chaos, with reduction in number of smooth loops. Above the critical energy, the Poincaré section is filled with scatter of points and thus showing that the dynamics is highly chaotic. The motion in this case is *ergodic*: almost all the orbits eventually explore all parts of the available phase space. The ergodicity implied that the star can eventually escape to infinity.
- Another instructive system is the Toda lattice [10], which models the propagation of waves in nonlinear lattice. In 1970’s this system enjoyed much attention due to its special kind of solutions called *solitons*, which are waves propagate through the medium without any change of shape. The physical significance of the solitons is very wide in

nature [11]. Ford and co-workers modelled the Toda lattice using equal point masses on a ring with exponential interactions and studied the dynamical aspects [12]. Their exhausting observations suggested that the system is integrable, albeit the nonlinear interactions. However, the subsequent study [13] had shown that the system can become chaotic provided the point particles have unequal masses.

- Nonlinear coupled oscillators are the ideal representatives of nonintegrable systems [14]. An important member of this family is the harmonic oscillators with nonlinear interaction which models, in appropriate co-ordinates, the dynamics of Hydrogen atom in an external uniform magnetic field. It was found in [15] that, in highly chaotic regimes the atom-field quantum interaction is highly influenced by the unstable periodic orbits. A compilation of literature in [16] provides a complete account on this topic.
- In addition to the Hamiltonian with smooth potential, there is an important class of discontinuous systems called *planar billiards*. Their Hamiltonian is of the form

$$H = \begin{cases} (p_x^2 + p_y^2)/2 & \text{inside a boundary } A \text{ in } xy\text{-plane} \\ \infty & \text{outside } A. \end{cases} \quad (1.6)$$

Here the particle motion consists of straight segments joined by specular reflections at A and dynamics is very sensitive to the form of A [17]. In this class of system, two well known models are Sinai billiard [18] and stadium billiard of Bunimovich [19]. Sinai's model consists of a particle moving in a square with identified edges containing a circular reflecting obstacle of radius R at the centre of square. The stadium billiard consists of a particle confined in two semi circles of radius R joined by parallel straight lines with length L . In the asymptotic limit, typical orbits of these billiards passes through almost every region within A . Equivalently, the 3D energy shell is fully explored by the orbits. In addition, there are also very few special short periodic unstable orbits which do not fill the region A . They play an important role in the corresponding quantum spectra.

1.2 Quantum chaos

Dual (matter-wave) nature of atomic systems demanded new law of nature i.e., quantum mechanics, subject to Bohr's correspondence principle. Quantum mechanics is a probabilistic theory and fundamental ingredient of it is the Heisenberg's uncertainty principle that prohibits precise determination of canonical variables like position and momentum of a particle simultaneously. As a consequence, the concept of trajectory does not exist in the new theory. However,

classical mechanics emerges as the limiting case of quantum mechanics as follows. Considering an ansatz that the quantum wave function is $\Psi(\mathbf{q}, t) = e^{iS(\mathbf{q}, t)/\hbar}$ where S is the classical action and \hbar is the Planck constant, in semiclassical limit ($\hbar \rightarrow 0$) time dependent Schrödinger equation is nothing but the time dependent Hamilton-Jacobi equation. We may notice that the limit $\hbar \rightarrow 0$ is highly singular.

Basic formulation of quantum mechanics for integrable systems in semiclassical limit is the Einstein-Brillouin-Keller (EBK) quantization [20]. In this formulation, quantized classical objects for N degrees of freedom system are the N dimensional invariant tori. To be precise, classical action along N independent circuits of the tori are expressed as integral multiples of \hbar . Since the phase space of integrable systems are completely filled with tori, they are quantizable using EBK method. On the other hand, in the nonintegrable case the tori are destroyed by the perturbation and hence the EBK quantization is no longer applicable. Although this difficulty was realized long back by Einstein himself [20], the package of challenges in dealing nonintegrable quantum systems were fully appreciated only after our improved understanding of classical physics. In this context, many novel approaches supported by numerical techniques paved way to what is now conventionally accepted as ‘quantum chaos’ - studies on nonintegrable quantum systems in semiclassical limit. Such studies are mainly focussed on quantum manifestations of chaotic dynamics in the semiclassical limit.

1.2.1 Eigenvalues

The lack of a quantization procedure for nonintegrable quantum systems was overcome by an alternative general semiclassical method, pioneered by Gutzwiller [21], and further developed by Balian and Bloch [22]. This method is based on associating density fluctuations of quantum energy levels to classical periodic orbits. For a given quantum system with the eigenvalue equation $H|\psi_n\rangle = E_n|\psi_n\rangle$, the spectral density is represented as

$$d(E) \equiv \sum_n \delta(E - E_n) = \bar{d}(E) + d_{\text{osc}}(E). \quad (1.7)$$

Here $\bar{d}(E)$ is the average density given by the Thomas-Fermi formula

$$\bar{d}(E) = \frac{1}{(2\pi\hbar)^N} \iint \delta(E - H(\mathbf{q}, \mathbf{p})) \, \mathbf{d}\mathbf{q} \, \mathbf{d}\mathbf{p} \quad (1.8)$$

such that a quantum state occupies the phase space cell of volume $(2\pi\hbar)^N$. This provides the density after smoothening over the coarsest scale. The term $d_{\text{osc}}(E)$ is the oscillatory correction represented in terms of *all* non-zero length periodic orbits of the corresponding classical system.

Considering the level spacing $\Delta E = E_{n+1} - E_n$, the average spacing is $\overline{\Delta E} \sim 1/\bar{d}(E) \sim \hbar^N$. Only at this scale, all delta spikes of the density positioned at the energy E_n are resolved.

Influence of periodic orbit of period T on the spectrum can be realized through the relation $\Delta E \sim \hbar/T$ [23]. This relation means that a single orbit of period T provides collective property (oscillatory clustering) of levels in the scale ΔE . That is shorter orbit gives spectral details on coarser scale while the longer ones on finer scale. Thus the complete spectral details are represented in terms of all the orbits upto the period $T \sim \hbar/\overline{\Delta E} \sim 1/\hbar^{N-1}$. This period is extremely long for the non-trivial classical case with $N > 1$. But approaching the finest scale $\overline{\Delta E}$ to get the complete spectrum is not practical for a chaotic system since the orbits are isolated and unstable and their number grows exponentially with the period as e^{hT}/T where h is the topological entropy [24]. Hence instead of acquiring complete knowledge of the spectrum, the level density *smoothed* over energy range $\Delta E \gg \overline{\Delta E}$ can be obtained by including all the necessary shorter orbits. With beautiful illustration Berry has shown in [23] that contribution of more and more orbits with longer period leads to the emergence of δ spikes in the spectrum.

The association of periodic orbits and the quantum spectra are well supported by spectral behaviour of many chaotic quantum systems. One of the encouraging observations is the quantum spectra of hydrogen atom in a strong external magnetic field. Both theoretical [15, 25] and experimental [26] studies on diamagnetic excited atom of hydrogen have confirmed that the spectral features are highly influenced by the periodic orbits. In addition, the spectra of microwave billiard [27] and tunnelling current through double barrier of quantum well in presence of magnetic field [28] have upheld the periodic orbit theory of spectra.

1.2.2 Eigenstates

It is then natural to ask whether it is possible to understand the quantum states also, in the semiclassical limit, through the knowledge of periodic orbits. Before answering this question, it is instructive to recapitulate some of the early attempts to distinguish the quantum states of nonintegrable systems from those of the integrable systems. A first and noted attempt in this direction was made by Percival [29]. He suggested that, in semiclassical limit there are regular and irregular states corresponding to two extreme sorts of classical motion. Since then it was of great concern to distinguish the quantum states of integrable and nonintegrable systems. Berry has first made use of Wigner function as a convenient tool to reveal some of the salient features of the above mentioned quantum states. The Wigner function of a state is defined as [30]

$$W(\mathbf{q}, \mathbf{p}) \equiv \frac{1}{(2\pi\hbar)^N} \int e^{-i\mathbf{p}\cdot\mathbf{y}/\hbar} \langle \mathbf{q} + \mathbf{y}/2 | \psi \rangle \langle \psi | \mathbf{q} - \mathbf{y}/2 \rangle d\mathbf{y}. \quad (1.9)$$

This function, which is not positive definite, roughly approximates to phase space density over the manifold explored by the classical orbit corresponding to the state $|\psi\rangle$. Starting from EBK quantization for integrable case, Berry [31] has shown that the Wigner function collapses on to the classical N dimensional invariant torus. This is in full correspondence with the classical

orbit confined on the torus. Although there is no known form for the semiclassical state of the nonintegrable system, in ergodic regime Voros suggested the microcanonical distribution as an approximation for the corresponding Wigner function [32]

$$W(\mathbf{q}, \mathbf{p}) = \left\{ \int \int \delta(E - H(\mathbf{q}, \mathbf{p})) d\mathbf{q} d\mathbf{p} \right\}^{-1} \delta(E - H(\mathbf{q}, \mathbf{p})). \quad (1.10)$$

Using this Berry argued that the quantum state is a Gaussian random function [33]. This is in some sense a reflection of the unpredictable nature of classical orbit that fills the energy surface ergodically. These results are in accordance with the Shnirelman's theorem [34] that the phase space invariants are the guiding factors for the morphology of quantum states, like the N -tori for the regular states and $2N - 1$ dimensional energy surface for the irregular states. In contrast to the periodic orbit theory approach, it was also believed that individual unstable orbits with measure zero are unlikely to support irregular quantum states.

One of the most striking results concerned with eigenfunctions are brought to light from Heller's numerical explorations on chaotic stadium billiard [35]. His analysis revealed that, in addition to typical eigenstates which appear to have more complex structures, there are also states that appear to be more regular such that their intensities are prominent in the vicinity of some of the unstable short periodic orbits. He refers this quantum imprints of periodic orbits on the states as 'scars'. This observation leads to the speculation that, besides the invariant set like the energy surface, set of periodic orbits could also influence morphological features of eigenstates. A first attempt to explain scarring phenomena within the frame work of periodic orbit theory was made by Bogomolny [36]. He shows that, analogous to spectral density, the intensity of eigenstates averaged over small range of spectra can be associated to periodic orbits. Berry also arrived a similar results using Wigner function representation of quantum states [37]. Theoretical investigations on systems like the nonlinearly coupled quartic oscillator [38], hydrogen atom in magnetic field [39] and experiments with microwave cavities [40] provide ample support for the scarring phenomena of chaotic quantum systems. Recently, semiconductor quantum well in presence of a uniform magnetic field [41] has emerged as a promising new experimental set up for the studies on quantum chaos. In this system, states of electron in the well that are scarred along some of the unstable periodic orbits are found to be responsible for tunnelling current through the barrier of the well.

1.2.3 Statistics

We have already seen that spectral density of quantum system is of the order \hbar^{-N} . Hence in the limit $\hbar \rightarrow 0$, the density is very large and it would be appropriate to study statistical behaviour of the spectrum. In the semiclassical limit, intuitively one may then expect that the degree of complexity of underlying classical dynamics could be reflected in the spectral

statistics in some way or the other. One of the first steps in this direction is made in [42] where the distribution $P(s)$ of nearest neighbour spacing $s = E_{n+1} - E_n$ is derived for integrable systems with $N > 1$. It is shown that spacings follow Poisson distribution i.e., $P(s) = \exp(-s)$. It is worth noting that this is also the spacing distribution of random numbers. An important feature of this distribution lies in the limiting case: $s \rightarrow 0$, $P(s) \rightarrow 1$. Thus the energy eigenvalues of regular system are uncorrelated and exhibit *level clustering*. Although deriving such a distribution is an impossible task for nonintegrable system, a first systematic numerical analysis was made in [43] for the chaotic billiard systems with random matrix theory (RMT) as a tool.

RMT is a well established theory, initiated by Wigner and further developed mainly by Dyson and Mehta [44], which describes spectral fluctuations of nuclear energy spectra. We may recollect that nucleus comprises numerous nucleons and their interactions among themselves are highly complex, and complete knowledge of nuclear interactions are contentious even today. Nevertheless, the RMT was conceived as a model for nuclear spectral fluctuations which does not require any complicated details of the nuclear interactions except few symmetry informations. To be more precise, the theory was built for eigenvalues of Hermitian matrix whose elements are random numbers chosen from Gaussian distributions. The symmetry requirements classify the comprising ensemble of Hermitian matrices into three classes. Among them Gaussian orthogonal ensemble (GOE) is relevant for our discussion. GOE is an ensemble of real matrices such that probability distribution of the matrix elements are invariant under orthogonal transformation. This ensemble represents Hamiltonian with time-reversal symmetry and no spin-1/2 interactions. A celebrated result of RMT is the Wigner distribution which predicts spacing distribution of the eigenvalues for the GOE class as

$$P(s) = \frac{\pi s}{2} \exp(-\pi s^2/4). \quad (1.11)$$

For the first time Bohigas et. al. [43] found that energy levels of a quantum particle confined in planar billiards, whose underlying classical motion is fully chaotic, also follow the above distribution. Noticing the limit $P(s) \rightarrow 0$ as $s \rightarrow 0$, it was conjectured that the spectrum of chaotic system exhibits RMT predicted *level repulsion*. The conjecture has been well supported by the spectra of various systems like magnetized Hydrogen atom [45], billiard shaped microwave cavity [46] etc. As an implication, RMT prediction of the spacing distribution emerges as touchstone to classify highly chaotic systems from the regular ones in the quantum domain.

1.3 Kicked rotor: a paradigm

We have already emphasized that area-preserving mappings are simple to study two degrees of freedom time independent Hamiltonian systems. It is then certainly of interest to find out an appropriate Hamiltonian system which corresponds to such mappings. It turns out that the Hamiltonian of the form

$$H(q, p, t) = \begin{cases} V(q)/\gamma & 0 < t < \gamma T \\ p^2/2(1 - \gamma) & \gamma T < t < T \end{cases} \quad (1.12)$$

where $0 < \gamma < 1$ generates such a mapping. The above Hamiltonian represents a particle which experiences an impulsive force due to the potential $V(q)$ during the time $0 < t < \gamma T$ and then it moves freely till the time T . This process is repeated periodically with period T . The dynamics of such externally driven systems can be chaotic as there are no constants of motion. Integrating the equations of motion for the above Hamiltonian over a period from $t = nT$ to $t = (n + 1)T$, n being an integer, yields the area-preserving mapping

$$\begin{aligned} q_{n+1} &= q_n + Tp_{n+1} \\ p_{n+1} &= p_n - T(\partial V/\partial q)_{q_n}. \end{aligned} \quad (1.13)$$

An instructive model of this kind is a rotor which is periodically kicked by a standing wave. This system is represented by the Hamiltonian

$$H = \frac{p^2}{2} + \frac{K}{4\pi^2} \cos(2\pi q) \sum_n \delta(n - t) \quad (1.14)$$

which was first introduced by Casati et. al. [47]. The associated mapping is the well known *standard map*

$$\begin{aligned} p_{n+1} &= p_n + (K/2\pi) \sin(2\pi q_n) \\ q_{n+1} &= q_n + p_{n+1} \pmod{1}. \end{aligned} \quad (1.15)$$

which is one form of the perturbed twist map that describes kick-to-kick dynamics of the rotor. Albeit its simple form, the standard map exhibits variety of dynamics ranging from regular to chaotic as strength of the kick K increases [48, 49]. It is worth remarking that the standard map approximates motion of Hydrogen atom in external electric field [50].

1.3.1 Dynamical localization

Quantum mechanically also the delta kick facilitates to write analytical form of kick-to-kick propagator by partial integration of the Schrödinger equation. Thus quantum dynamics of the

rotor can be conveniently studied using quantum analogue of the classical map. The quantum kicked rotor has been recognized as a paradigm of quantum chaos [51]. The kick provides periodic input of energy to the system, and classically very large kicking strength results to chaos assisted unbounded diffusion in kinetic energy of the rotor. An important result of quantization is that in generic case the energy is initially diffusive and then attains a quasiperiodic saturation [52]. To understand this striking phenomena of ‘quantum suppression of classical diffusion’ it will be appropriate to delineate a problem in solid state physics.

Conduction of electronic current through atomic lattice is one of the fundamental problems in solid state physics. The electronic eigenstate is represented in tight-binding approximation as

$$H_{mm}\psi_m + \sum_{n \neq m} H_{mn}\psi_n = E\psi_m. \quad (1.16)$$

Here ψ_n , H_{nn} are the components of electronic eigenstate and energy associated to n th lattice site respectively. E is the eigenvalue of the state and H_{mn} is the hopping element. We may note that behaviour of ψ_n crucially depends on H_{nn} . For crystal lattice, H_{nn} is constant and ψ_n corresponds to Bloch states. These are extended states which are responsible for transport through the lattice. On the other hand, if the crystal is doped such that the set $\{H_{nn}\}$ is a random sequence then the transport is significantly suppressed. Anderson showed that the randomness in the on-site potential begets destructive quantum interference such that the electronic states are exponentially localized in the lattice site [53]. This well known *Anderson localization* provides a plausible mechanism for the suppression of electronic transport through the random lattice.

It has been shown in [54] that the Eqn. (1.16) also represents the rotor model with $\{H_{nn}\}$ being a ‘pseudorandom’ sequence in the generic case and ψ_n being component of rotor eigenstate (here it is called quasienergy state) in momentum representation. This one-to-one mapping of rotor model to Anderson model show that generic rotor states are *exponentially localized in momentum space*. It is remarkable to notice that unlike the Anderson model, kicked rotor is a deterministic system. Nevertheless the rotor states are localized and the randomness which is responsible for the localization is of dynamical origin. Localization of this kind is termed as *dynamical localization*. This phenomenon is reflected in the kicked rotor as suppression of chaos assisted diffusion upon quantization.

An important experiment to validate dynamical localization is an atom-optics realization of the delta kicked rotor [55]. In this experiment nearly 10^5 sodium atoms are trapped and laser cooled in a magneto-optic trap (MOT) [56]. Within the trap the atoms are Gaussian distributed both in the position and momentum. The sample of atoms then interact with a pulsed standing wave of a laser light. As a consequence, the momenta of excited atoms are redistributed. In order to evaluate the resultant momentum distribution, atoms are allowed for a time t_{drift} to

settle in their new widened spatial distribution. They are then frozen in their positions with the trapping lasers to form ‘optical molasses’. The fluorescent image of the molasses, recorded in a charged-coupled-device (CCD) camera, gives the new spatial distribution of the atoms. From this distribution and the time t_{drift} , the resultant momentum distribution of the atoms is evaluated. This process is repeated for N number of kicks. Shown in Fig. 1.1 is the average kinetic energy of the atomic sample as a function of number of kicks. It is observed that for initial few kicks the atomic energy follows the classical diffusion. As the number of kicks increases, the energy deviates from the classical behaviour and saturates at the value predicted by the localization theory. The measured distribution in momentum also supports the expected exponential localization. These results confirm the dynamical localization and the subsequent quantum suppression of the classical diffusion.

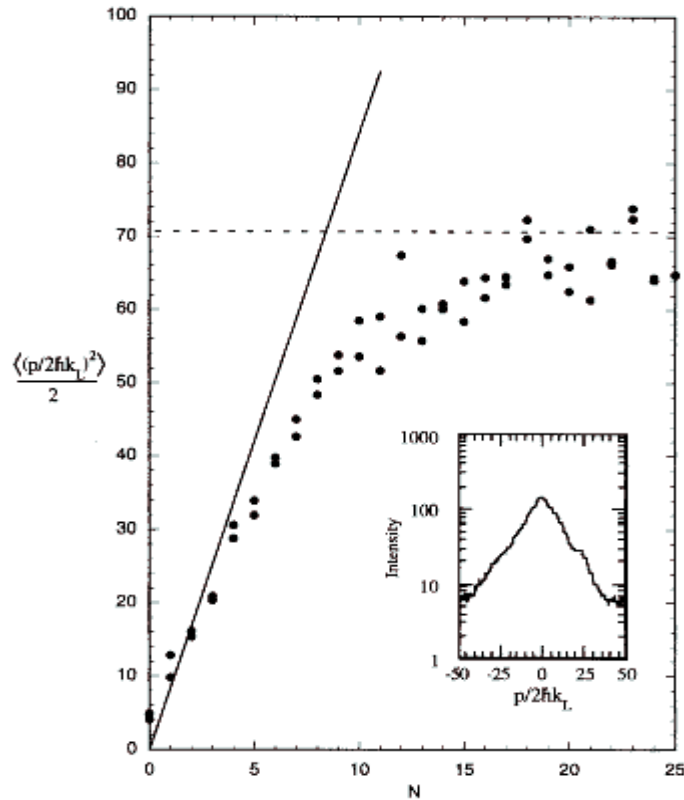


Figure 1.1: *Straight line represents the classical diffusion in kinetic energy of the rotor in highly chaotic regime. Solid dots are the experimentally measured average kinetic energy of the atoms. Inset shows the exponential fall of momentum distribution of the excited atoms [55].*

Dynamical localization is not a unique phenomenon of the delta kicked rotor and it can be observed in other systems as well. Experimental developments on microwave ionization of Hydrogen atom [57] has evoked enormous interest in 1980's to study the ionization mechanism

for simple one-dimensional system

$$H = \frac{p^2}{2} - \frac{1}{|z|} + \epsilon z \cos(\omega t) \quad (1.17)$$

which represents a 1D Hydrogen atom interacting with an external microwave field. In chaotic regime, it has been experimentally verified that the threshold field for ionization increases unlike the classical predictions [58]. This is due to localization that occurs in the quantum excitations. Thus Hydrogen atom in external field also serves as an ideal testing ground for the dynamical localization. The interaction of a beam of atoms with modulated standing light wave represented by the Hamiltonian of the form [59]

$$H = \frac{p^2}{2} - \epsilon \cos[2k(x - \Delta L \sin \omega t)] \quad (1.18)$$

is also another system which displays localization. An experimental realization of this system using beams of ultra-cold atoms has shown that [60], when the system is classically chaotic, light induced momentum transfer to the atoms is limited due to the localization. Thus the dynamical localization is an important phenomenon by which the quantum systems significantly differ from the corresponding classical systems in the chaotic regime.

1.4 Motivation for the thesis

As we have seen that until now much work has been done on chaotic systems and on their quantum counterpart with the object of revealing quantum mechanical manifestations of classical chaos. Most of the work has used smooth Hamiltonian systems which are in general integrable systems with smooth perturbation. For these systems KAM theorem is valid, on increasing the perturbation the systems change from regular to chaotic and the underlying transition is gradual. This scenario has been widely studied in two degree of freedom systems or equivalently area preserving maps. However, there are conditions upon which the KAM theorem rests that may not always be satisfied by certain systems of physical interest. In particular if the perturbation is *not* sufficiently smooth or even discontinuous, the KAM scenario may break down. Large scale chaos may instantaneously develop in the system. One other way is that the KAM scenario fails when the unperturbed system is fully resonant, as in the Kepler problem. Let us focus only on non-KAM behaviour of the former kind.

To begin with we shall discuss the prevalence of systems where the non-KAM scenario may be seen. The simplest systems where Hamiltonian chaos can develop is the so called 1.5 degree of freedom system, which are time dependent one-degree of freedom systems. Thus consider the driven rotor Hamiltonian

$$H = \frac{p^2}{2} + f(t)V(\theta) \quad (1.19)$$

where $V(\theta)$ is an external potential that is periodic with period 2π , and $f(t)$ is a periodic function of time with period T . If $V(\theta)$ is sufficiently smooth, the KAM theorem scenario combined with the Poincaré-Birkhoff theorem provides the generic behaviour. The smoothness or at least continuity of $V(\theta)$ is provided by the periodic boundary conditions in angular position of the rotor. Introducing discontinuous potentials will lead to delta function forces equivalent to walls of certain heights. This brings us to a natural class of systems where non-KAM behaviour will be the rule rather than exception: *externally forced particles in wells*. This forms a broad class of systems which have evoked considerable interest in recent years since the development of quantum wells. Quantum wells are semiconductor fabricated structures that are potential wells for the electrons. One of the recent experiments [41] has demonstrated that system comprising electron inside the quantum well in presence of external electromagnetic field is a new testing ground for our understanding on quantum chaos.

1.4.1 An illustration

In fact the simplest of such systems involve a particle in one-dimensional infinite square wells (1D billiards) with time dependent external fields. Consider as an example the Hamiltonian

$$H = H_0 + \epsilon \cos\left(\frac{2\pi x}{\lambda}\right) \cos(\omega t) \quad (1.20)$$

where $H_0 = p^2/2 + V_{sq}(x; a)$, describing such a particle. The potential $V_{sq}(x; a)$ is the confining infinite square well potential of width $2a$, centered at the origin (see Fig. 1.2). Here ϵ and λ are field strength and wavelength of the external field which is being modulated in time with frequency ω .

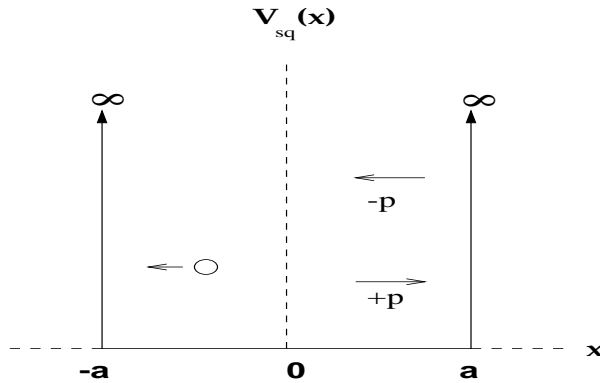


Figure 1.2: Particle in 1D infinite square well potential.

The equations of motion of the particle within the square well are

$$\dot{x} = p \quad ; \quad \dot{p} = \frac{2\pi}{\lambda} \epsilon \sin\left(\frac{2\pi x}{\lambda}\right) \cos(\omega t). \quad (1.21)$$

It is easy to verify that Eqn. (1.21) is invariant under the transformation

$$\begin{aligned} t &\rightarrow \omega_0 t, & \epsilon &\rightarrow \epsilon / (2a\omega_0)^2 \\ x &\rightarrow x/2a, & \lambda &\rightarrow \lambda/2a \\ p &\rightarrow p/2a\omega_0, & \omega &\rightarrow \omega/\omega_0. \end{aligned} \quad (1.22)$$

Here the frequency ω_0 , which sets the new time scale, is arbitrary. Note that the new scaled variables and parameters are referred by the old symbols and they are dimensionless. Setting $\omega_0 = \omega$ in the above transformation, the system has effectively two parameters *viz.* ϵ and $R = 2a/\lambda$. Here R is the ratio of two length scales of the system i.e., well width and field wavelength.

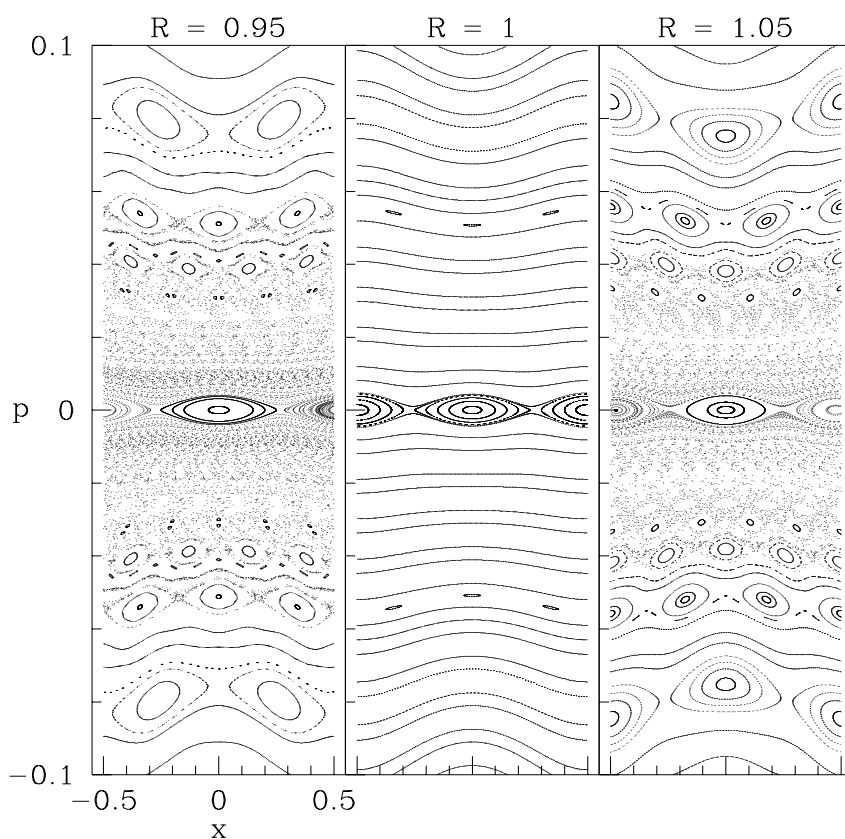


Figure 1.3: Typical phase space of the system governed by the Hamiltonian in (1.20) with dimensionless parameters $\epsilon = 0.001$ and $\omega = 1$. The lower momentum region is increasingly chaotic when the length scales do not match.

The presence of two competing length scales, provides a rich range of non-KAM behaviours. In particular if the dimensionless ratio R is a non-integer there is a possibility of observing non-KAM phenomena. Under the perturbation we can roughly expect that states whose absolute value of the initial momentum is less than $\sqrt{2|\epsilon|}$ will be most affected. Thus low energy states will be most affected by the time-dependent forces. Fig. 1.3 shows the effect of the parameter R . While for $R = 1$ the system is essentially KAM type and has KAM tori interspersed with resonances, any small deviation of R away from unity destroys low energy KAM curves and leads to increased chaos. Fig. 1.4 shows the fate of an individual KAM torus for which $R = 1$ is a ‘bifurcation’ point in parameter space and changes stability on either side. We expect such behaviour to be generic to a large class of similar systems.

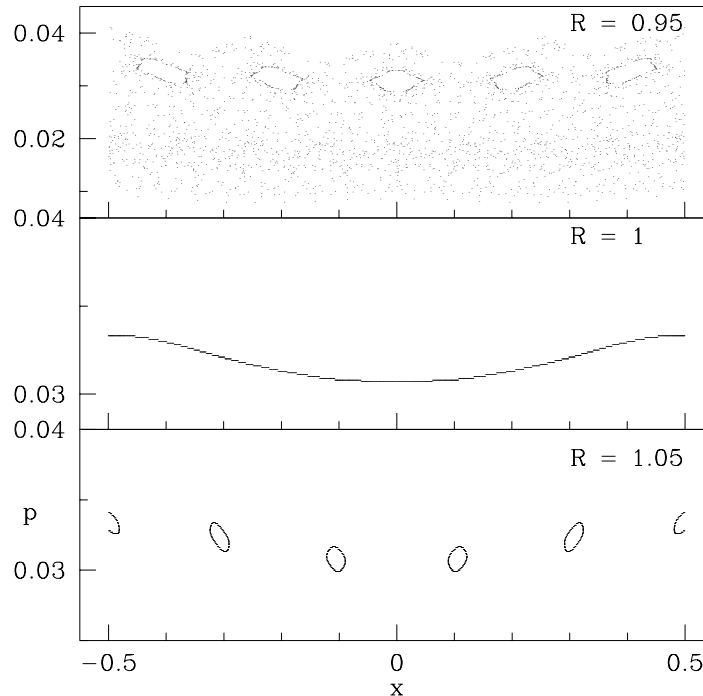


Figure 1.4: *Shown are orbits of Fig. 1.3 having identical initial conditions. The initial condition corresponds to a KAM torus in the lower momentum region for $R = 1$ (the negative momentum region is not shown here). Note the abrupt change in the stability and the non-generic features of the resultant phase space structures.*

We shall note that some aspects of the classical motion of a particle in an infinite square well potential in presence of an uniform monochromatic external field are already studied [61]. Quantum mechanically also similar systems have been introduced as a model of quantum chaos [62, 63]. However, in all these earlier works there were no issues of competing length scales.

Consequently, understanding on the above mentioned length scale induced non-KAM scenarios and their quantum mechanical manifestations are completely missing. One of the main motivation of this thesis is to fill this void. In this thesis we explore in great detail the classical and quantum mechanical implications of naturally emerging competing length scales.

1.4.2 Outline of the thesis

The thesis is organized as follows. In *Chapter 2*, we introduce one simplest possible system which is appropriate for our investigation. Using one generalization of the standard map, we study the classical dynamics with main focus on non-KAM transition to chaos. In *Chapter 3*, the corresponding quantum system is analyzed using quantum map. Here, influences of the length scales on the quantum system are studied in detail. In *Chapter 4*, attention is given on special orbits of the system called ‘accelerator modes’ which are responsible for anomalous classical transport in chaotic regimes. Possibility of such modes and their consequences in the quantum system have been explored. In *Chapter 5*, torus quantization of the classical map is studied in detail as a model of bounded Hamiltonian system. At the end of each chapters we summarize the results. Finally, we conclude the thesis with a brief outlook.

2. Classical map

2.1 Introduction

One dimensional time periodic kicked systems have their own privileged place in the study of Hamiltonian chaos. In this family of systems, a natural choice to understand the issue of competing length scales and subsequent non-KAM scenario is given by the Hamiltonian

$$H = \frac{p^2}{2M} + V_{sq}(x) + \epsilon \cos\left(\frac{2\pi x}{\lambda}\right) \sum_{j=-\infty}^{\infty} \delta\left(j - \frac{t}{T}\right). \quad (2.1)$$

This Hamiltonian corresponds to a particle of mass M , trapped inside the infinite square well $V_{sq}(x)$, in presence of time periodic impulsive external field. The square well of width $2a$ is centred at the origin. The external field is characterized with the strength ϵ and the wavelength λ . The impulse is accomplished using train of delta functions with period T . Recollecting the Poisson summation formula

$$\sum_{j=-\infty}^{\infty} \delta\left(j - \frac{t}{T}\right) = \sum_{n=-\infty}^{\infty} \cos(n\omega t)$$

where $\omega = 2\pi/T$ is the pulse frequency, we have

$$\epsilon \cos\left(\frac{2\pi x}{\lambda}\right) \sum_{j=-\infty}^{\infty} \delta\left(j - \frac{t}{T}\right) = \epsilon \sum_{n=-\infty}^{\infty} \cos\left(\frac{2\pi x}{\lambda} - n\omega t\right). \quad (2.2)$$

That is, the effect of impulsive field is the same as that of an infinite number of travelling waves with identical amplitudes and frequencies being multiples of pulse frequency.

The stroboscopic map, relating the dynamical variables immediately after successive kicks, can be derived in a standard manner and results in the following:

$$\begin{aligned} x_{n+1} &= (-1)^{b_n} (x_n + p_n T/M) + (-1)^{b_n+1} \text{sgn}(p_n) 2ab_n \\ p_{n+1} &= (-1)^{b_n} p_n + (2\pi\epsilon T/\lambda) \sin(2\pi x_{n+1}/\lambda) \end{aligned} \quad (2.3)$$

where $b_n \equiv \left\lceil \frac{1}{2a} \{ \text{sgn}(p_n)(x_n + p_n T/M) + a \} \right\rceil$ is the number of bounces of the particle at the walls during the interval between the n th and the $(n+1)$ th kick. Here $\text{sgn}(\dots)$ and $\lceil \dots \rceil$ stand for sign and integer part of the argument respectively. The dynamical variables x_n, p_n are the position and momentum of the particle just after the n th kick; $\text{sgn}(p_n) = \pm 1$, depending on whether $p_n > 0$ or $p_n < 0$. Although $\text{sgn}(p_n)$ is discontinuous and undefined for $p_n = 0$, one can see easily from the map that either of the values (± 1) can be taken for $\text{sgn}(p_n)$ as this does

not alter the dynamics. Note that whenever the particle hits any of the two walls, it bounces back with instantaneous sign change in its momentum.

With the following scaling

$$X_n = \frac{x_n}{2a}, \quad P_n = \frac{p_n T}{2aM}, \quad K = \frac{2\epsilon\pi^2 T^2}{aM\lambda}, \quad R = \frac{2a}{\lambda} \quad (2.4)$$

the above map be written in dimensionless form as

$$\begin{aligned} X_{n+1} &= (-1)^{b_n}(X_n + P_n) + (-1)^{b_n+1} \text{sgn}(P_n)b_n \\ P_{n+1} &= (-1)^{b_n}P_n + (K/2\pi) \sin(2\pi R X_{n+1}) \end{aligned} \quad (2.5)$$

where $b_n = \left[\text{sgn}(P_n)(X_n + P_n) + \frac{1}{2} \right]$. We refer to this map as the *well map*. Note that K and R are the only two effective parameters of the well map. Here K is proportional to the strength of the external field; R is the ratio of the width of the well to the wavelength of the external field. We do not impose any constraints on R , for example, those imposed while considering standing waves in a cavity, but allow all values. Evidently, $|X_n| \leq 1/2$ or $|x_n| \leq a$ as the particle motion is confined between two rigid walls.

2.2 Generalized standard map

The phase space of the well map is a two dimensional plane with reflective boundary in scaled position X and unbounded in scaled momentum P . Moreover, the map is complex in its form. However, our analysis of the well map may be simplified to great extent on realizing the close relation between dynamics of the unperturbed particle in the well and that of the free rotor (i.e, particle moving on a circle). The difference between the free particle inside the well and the free rotor is in the boundary conditions. Both the free motions are same unless the particle hits the walls. The correspondence between them is made explicit in the following way.

Let us consider the dynamics of a free rotor in discrete unit time steps, which is the map relating successive angles θ_n and angular momenta J_n :

$$\begin{aligned} \theta_{n+1} &= \theta_n + J_n \pmod{1} \\ J_{n+1} &= J_n. \end{aligned} \quad (2.6)$$

Here the motion is confined on a cylinder $[-1/2, 1/2) \times (-\infty, \infty)$, and this is the unperturbed twist map. Similarly the discretized free motion in a well of unit width is

$$\begin{aligned} X_{n+1} &= (-1)^{b_n}(X_n + P_n) + (-1)^{b_n+1} \text{sgn}(P_n)b_n \\ P_{n+1} &= (-1)^{b_n}P_n. \end{aligned} \quad (2.7)$$

Denoting $S_n \equiv (\theta_n, J_n)$, and $W_n \equiv (X_n, P_n)$ if both the maps are iterated with the same initial conditions i.e., $W_0 = S_0$, then we find a relation between the n th iterate as

$$W_n = (-1)^b S_n \quad ; \quad b = \sum_{i=0}^{n-1} b_i \quad (2.8)$$

where b is the *total* number of bounces of the particle after $(n - 1)$ iterates. That is, the n th iterates of both the maps *at most differ by sign*. Since the maps (2.6) and (2.7) have reflection symmetry about the origin, the particle dynamics is quantitatively same as the rotor dynamics. Now if we introduce nonlinear perturbation to the twist map such that the resultant map is

$$\begin{aligned} \theta_{n+1} &= \theta_n + J_n \quad (\text{mod } 1) \\ J_{n+1} &= J_n + (K/2\pi) \sin(2\pi R\theta_{n+1}). \end{aligned} \quad (2.9)$$

It is easy to see that the relation (2.8) still exists between the well map and the perturbed twist map. The time reversal of the perturbed twist map is

$$\begin{aligned} J_{n+1} &= J_n + (K/2\pi) \sin(2\pi R\theta_n) \\ \theta_{n+1} &= \theta_n + J_{n+1} \quad (\text{mod } 1) \end{aligned} \quad (2.10)$$

and we call this map as the *generalized standard map* (GSM).

From the above description it is clear that quantitative dynamical features are *same for the well map and the GSM*. Thus in attempting to analyze the dynamics of the well map, it is sufficient to understand the dynamics of the GSM. Also the map (2.10) is easier to handle than the well map, as it is only a slightly generalized version of the well known standard map ($R = 1$) of kicked rotor [47, 48, 49]. When it is stated that the standard map is a one parameter system the implicit assumption is that there is only one length scale. Here there are naturally *two* length scales whose ratio is the cause of many interesting effects as we shall see. In what follows we discuss dynamical behaviour of the GSM in detail. Throughout the present study we consider K and R to assume *real positive* values only.

2.3 Transition to chaos

For the standard map (GSM with $R = 1$), when $K < 1$, the dynamics is nearly regular. The phase space is filled with large number of KAM tori which are *rotationally invariant circles* [64] extending across the phase plane. These closed loops \mathcal{C} encircle the cylinder and are invariant, meaning that $\mathcal{T}\mathcal{C} = \mathcal{C}$, where \mathcal{T} is an area preserving *continuous* transformation on the cylinder (for instance Eq.(2.10) with $R = 1$). KAM tori are the principal barriers for the unstable orbits to diffuse in phase space. As K increases there is a *smooth* transition from regular to chaotic

behaviour with a reduction in the number of KAM tori [65]. Dynamical changes of KAM tori with increase of K are discussed in [66]. At $K \approx 1$ all the KAM tori disappear from the phase space [67]. For very large K ($\gg 1$) the dynamics is chaotic and diffusive. In general, for integer values of R , the map is continuous and takes the form of standard map with $K \rightarrow KR$. Hence the dynamical transitions are identical with that of the standard map.

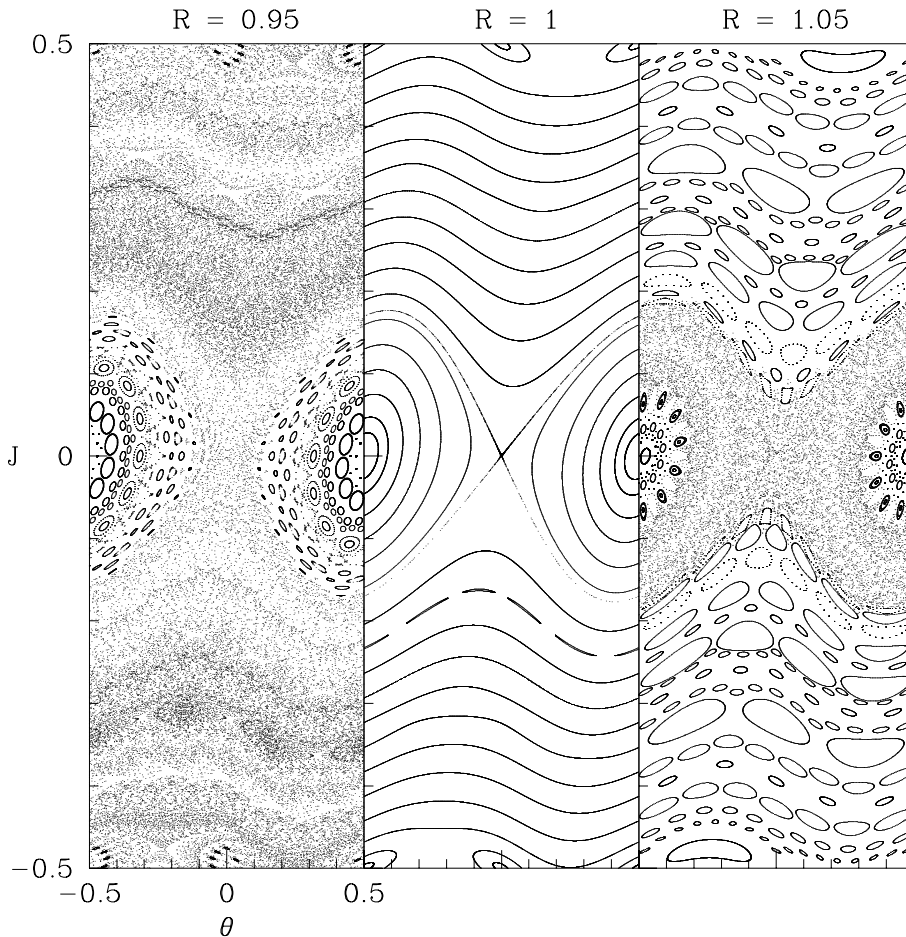


Figure 2.1: *Phase space portrait of the GSM with $K = 0.3$. We have shown the phase space of unit square since GSM is periodic in J and θ with unit period. For $R = 1$, the dynamics is nearly regular wherein many smooth KAM tori are seen. When R departs from unity the dynamics is increasingly complex and no KAM tori are seen. This may be compared to the lower momentum region in Fig. 1.3.*

When R assumes non-integer values the situation is entirely different from the earlier case, particularly when K is small. A typical phase space portrait in Fig. 2.1 depicts an interesting abrupt transition to chaos. While the phase space is nearly regular for $R = 1$, it is more complex

with the coexistence of both regular and chaotic orbits even for small departure of R from unity. Moreover, in the “non-standard map” case no KAM tori exist in the phase space. It is to be noted that all these features are very similar to the length scale induced chaos and non-KAM scenario which we discussed previously in the Chapter 1. Thus the GSM, albeit simple in form, qualifies as the “standard map” for non-KAM systems like externally forced particle in potential well.

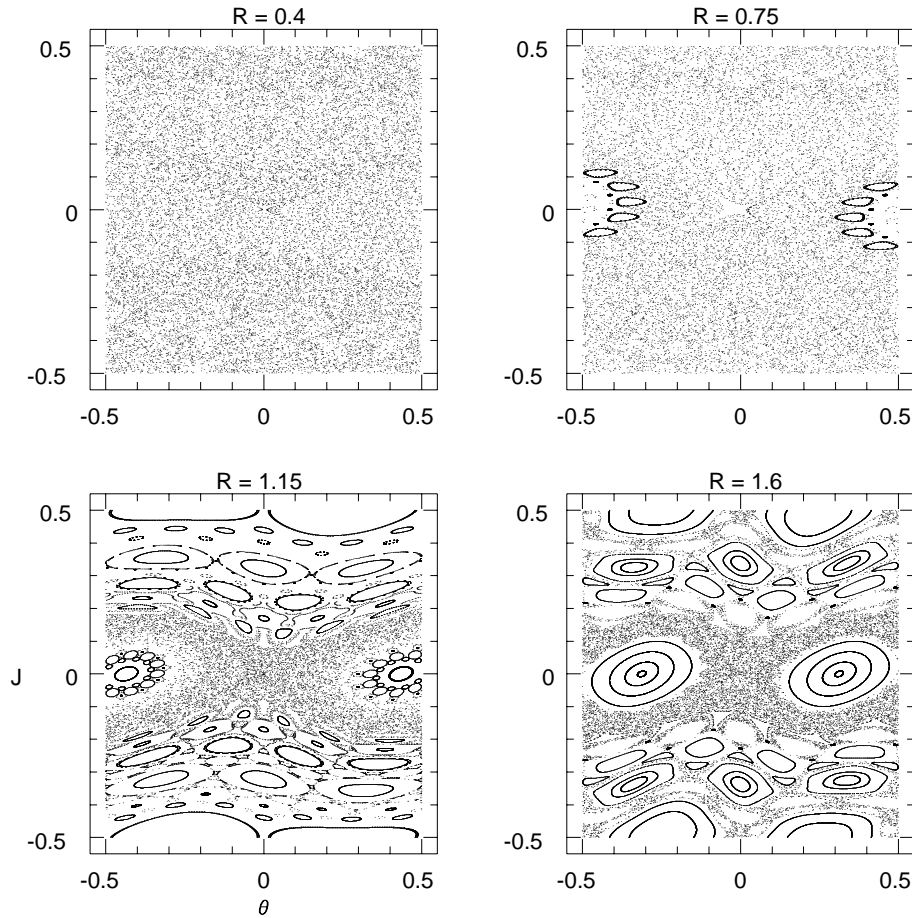


Figure 2.2: Phase space portrait for $K = 0.3$ to illustrate more effects of non-integer R values.

A careful observation of Fig. 2.1 reveals that stability nature of different regions of the phase space are different with respect to R . The regions of KAM tori ($R = 1$) are replaced by unstable chaotic orbits for $R < 1$. On the other hand, those regions are filled with chains of stable islands for $R > 1$. In contrast, the regions around the stable fixed point $(0, 1/2)$, i.e, principle resonance zones, have hierarchical stable structures for both the cases of $R \neq 1$. Similarly, the regions near the separatrix are unstable and chaotic for $R \neq 1$. Thus the entire

standard map may be regarded as being poised at a point of bifurcation when considered as a function of the parameter R . In general, no KAM tori appear in the phase space if $R \neq j$ (j is a positive integer) for however small K may be. The dynamics is either mixed or chaotic for non-integer R . This is of course due to the discontinuity in the map when R assumes non-integer values. In other words, there are no closed loops \mathcal{C} encircling the cylinder such that $\mathcal{T}'\mathcal{C} = \mathcal{C}$, where \mathcal{T}' is the transformation defined by GSM with non-integer values of R . The point of discontinuity in \mathcal{T}' arises at $\theta = -1/2$ (or $1/2$).

In Fig. 2.2 more phase space portraits are shown to illustrate the influence of non-integer R . The absence of KAM tori in the phase space is evident in all the cases, however, the dynamics for the cases $R < 1$ and $R > 1$ are clearly distinguishable. The former is more chaotic and the phase space is almost filled with unstable orbits. On the other hand, both regular and chaotic regions are seen in the latter. But for large K ($\gg 1$), there is no such apparent difference in dynamics between the above two cases as K is the leading chaos parameter. This discontinuous dynamics implies the failure of both KAM and Poincaré-Birkhoff scenarios. The modifications that may occur are little understood, and Chirikov in [68] points out that the piecewise linear sawtooth map

$$\begin{aligned} p_{n+1} &= p_n + \alpha x_n \\ x_{n+1} &= x_n + p_{n+1} \pmod{1} \end{aligned} \quad (2.11)$$

when K is a non-integer such that $-4 < \alpha < 0$ is one such system where extremely complicated locally stable motions occur and “it is not at all clear what could be a meaningful description, if any, of this apparently trivial model”. The particle in a well naturally gives rise to a nonlinear generalization of the sawtooth map and below we show how a simple method may give us significant local stability information that elucidates the observed dramatic transition to chaos.

2.4 Stability analysis: new approach

In the absence of KAM theorem for irrational tori and the Poincaré-Birkhoff theorem for rational tori, we apply a kind of local analysis to understand the change in stability of the orbits with respect to R . Assuming that K is small (< 1), let us denote an orbit of GSM (with $R = j$, positive integer) as $\{\tilde{\theta}_n, \tilde{J}_n\}$. This satisfies the following mapping:

$$\begin{aligned} \tilde{J}_{n+1} &= \tilde{J}_n + (K/2\pi) \sin(2\pi j \tilde{\theta}_n) \\ \tilde{\theta}_{n+1} &= \tilde{\theta}_n + \tilde{J}_{n+1} \pmod{1}. \end{aligned} \quad (2.12)$$

Also consider an orbit $\{\theta_n, J_n\}$ of the GSM with $R = j + \mu$ and $|\mu| \ll 1$, with the same initial conditions as the above orbit. On introducing the differences $\Delta\theta_n = \theta_n - \tilde{\theta}_n$; $\Delta J_n = J_n - \tilde{J}_n$,

it is possible to write an exact mapping equation for $\Delta\theta, \Delta J$ as

$$\begin{aligned}\Delta J_{n+1} &= \Delta J_n + (K/2\pi) \left\{ \sin\left(2\pi R(\tilde{\theta}_n + \Delta\theta_n)\right) - \sin(2\pi j\tilde{\theta}_n) \right\} \\ \Delta\theta_{n+1} &= \Delta\theta_n + \Delta J_{n+1}.\end{aligned}\tag{2.13}$$

Expanding in terms of $\Delta\theta_n$ and retaining first order terms leads to a time dependent force and the non-autonomous linear set of equations

$$\begin{aligned}\Delta J_{n+1} &= \Delta J_n + KR \cos(2\pi R\tilde{\theta}_n)\Delta\theta_n + A_n \\ \Delta\theta_{n+1} &= \Delta\theta_n + \Delta J_{n+1}\end{aligned}\tag{2.14}$$

where

$$A_n \equiv \frac{K}{2\pi} \left\{ \sin(2\pi R\tilde{\theta}_n) - \sin(2\pi j\tilde{\theta}_n) \right\}.$$

The behaviour of such linear non-autonomous equations can be quite complex (compare for instance the Mathieu differential equation which also arises in linear stability analysis). For the analysis on stability of the orbits, we wish be intuitive and derive rough but useful estimates. Although we never expand R about an integer, here we assume that this excursion is small, so that the non-autonomous stability equations can be treated perturbatively. Appealing to the method of averaging we simply replace the time dependent force by its time average. The limitation of this is pointed out further ahead.

Considering the orbit $\{\tilde{\theta}_n, \tilde{J}_n\}$ to be the KAM torus orbit which correspond to $R = j$. Since the motion is ergodic in $\tilde{\theta}$, we replace the time average by an equivalent space average with uniform measure. Thus

$$\cos(2\pi R\tilde{\theta}_n) \approx \mathbf{g}(R) = \int_{-1/2}^{1/2} \cos(2\pi Rx) dx\tag{2.15}$$

This procedure leads us to simple linear map:

$$\begin{aligned}\Delta J_{n+1} &= \Delta J_n + (K/\pi) \sin(\pi R)\Delta\theta_n + A_n \\ \Delta\theta_{n+1} &= \Delta\theta_n + \Delta J_{n+1}\end{aligned}\tag{2.16}$$

and its stability can be seen from the corresponding Jacobian matrix which gives the stability condition: $|2 + (K/\pi) \sin(\pi R)| < 2$. Substituting $R = j + \mu$, the stability condition becomes

$$-\frac{4\pi}{K} < (-1)^j \sin(\pi\mu) < 0.\tag{2.17}$$

This implies that if j is odd KAM tori which exist at $R = j$ are stable for $\mu > 0$ and unstable for $\mu < 0$; converse is the case if j is even. Shown in Fig. 2.3 are the typical stability changes

of KAM orbit as R varies. Thus the above stability condition satisfactorily explains the observation. Although μ is small in the above analysis, our numerical observation show that the stability condition (2.17) is satisfied even for large values of μ . Here we can think of the integer R values as bifurcation points for entire set of KAM tori orbits. This explains majority of the phase space features seen earlier.

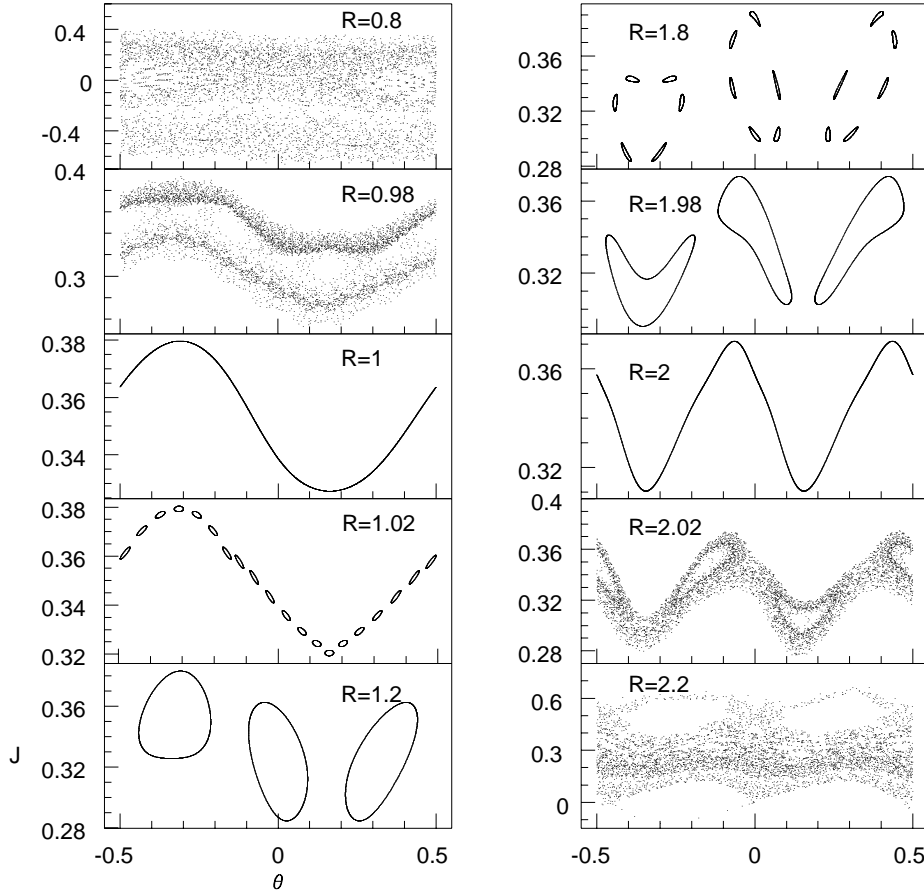


Figure 2.3: Fate of an orbit with initial condition $S_0 = (0.25, 0.33)$ as R varies. The orbit corresponds to KAM torus for integer R . Right column ($j = 1$): the orbit becomes unstable and chaotic for $\mu < 0$ while it becomes chain of stable islands for $\mu > 0$; Left column ($j = 2$): the stability is reversed and can be compared with the right column.

To quantify the degree of complexity of the orbit shown in Fig. 2.3, we calculate the Lyapunov exponents which measure the rate at which the neighbourhood orbit diverge from the given orbit in the tangent space. The GSM in tangent space is given by

$$\begin{pmatrix} \delta J_{n+1} \\ \delta \theta_{n+1} \end{pmatrix} = \mathbf{M}_n \begin{pmatrix} \delta J_n \\ \delta \theta_n \end{pmatrix} ; \quad \mathbf{M}_n = \begin{pmatrix} 1 & KR \cos(2\pi R\theta_n) \\ 1 & 1 + KR \cos(2\pi R\theta_n) \end{pmatrix} \quad (2.18)$$

where \mathbf{M}_n is the Jacobian matrix evaluated at n th iterate. Consequently

$$\begin{pmatrix} \delta J_n \\ \delta \theta_n \end{pmatrix} = \tilde{\mathbf{M}} \begin{pmatrix} \delta J_0 \\ \delta \theta_0 \end{pmatrix} ; \quad \tilde{\mathbf{M}} = \prod_{i=0}^{n-1} \mathbf{M}_i \quad (2.19)$$

and the exponents are given by

$$\Lambda_{\pm} = \lim_{n \rightarrow \infty} \frac{1}{n} \ln |\lambda_{\pm}(n)| \quad (2.20)$$

where $\lambda_{\pm}(n)$ are the eigenvalues of the matrix $\tilde{\mathbf{M}}$. Since we are considering the area-preserving mapping the two exponents are such that $\Lambda_+ + \Lambda_- = 0$. The maximum exponent $\Lambda_+ = 0$ for the regular orbit and $\Lambda_+ > 0$ for the chaotic case.

R	0.8	0.98	1.0	1.02	1.2	1.8	1.98	2.0	2.02	2.2
Λ_+	0.24	0.083	0.004	0.0	0.003	0.003	0.005	0.005	0.04	0.21

From the table we see that the exponent is positive for $R < 1$ and for $R > 2$ showing that the orbit is chaotic in these cases. For $1 \leq R \leq 2$ the exponent is nearly zero as the orbit corresponds to regular case (see Fig. 2.3).

Now we dwell on other regions of phase space, for instance the chaotic regions around the origin in Fig. 2.1, where the above procedure fails. In the interior of the original 0/1 resonance (at $R = 1$) even a reversal of the stability criteria is observed. Origin of the phase space, hyperbolic fixed point, is not affected by R and this is the genesis of chaos. Smooth stable and unstable manifolds of the hyperbolic fixed point that exist for $R = 1$ can not exist for $R \neq 1$ as they would then represent rotationally invariant curves. Therefore the presence of the hyperbolic point necessarily implies chaos.

Within the framework of the stability analysis done earlier what has failed around the hyperbolic fixed points is the assumption of uniform measure. If we think of the simple pendulum we are moving from energetic rotational motions (KAM tori) to slow oscillations of large amplitude and clearly the time is spent preferentially around the turning points. Also the replacement with time averages will fail as the time scales involving fast θ motions and slow ΔJ motions become comparable. The latter effect becomes important as we move into the 0/1 resonance region. Note that the existence of two different time scales is initial value dependent and is present in the standard map as well, *i.e.*, it does not arise as a result of the presence of the additional parameter R .

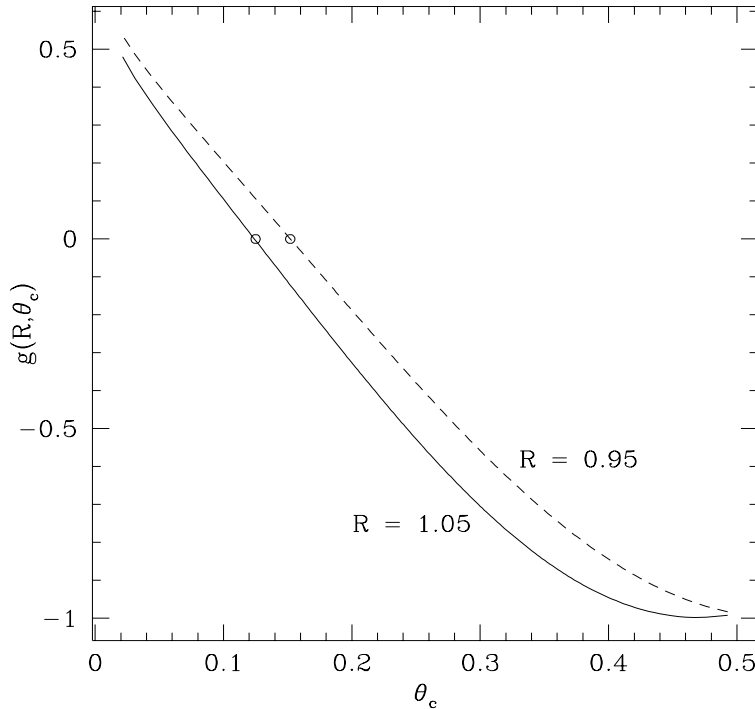


Figure 2.4: The function $g(R, \theta_c)$ is plotted with the turning point θ_c of the pendulum. Positiveness of g corresponds to the instability of some GSM orbits. The points at which g changes its sign are shown with the open circle.

The modified measure can be approximated by considering the simple pendulum. We now take $j = 1$ for simplicity and consider only excursions of R from unity. The term $\cos(2\pi R\tilde{\theta}_n)$ in Eq. (2.14) is replaced with the ergodic average:

$$\cos(2\pi R\tilde{\theta}_n) \approx g(R, \theta_c) = \left\{ \int_{\theta_c}^{1/2} \frac{dx}{\sqrt{E - \cos(2\pi x)}} \right\}^{-1} \int_{\theta_c}^{1/2} \frac{\cos(2\pi R x) dx}{\sqrt{E - \cos(2\pi x)}}. \quad (2.21)$$

Here $-1 \leq E \leq 1$ is the scaled energy and θ_c is the turning point given by $\cos(2\pi\theta_c) = E$. This is shown in Fig. 2.4 and the point where g crosses zero from above ought to be a point where stability is recovered. This then explains the uniform chaos around the hyperbolic fixed point for $R \neq 1$. This also explains the stability around the point $S = (1/2, 0)$. However the interior of the resonance is not accessible to the simple theory. Remarkably Fig. 2.4 predicts a recovery of stability at $\theta_c \approx 0.15$ which is seen for $R = 0.95$ while stability is recovered at a much higher value of θ_c for $R = 1.05$ and is not seen in Fig. 2.4. This fact may be attributed to the failure of the averaging procedure in analyzing non-autonomous equations and have no other recourse than Eq. (2.14) itself.

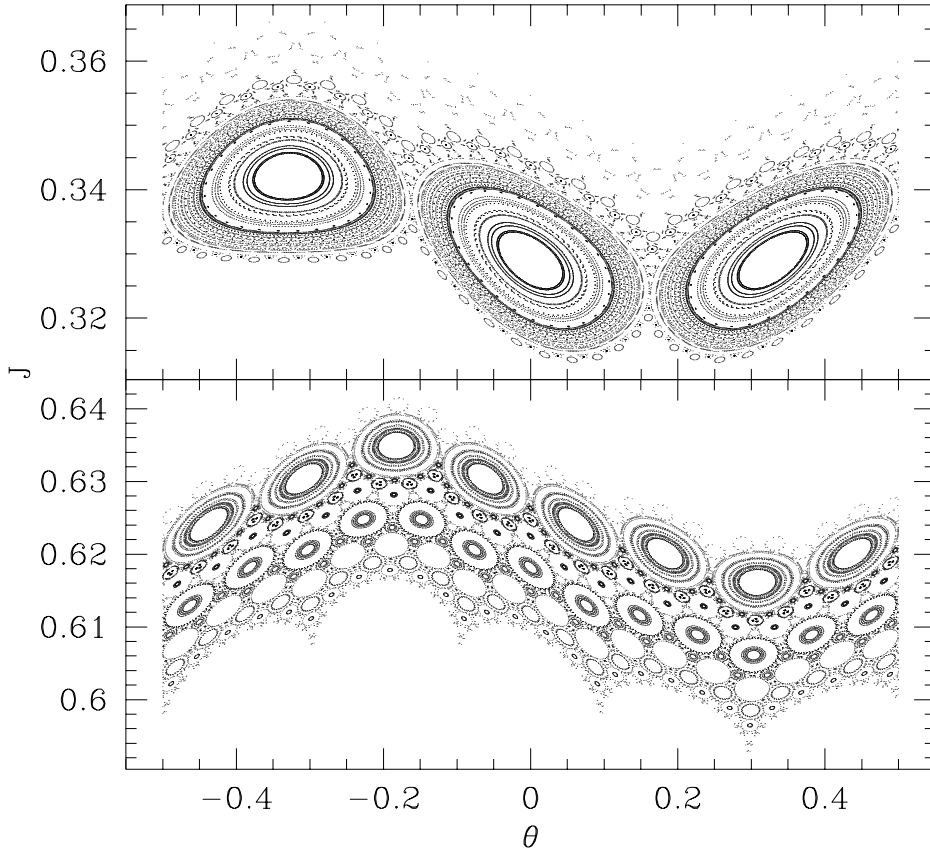


Figure 2.5: *Orbits with initial conditions on the line $J = 1/3$ (top) and $J = (\sqrt{5} - 1)/2$ (bottom) for $K = 0.1$ and $R = 1.05$.*

As we have noted, hyperbolic fixed point generates chaos for $R \neq 1$. Let us further move on to the region of phase space for $R \gtrsim 1$ where there are lack of chaos with total absence of hyperbolic points. The Poincaré-Birkhoff theorem concerning the breakup of rational tori into an equal number of hyperbolic and elliptic periodic points is clearly violated. In fact the modified scenario seems to be the creation of *only* elliptic fixed points for $R \gtrsim 1$ and *only* hyperbolic points for $R \lesssim 1$. To illustrate this we have shown in Fig. 2.5 the fate of points on the lines $J = 1/3$ and $J = (\sqrt{5} - 1)/2$. While in the former case three elliptic islands emerge prominently, in the latter one can see chains of elliptic islands with the clear hierarchy of the number of islands $5, 8, 13, 21, 34 \dots$ deriving from the Fibonacci sequences generating closer approximations to the golden mean. These island chains alternate as the ratios approach the golden mean. As a limiting case we may think of a golden mean chain, but we have, of course,

not rigorously proved its existence. There appear to be two types of orbits in the stable regions: those that form an island chain and those that meander in the interstitial spaces between island chains on presumably a fractal set. These would then be examples of strange non-chaotic sets in Hamiltonian mechanics.

Thus simple methods provide detailed understanding of very complicated dynamics and dramatic stability changes that emerge from the natural length scales or the discontinuity. We may also speculate that tuning the length scales would lead a good way of controlling or enhancing chaos. While our study has been for Hamiltonian systems, dissipative systems may also display such a behaviour.

2.5 Hyperbolic regime

In this section we discuss another peculiar property of the GSM. The trace of the Jacobian matrix (2.18) is given by

$$|\text{Tr } \mathbf{M}_n| = |2 + KR \cos(2\pi R\theta_n)|. \quad (2.22)$$

Since $|\theta_n| \leq 1/2$, for $R \leq 1/2$ the trace is such that $|\text{Tr } \mathbf{M}_n| > 2$ (for $R = 1/2$, $|\text{Tr } \mathbf{M}_n| = 2$ only at $|\theta_n| = 1/2$). We remind that this range of θ_n is the *entire* configuration space and $\theta_n = \pm 1/2$ represent the wall boundaries. Since the Jacobian is only a function of the angle and not a function of action at a given phase space point, we conclude that the Jacobian has real eigenvalues *throughout* the phase space. In other words, the system is completely chaotic or hyperbolic for $R \leq 1/2$. This implies that there are contracting and expanding real directions or alternatively stable and unstable manifolds throughout phase space [69]. It is worth remarking that very few dynamical models are exactly known to be hyperbolic systems. These include the sawtooth map [70, 71], the baker map and flows on surfaces of constant negative curvature [72]. The standard map even for large values of the parameter K is not proven to be hyperbolic. Thus in this context, we place the fact that GSM has a parameter range for which it is hyperbolic for all positive values of the parameter K . The phase space of one such case is shown in Fig. 2.2.

The similarity of the GSM, when $R \leq 1/2$, with the piecewise linear sawtooth map (2.11) is made clear by the following linear approximation. In this regime, the force $\sin(2\pi R\theta_n)$ in the GSM is monotonic and we have the linear approximation as $\sin(2\pi R\theta_n) \approx 2 \sin(\pi R)\theta_n$. This leads to $|\text{Tr } \mathbf{M}_n| \approx |2 + (K/\pi) \sin(\pi R)|$. The Lyapunov exponents in this approximation are given by

$$\Lambda_{\pm} \approx \ln(y \pm \sqrt{y^2 - 1}) \quad ; \quad y = 1 + (K/2\pi) \sin(\pi R). \quad (2.23)$$

It is clear from Fig. 2.6 that the approximated exponent fits fairly well with the actual one. Similar agreement was seen for a wide range of initial conditions and different values of K as well. This shows the validity of the above linear approximation for the force when $R \leq 1/2$, which enables us to understand the gross behaviour of the Lyapunov exponents in this regime. We note that the usual linear approximation $\sin(2\pi R\theta_n) \approx 2\pi R\theta_n$ near the origin was found not to be as good as the above approximation.

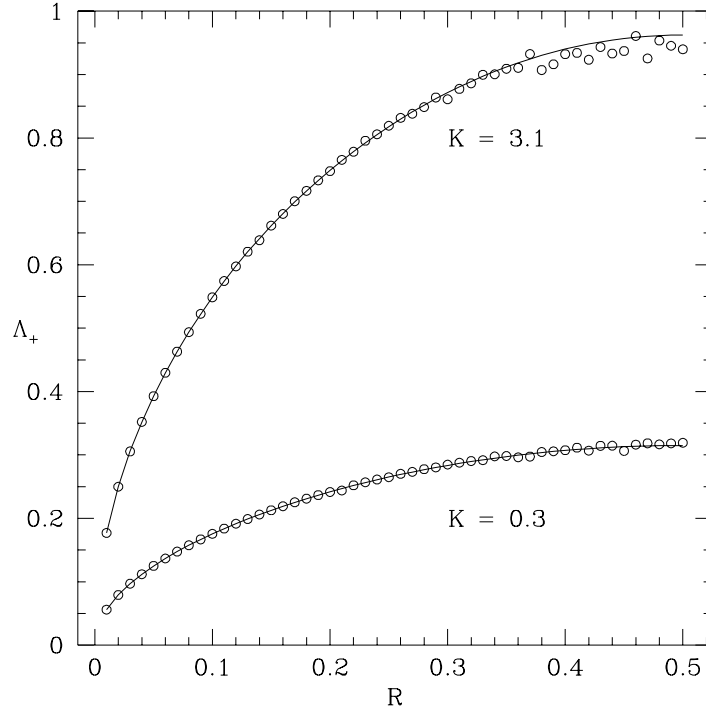


Figure 2.6: *Positive Lyapunov exponent (circles) of an orbit of the GSM for two K values. It is calculated from the procedure which is described earlier. The solid curve is the approximated exponent given by Eq. (2.23).*

2.6 Diffusion

One of the striking results in the study of nonlinear phenomena has been the similarity to many body thermodynamic property such as diffusion. The fact that deterministic dynamical systems can give rise to diffusive behaviour reminiscent of stochastic processes like random walks, has led to the speculation that indeed a lot of macroscopic stochastic behaviour can be pinned onto microscopic deterministic chaos [73, 74]. Diffusion in a dynamical variable u_n can be characterized by long time behaviour of its variance σ^2 . Considering that the variance has

time dependence

$$\sigma^2(n) = \langle u_n^2 \rangle - \langle u_n \rangle^2 \sim n^\gamma \quad (2.24)$$

where $\langle \dots \rangle$ stands for ensemble average, γ is a characteristic exponent and n being the discrete time. The rate of change of variance in long time limit is defined as the diffusion coefficient:

$$D = \lim_{n \rightarrow \infty} \frac{\sigma^2(n)}{n}. \quad (2.25)$$

In general $0 < \gamma \leq 2$ and the diffusion processes are classified accordingly.

The central limit theorem (CLT) implies that $\gamma = 1$ and such is the case for most diffusion processes and is hence called *normal*. Generalized simple one dimensional random walk problem [75], with u_n as the total displacement of the random walker at the n th step, substantiates the CLT and the probability distribution function $\rho(u)$ in the long time limit converges to the Gaussian form

$$\rho(u) = \frac{1}{\sqrt{2\pi\sigma^2}} \exp \left\{ \frac{-(u - \langle u \rangle)^2}{2\sigma^2} \right\} \quad (2.26)$$

with $\sigma^2 \sim n$. If there is long time correlation, which is dominated by rare events such as sticking and flights, diffusion becomes *anomalous* ($\gamma \neq 1$) in which case the limit in Eq. (2.25) does not exist and the CLT fails to explain these processes. Flights are the events in which the random walker can travel for long distances in spurts and the mean square of the flight length diverges. They are called *Lévy flights* [76, 77], characterized by *superdiffusion* ($\gamma > 1$). The Lévy flights are common in many applications of physics [78]. On the other hand, sticking [76] is a strange phenomenon occurring in deterministic kinetics, when chaotic orbits get trapped for long time by cantori (broken KAM tori) around stable islands in the mixed phase space. Such stickiness leads to *subdiffusion* ($\gamma < 1$), where the average time duration at each step diverges. The case $\gamma = 2$, which we will encounter in Chapter 4, corresponds to the ballistic motion.

From the earlier discussion we have seen that the phase space of the GSM, even for small K , does not have any KAM tori if $R \neq 1$ (in general for non-integer). This could cause the dynamics to be chaotic and there is a possibility of diffusion in momentum J . More over, for $R < 1$ the dynamics is mostly chaotic while for $R > 1$ it is mixed with the coexistence of regular and chaotic orbits in the phase space. This implies that the diffusion must be strongly affected by the parameter R . Taking $u_n = J_n - J_0$, jump in the momentum J at the n th iteration, we observe from Fig. 2.7 that the diffusion is normal for $R < 1$. However, the diffusion coefficient is small since K is small. The coefficient is maximum at $R = 1/2$, where the discontinuity of the GSM is maximum in the shown range; then it falls to zero when R approaches zero or unity. The force term $\sin(2\pi R\theta)$ approaches to zero with R and the diffusion is highly limited,

presumably due the cantori, and hence fall in diffusion coefficient. At $R = 1$, the exponent γ sharply falls down to zero, where there is no diffusion as the KAM tori are present in the phase space.

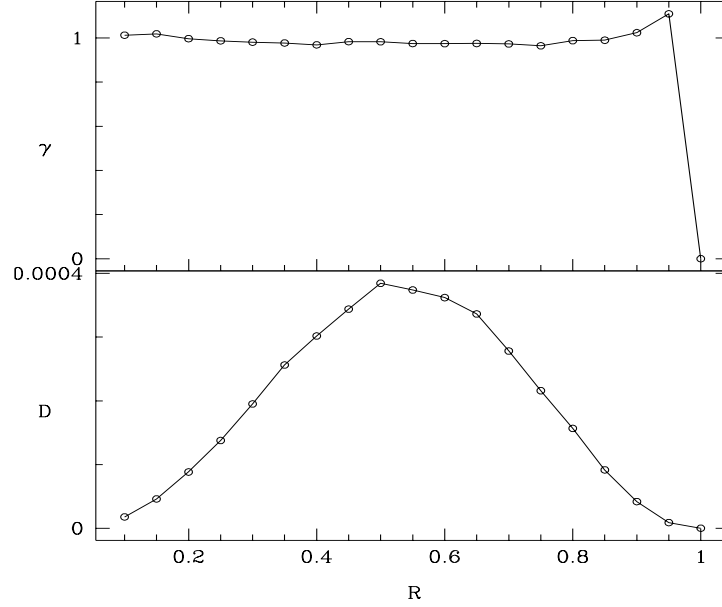


Figure 2.7: *The characteristic exponent γ and the diffusion coefficient D for $R \leq 1$ with $K = 0.1\pi$. We have taken an ensemble of 10^4 initial conditions distributed uniformly in a small square, centred at $(0.3, 0.3)$ with side 0.1 , and evolved each of them for 5000 time steps. The ensemble is chosen such that it does not contain any regular orbits. Notice that there are some small regular regions seen for $1/2 < R < 1$ in Fig. 2.1 and Fig. 2.2. However, the diffusive nature of the chaotic orbits are not influenced by those regular regions.*

For $1 < R < 2$ we have seen that the phase space is mixed with regular and chaotic orbits. The phase space has no KAM tori and instead there are many chains of stable islands. However, we expect that any diffusion of the chaotic orbits will be limited by the sticky regions around the stable islands. In fact the stickiness is so overwhelming that our numerical results that indicate subdiffusion ($\gamma < 1$) in this parametric regime do not converge even after long time iterations of large ensembles. In these kinds of situation, characterization by a simple diffusion process may be inappropriate. More interesting and meaningful measures may be quantities like Poincaré return time distribution [79] and exit time [80] of the chaotic orbits. Alternatively, we may characterize the dynamics by the two-time correlation function $f(\tau)$, which is defined as

$$f(\tau) = \lim_{n \rightarrow \infty} \frac{1}{n} \sum_{i=0}^n \theta_i \theta_{i+\tau}. \quad (2.27)$$

In Fig. 2.8 typical time correlations of an orbit which is chaotic for $R \neq 1$ are shown. The oscillations in $f(\tau)$ for $R = 1$ implies the existence of non-vanishing long time correlation as a characteristic of regular case. For $R = 0.9$, the orbit is chaotic and diffusive in J without any constraint. In this case $f(\tau)$ falls to zero after a small initial oscillation indicating rapidly uncorrelating motion. On the other hand, for $R = 1.1$ though the orbit is chaotic, there are long time correlations. The persistence of these correlations may be associated to the fact that the diffusion of the orbit is highly suppressed by the presence of chains of regular islands. The non-diffusive chaotic orbit occupies the boundaries of regular islands (sticky regions) which can retain the long time correlation. Thus we indicate another way in which the presence of island chains affect the dynamical behaviour even in the absence of rotationally invariant circles: it could for all practical purposes suppress diffusion while retaining long time correlations.

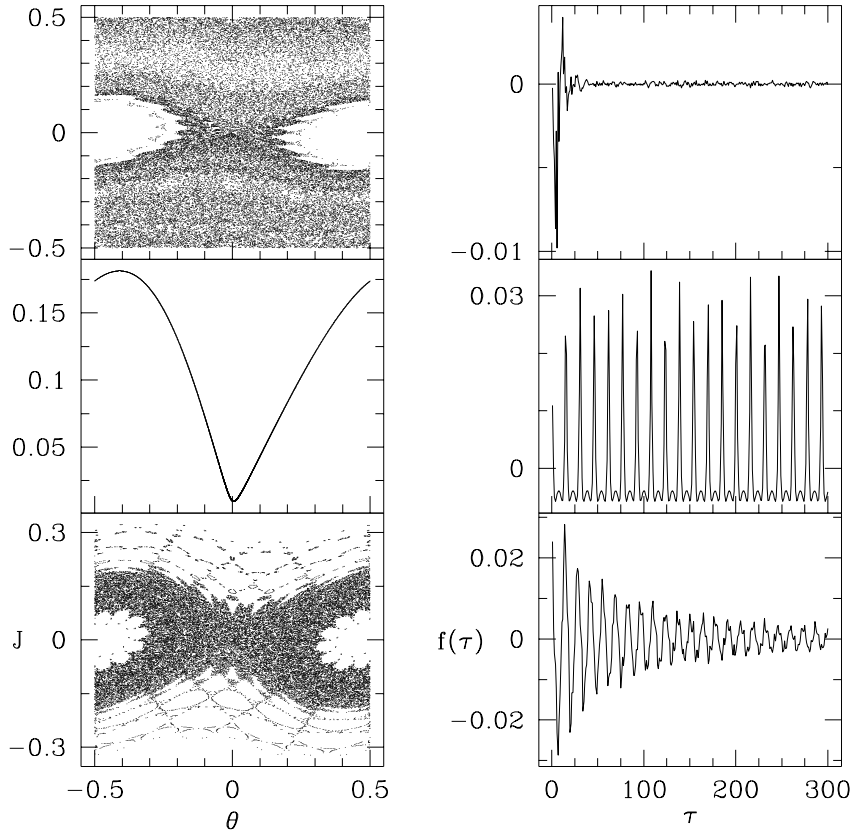


Figure 2.8: *Left column: an orbit with $S_0 = (0.01, 0.01)$ for $K = 0.1\pi$ and $R = 0.9, 1, 1.1$ from top to bottom. The orbit corresponds to a KAM torus near to the separatrix for $R = 1$ and it is chaotic for $R \neq 1$ (for $R = 0.9$, $\Lambda_+ = 0.2$ and for $R = 1.1$, $\Lambda_+ = 0.1$). Right column: corresponding two-time correlation of the orbit.*

Further we investigate the diffusion when K is large (i.e., $K \gg 1$). In this regime the phase space is highly chaotic and D is predominantly governed by K since this is the leading chaos parameter. However, here we are interested in R dependence of D to contrast from the known results for $R = 1$. We have

$$u_n = J_n - J_0 = \frac{K}{2\pi} \sum_{i=0}^{n-1} \sin(2\pi R\theta_i) \quad (2.28)$$

and

$$\begin{aligned} u_n^2 &= \left(\frac{K}{2\pi}\right)^2 \left(\sum_{i=0}^{n-1} \sin(2\pi R\theta_i)\right)^2 \\ &= \left(\frac{K}{2\pi}\right)^2 \left\{ \sum_{i=0}^{n-1} \sin^2(2\pi R\theta_i) + 2 \sum_{i=0}^{n-2} \sum_{j=i+1}^{n-1} \sin(2\pi R\theta_i) \sin(2\pi R\theta_j) \right\}. \end{aligned} \quad (2.29)$$

With the definition of ensemble average

$$\langle g \rangle \equiv \int \int g(\theta, J) d\theta dJ \quad (2.30)$$

integrated averaged over all possible points (θ, J) in the fundamental domain of the phase space i.e., from $-1/2$ to $1/2$ for both the variables, we introduce $C(\tau) = \langle \sin(2\pi R\theta_i) \sin(2\pi R\theta_{i+\tau}) \rangle$ as the force-force correlation. Note that $C(\tau)$ is invariant under time translation. Assuming that $C(\tau)$ falls off rapidly with τ , which is the case of chaotic systems, the diffusion coefficient is given by

$$D = \left(\frac{K}{2\pi}\right)^2 \left\{ C(0) + 2 \sum_{\tau=1}^{\infty} C(\tau) \right\}. \quad (2.31)$$

In general first few terms may be sufficient for the chaotic systems due to the absence of higher order correlation. The zeroth order correlation is

$$C(0) = \frac{1}{2} \left\{ 1 - \frac{\sin(2\pi R)}{2\pi R} \right\} \quad (2.32)$$

and the first order correlation is

$$\begin{aligned} C(1) &= \langle \sin(2\pi R\theta_i) \sin(2\pi R\theta_{i+1}) \rangle \\ &= \langle \sin(2\pi R\theta_{i-1}) \sin(2\pi R\theta_i) \rangle \\ &= \int \int \sin(2\pi R(\theta \pmod{1} - J)) \sin(2\pi R\theta) d\theta dJ \end{aligned}$$

$$= \iint \sin(2\pi R(\theta - J + l)) \sin(2\pi R\theta) d\theta dJ \quad (2.33)$$

where $l \equiv l(\theta, J; K, R)$ is an integer. For $R = j$, $\sin(2\pi R(\theta - J + l)) = \sin(2\pi R(\theta - J))$ and in this case $C(1) = 0$. Similarly we can show that $C(2) = -J_2(jK)$ where $J_2(x)$ is the Bessel function of first kind. Although higher order correlations are more complicated, for the standard map D is calculated upto fourth order correlation [49]. In [81] D is calculated using different methods and since then the Bessel function oscillation of the diffusion coefficient for the standard map is well known.

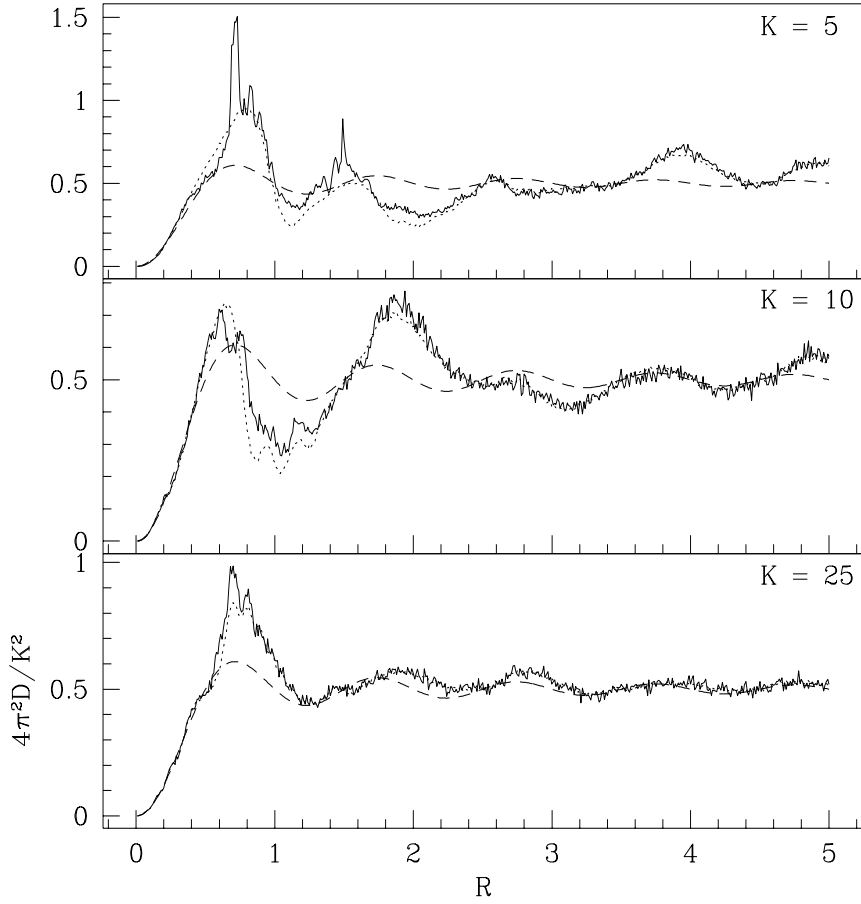


Figure 2.9: Diffusion coefficient for three large values of K are shown. Solid lines correspond to the actual coefficient, the dashed lines correspond to $C(0)$ and the dotted lines correspond to $C(0) + 2C(2)$. For this calculation, an ensemble of 2500 points evolved each of them for 300 time steps. Results are independent of the ensemble.

For non-integer R , $\sin(2\pi R(\theta - J + l)) \neq \sin(2\pi R(\theta - J))$. In this case, for a given K and R the above integration becomes the sum of integration over the cells Ω_l :

$$C(1) = \sum_l \iint_{\Omega_l} \sin(2\pi R(\theta - J + l)) \sin(2\pi R\theta) d\theta dJ. \quad (2.34)$$

Hence $C(1)$ itself is not calculable in straight forward manner. However, we have found numerically that $C(1) \approx 0$, when K is large. Since $C(2)$ is even more difficult here we calculate it numerically. Fig. 2.9 shows typical behaviour of diffusion coefficient as R varies. We may notice that these oscillations significantly differ from the Bessel function oscillations of the standard map. We also find that D is well approximated upto $C(2)$, implying that higher order correlations are negligible. However, the large deviations around $R = 0.7$ for $K = 5$ may be due to the presence of small regular regions (not shown) embedded in the chaotic phase space. In the hyperbolic regime, i.e., $R \leq 1/2$, $C(0)$ itself is sufficient to reflect the behaviour of D . It is worth remarking that for the saw-tooth map all the higher order correlations are shown to be zero and D depends only on $C(0)$ in the hyperbolic regime [70]. In this context, we speculate that for hyperbolic systems all higher order correlations are insignificant.

2.7 Summary

In this Chapter we have introduced a particle confined in one-dimensional infinite square well potential in presence of time periodic impulsive external field as a simple and instructive model for externally forced particle in well. Kick-to-kick classical dynamics of the particle is investigated in detail with the help of one generalization of the standard map. The virtue of generalization lies in the natural introduction of two competing length scales *viz.* well width and the field wavelength.

The ratio of the length scales R is found to be decisive for the dynamics particularly when the external field strength is small. When R is integer the dynamics is nearly regular while it can be chaotic if R is non-integer. This is because the map is continuous for integer R and discontinuous otherwise. The resulting non-KAM scenario and the transition to chaos for non-integer R has been studied. In particular, the absence and fate of irrational tori under perturbation is fairly understood using a simple stability theory. We have observed an alternative to Poincaré-Birkhoff scenario wherein the rational tori under perturbation becomes either stable or unstable points. When $R \leq 1/2$, the map is found to be hyperbolic - a rare class of dynamical system.

We have studied the transport property in different chaotic regimes. In the mixed phase space, although the KAM tori are absent, diffusive nature of the chaotic orbits is highly suppressed by the presence of some regular islands. In highly chaotic regimes, the diffusion coefficient is essentially governed by the first few force-force correlation.

3. Quantum map

3.1 Introduction

We now consider the quantum dynamics of the particle inside the infinite square well potential well in presence of time periodic (period T) impulsive field, and it can be easily studied using iterative quantum map:

$$|\Psi(t + T)\rangle = U|\Psi(t)\rangle \quad ; \quad |\Psi(t + nT)\rangle = U^n|\Psi(t)\rangle \quad (3.1)$$

where U is the one time period quantum propagator and n represents the n th kick. The quantum map, analogous to the classical map discussed in Chapter 2, describes kick-to-kick quantum dynamics. Although the Hilbert space of the quantum system is infinite dimensional, for all practical purposes, it is large but finite N -dimensional space. However, care must be given in making sure that this artificial truncation does not influence the system.

Since the Schrödinger equation is a first order linear differential equation, in the truncated space there exist N linearly independent solutions. For time periodic Hamiltonian with period T , according to Floquet theorem for linear system [82] the solutions of the Schrödinger equation are of the form $|\psi_j(t + T)\rangle = e^{-i\alpha_j}|\psi_j(t)\rangle$ where $j = 1, 2, \dots, N$; α_j are real and distinct i.e., between 0 and 2π . In other words the solutions satisfy the eigenvalue equation

$$U|\psi_j(t)\rangle = e^{-i\alpha_j}|\psi_j(t)\rangle \quad ; \quad \alpha_j = \frac{E_j T}{\hbar}. \quad (3.2)$$

The states $|\psi_j(t)\rangle$ are called *quasienergy states* and E_j are the *quasienergies* [83]. Then the quasienergy states can be written as

$$|\psi_j(t)\rangle = e^{-iE_j t/\hbar}|\phi_j(t)\rangle \quad ; \quad |\phi_j(t + T)\rangle = |\phi_j(t)\rangle. \quad (3.3)$$

The states $|\phi_j(t)\rangle$, called *steady states*, and the quasienergies E_j are analogous to the stationary states and energies of the conservative system [84]. It is to be noted that the inner product of two arbitrary solutions of the Schrödinger equation for arbitrary time dependent Hamiltonian is independent of time due to hermiticity of the Hamiltonian. As a consequence $\langle\psi_j(t)|\psi_{j'}(t)\rangle = \delta_{jj'}$, i.e., the quasienergy states are orthogonal. At any give time t , they form a complete set in the N -dimensional space. By the superposition principle, general solution of the Schrödinger equation with time periodic Hamiltonian with period T is then given by $|\Psi(t)\rangle = \sum_j c_j |\psi_j(t)\rangle$ where c_j are constants. With this the quantum map is

$$|\Psi(t + nT)\rangle = \sum_j c_j e^{-i\alpha_j n} |\psi_j(t)\rangle. \quad (3.4)$$

It is to be noted that t is arbitrary. Thus the quasienergies and quasienergy states play central role in the time periodic Hamiltonian system. They can be obtained by diagonalizing the matrix form of U in some suitable basis states.

3.2 Matrix form of quantum propagator

For the Hamiltonian (2.1), by integrating the Schrödinger equation from just after one kick to the next kick, we can write the quantum propagator can be written as

$$U = \exp \left\{ -ik \cos \left(\frac{2\pi x}{\lambda} \right) \right\} \exp \left\{ -i \frac{H_0 T}{\hbar} \right\} \quad (3.5)$$

where $k = \epsilon T / \hbar$. Note that the propagator is the quantum counter counter part of the well map and not that of the GSM. In Chapter 5, we will be discussing quantum propagator of the GSM in detail. Natural choice of basis for the U -matrix is the eigenstates of the unperturbed Hamiltonian H_0 :

$$H_0 |n\rangle = \mathcal{E}_n |n\rangle \quad (3.6)$$

where $n = 1, 2, 3, \dots$. The energy eigenfunctions and eigenvalues are

$$\langle x | n \rangle = \begin{cases} \frac{1}{\sqrt{a}} \cos\left(\frac{n\pi x}{2a}\right), & \text{for } n \text{ odd} \\ \frac{1}{\sqrt{a}} \sin\left(\frac{n\pi x}{2a}\right), & \text{for } n \text{ even} \end{cases} ; \quad \mathcal{E}_n = \frac{n^2 \pi^2 \hbar^2}{8Ma^2}. \quad (3.7)$$

The U -matrix is then given by

$$U_{mn} = \langle m | U | n \rangle = \langle m | \exp \{ -ik \cos(2\pi x / \lambda) \} | n \rangle e^{-in^2 \tau} \equiv F_{mn} e^{-in^2 \tau} \quad (3.8)$$

where we have defined an effective Planck constant as

$$\tau \equiv \frac{\pi^2 \hbar T}{8Ma^2}. \quad (3.9)$$

As the external field preserves parity we have

$$F_{mn} = \begin{cases} 0, & \text{if } m + n \text{ is odd} \\ \frac{1}{2\pi} \left\{ Q_{\frac{m-n}{2}} - (-1)^n Q_{\frac{m+n}{2}} \right\}, & \text{if } m + n \text{ is even} \end{cases} \quad (3.10)$$

where

$$Q_l = \int_{-\pi}^{\pi} \cos(l\theta) e^{-ik \cos(R\theta)} d\theta \quad (3.11)$$

and $\theta = \pi x/a$. We note that Q_l is a Bessel function integral for integer R , while for non-integer R the integral constitutes a kind of ‘‘incomplete’’ Bessel function. Invoking the Bessel function $J_s(k)$ through the following identity

$$e^{-ik \cos \theta} = \sum_{s=-\infty}^{\infty} (-i)^s J_s(k) e^{-is\theta}$$

the above integral can be evaluated as a series:

$$Q_l = 2\pi J_0(k) \delta_{l,0} + 2 \sum_{s=1}^{\infty} (-i)^s J_s(k) C_s \quad (3.12)$$

where

$$C_s = \int_{-\pi}^{\pi} \cos(l\theta) \cos(sR\theta) d\theta = \begin{cases} \frac{(-1)^l 2sR \sin(sR\pi)}{(sR)^2 - l^2}, & \text{for } sR \neq |l| \\ \pi, & \text{for } sR = |l|. \end{cases}$$

The relation $J_{-s}(k) = (-1)^s J_s(k)$ has been used in Eq.(3.12). Note that if R is an integer, Eq.(3.12) simplifies to

$$Q_l = 2\pi \sum_{s=0}^{\infty} (-i)^s J_s(k) \delta_{|l|,sR} \quad (3.13)$$

i.e., the integral becomes a single Bessel function.

The forms of Q_l allow us to assess the fall of the matrix elements of the unitary matrix U_{mn} . For integer R the matrix can be essentially banded as the matrix elements fall off exponentially after a certain cutoff. For $R = 1$, as is well known and also can be seen from above that for $l > k$ the matrix elements fall off exponentially, where l measures the distance from the diagonal. On the other hand when R is not an integer, apart from the Bessel function terms, there are terms that are falling only algebraically in l . For instance when $R = 1/2$ we have

$$Q_l = 2\pi(-1)^l J_{2l}(k) + (-1)^l 8 \sum_{s=1,3,5,\dots}^{\infty} \frac{(-i)^s s \sin(s\pi/2)}{s^2 - 4l^2} J_s(k). \quad (3.14)$$

The infinite series gets effectively cut-off for $s > k$. The finite sum has terms that only decay as l^{-2} . Fig. 3.1 shows that Q_l falls as l^{-2} even for other non-integer R values. Thus non-integer R values imply an important characteristic of the unitary quantum map: the algebraic fall of matrix elements, as opposed to the exponential fall characterizing integer R . In fact we may speculate whether non-KAM systems are *always* characterized by algebraic decaying matrix elements in the unperturbed basis. It is generally believed that localization properties of the eigenfunctions crucially depend on the way in which matrix elements fall.

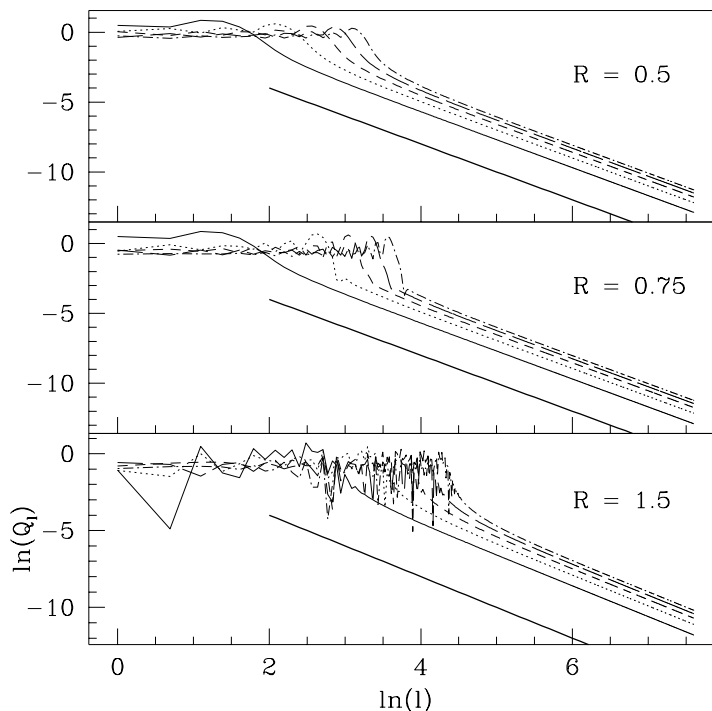


Figure 3.1: Shown are the behaviour of Q_l with $10 \leq k \leq 50$ for different non-integer values of R . The thick line l^{-2} is drawn to guide the eye.

The perturbing potential $\cos(2\pi x/\lambda)$ preserves the parity of H_0 , and hence U has the symmetry of parity. In addition, the system has a spatial translational symmetry when R is an integer. Let us define a transformation for integer R as

$$\mathcal{T}f(X) = f((X + 1/R) \bmod 1) \quad (3.15)$$

such that $\mathcal{T}^R f(X) = f(X)$. \mathcal{T} has the eigenvalues $\beta_l = \exp(i2\pi l/R)$ where $l = 0, 1, 2, \dots, (R-1)$. The commutation relation $[U, \mathcal{T}] = 0$ leading to $\mathcal{T}|\psi\rangle = \beta_l|\psi\rangle$. For $R = 2$, $\beta_l = \pm 1$; in this case we consider only the states that correspond to $\beta_l = 1$. It is to be noted that the dimensionless quantum parameters k and τ are related to the classical parameters through the relation

$$\frac{K}{R} = 8k\tau. \quad (3.16)$$

The semiclassical limit is $k \rightarrow \infty$ and $\tau \rightarrow 0$, such that $k\tau$ is fixed. Any arbitrary state of the system at a given time in the unperturbed basis is $|\Psi(t)\rangle = \sum_n \Psi_n(t)|n\rangle$ and its time evolution is given as $\Psi_m(t+T) = \sum_n U_{mn}\Psi_n(t)$. It is to be noted that for a given k the infinite series in Eq. (3.12) can be approximated to a finite series up to say $s = s'$ such that $s' > k$ where the

Bessel function $J_s(k)$ decays exponentially. Since the quantum dynamics is implemented with finite number, N , of basis states, we need to ensure that this artificial truncation does not affect the calculations. The limit

$$\lim_{n \rightarrow \infty} \sum_{n=1}^N |\Psi_n(t)|^2 \rightarrow 1 \quad (3.17)$$

has been used for this purpose.

3.3 Special case: kicked rotor

It was shown in the previous Chapter that standard map of the kicked rotor is the special case ($R = 1$) of the well system. It is natural to expect such connection in the quantum systems also. In fact, in this section we show that when $R = 1$ the quantum well system is nothing but the quantum kicked rotor. For that let us consider the Hamiltonian of the kicked rotor moving in a circle of radius r as

$$\bar{H} = \frac{p_\theta^2}{2r^2} + \epsilon \cos(\theta) \delta_T \quad (3.18)$$

where p_θ, θ are the angular momentum and angle of the rotor. Here δ_T stands for the train of periodic delta function with period T . The kick to kick quantum propagator in angular momentum basis $\langle \theta | n \rangle = e^{in\theta} / \sqrt{2\pi}$ is given by

$$\bar{U}_{mn} = \langle m | \bar{U} | n \rangle = (-i)^{m-n} J_{m-n}(k) e^{-in^2 \bar{\tau}/2} \quad (3.19)$$

where $k = \epsilon T / \hbar$ and $\bar{\tau} = \hbar T / r^2$ with $m, n = 0, \pm 1, \pm 2 \dots$. Since \bar{H} preserves parity symmetry, the quasienergy states are either even or odd i.e., $\langle \theta | \bar{\psi}_j \rangle = \pm \langle -\theta | \bar{\psi}_j \rangle$ or $\langle n | \bar{\psi}_j \rangle = \pm \langle -n | \bar{\psi}_j \rangle$. Then the eigensystem of the propagator

$$\sum_{n=-\infty}^{\infty} \bar{U}_{mn} \langle n | \bar{\psi}_j \rangle = e^{-i\bar{\alpha}_j} \langle m | \bar{\psi}_j \rangle \quad (3.20)$$

is reduced to

$$\sum_{n=0}^{\infty} \tilde{U}_{mn} \langle n | \bar{\psi}_j \rangle = e^{-i\bar{\alpha}_j} \langle m | \bar{\psi}_j \rangle \quad ; \quad \tilde{U}_{mn} = \bar{U}_{mn} - \bar{U}_{m,-n} \quad (3.21)$$

by considering only the odd states. Notice that the above equation remains the same if we replace m by $-m$ since $\bar{U}_{mn} = \bar{U}_{-m,-n}$. Thus it is sufficient to consider only m with positive integers. Invoking the integral form of the Bessel function through the relation [85]

$$(-i)^n J_n(k) = \frac{1}{\pi} \int_0^\pi e^{-ik \cos \theta} \cos(n\theta) d\theta$$

the parity reduced propagator matrix is

$$\tilde{U}_{mn} = \frac{2}{\pi} e^{-in^2\bar{\tau}/2} \int_0^\pi \sin(m\theta) \sin(n\theta) e^{-ik \cos \theta} d\theta \quad (3.22)$$

where $m, n = 1, 2, \dots$

On the other hand, the well system also has the parity symmetry. Considering only the odd states of the well system, the quantum propagator is

$$U_{mn} = \frac{1}{a} e^{-in^2\tau} \int_{-a}^a \sin\left(\frac{m\pi x}{2a}\right) \sin\left(\frac{n\pi x}{2a}\right) e^{-ik \cos(2\pi x/\lambda)} dx \quad (3.23)$$

where $m = 2l, n = 2l'$ with $l, l' = 1, 2, \dots$. With the substitution $\theta = \pi x/a$ and setting $R = 1$, the above matrix element becomes

$$U_{ll'} = \frac{2}{\pi} e^{-i4l^2\tau} \int_0^\pi \sin(l\theta) \sin(l'\theta) e^{-ik \cos \theta} d\theta. \quad (3.24)$$

Now the matrix elements \tilde{U}_{mn} and $U_{ll'}$ are identical provided $\bar{\tau} = 8\tau$ or $\pi r = a$. Combining this condition with $R = 1$ ($2a = \lambda$) we have $2\pi r = \lambda$. That is, the intrinsic assumption made in the kicked rotor system is that the wavelength of the impulsive field is equal to the perimeter of the circle on which the rotor moves. In other words, *kicked rotor has a single length scale*. Since the parity symmetry reduced U -matrix of the rotor is identical to that of the well system for $R = 1$, in this case odd states of the rotor correspond to the odd states of well system, while the even states have a similar relationship. Thus all that is known for the quantum kicked rotor, including exponential localization of eigenstates, may be carried over to the well system with $R = 1$. This allows us to address interesting questions of deviations from the kicked rotor in a single model arising from the two competing length scales.

3.4 Quantum resonance

Here we investigate whether the parameter R has any effect on the important phenomenon of “quantum resonance”. We notice that the unperturbed motion of the particle, given by the Hamiltonian H_0 , between the kicks simply adds phase to the wave function components (when expressed in the unperturbed basis, as in Eq. (3.8)). At full resonance ($\tau = 2\pi$), the unperturbed motion between the kicks is absent. In this case, without loss of generality, the time evolution of an arbitrary state of the system is

$$|\Psi(t)\rangle = e^{-ik \cos(2\pi x/\lambda)t} |\Psi(0)\rangle \quad (3.25)$$

and thus $|\Psi(t)|^2 = |\Psi(0)|^2$. Note that here t is the number of kicks. In the position representation the above equation is written as

$$\Psi(x, t) = e^{-ik \cos(2\pi x/\lambda)t} \Psi(x, 0) \quad (3.26)$$

and then the kinetic energy of the particle after t kicks is

$$\begin{aligned} E(t) &= \langle \Psi(t) | \hat{p}^2 | \Psi(t) \rangle \\ &= \frac{-\hbar^2}{2M} \int_{-a}^a \Psi^*(x, t) \frac{\partial^2}{\partial x^2} \Psi(x, t) dx. \end{aligned} \quad (3.27)$$

Using the relation

$$i \left(f^* \frac{\partial f}{\partial x} - f \frac{\partial f^*}{\partial x} \right) = 2 \operatorname{Re} \left(i f^* \frac{\partial f}{\partial x} \right)$$

where $\operatorname{Re}(\dots)$ is the real part of the argument, and the boundary condition $\Psi(a, t) = 0$, the kinetic energy becomes

$$\begin{aligned} E(t) = E(0) &+ \frac{-\hbar^2}{2M} \left\{ \left(\frac{4\pi kt}{\lambda} \right) \int_{-a}^a \sin \left(\frac{2\pi x}{\lambda} \right) \operatorname{Re} \left\{ i \Psi^*(x, 0) \frac{\partial \Psi(x, 0)}{\partial x} \right\} dx \right. \\ &\left. - \left(\frac{2\pi kt}{\lambda} \right)^2 \int_{-a}^a |\Psi(x, 0)|^2 \sin^2 \left(\frac{2\pi x}{\lambda} \right) dx \right\}. \end{aligned} \quad (3.28)$$

In the limit $t \rightarrow \infty$ the energy grows quadratically with the number of kicks. If $|\Psi(0)\rangle = |n\rangle$, i.e., the initial state is one of the unperturbed states itself, then $\operatorname{Re}(\dots) = 0$ and hence the energy is purely quadratic. In this case the energy can be found exactly as

$$E(t) = E(0) \left\{ 1 + \left(\frac{ktR}{n} \right)^2 (2 - A) \right\} \quad (3.29)$$

where

$$A = \begin{cases} \frac{\sin(2\pi R)}{\pi R} \left(\frac{n^2}{n^2 - 4R^2} \right) & \text{if } n \neq 2R \\ (-1)^{n+1} & \text{if } n = 2R. \end{cases}$$

Since $A \neq 2$, we observe that the quadratic energy growth is unaffected by the length scale ratio R . Numerically we have found that this behaviour is also seen when τ is rational multiples of 2π . Thus the quantum resonance phenomena of the well system is very similar to that of the kicked rotor [86]. In the resonance condition, i.e., τ is rational multiples of 2π , the quasienergy states are extended in the Hilbert space and they are unnormalized. They are very similar to Block waves of electronic eigenstates in crystal lattice. Thus the diffusion in energy at the resonance can be compared with the electronic transport due to the extended Block waves in

the lattice problem. Recent experiments on atoms in presence of pulsed standing light wave, the atom-optics realization of delta-kicked rotor, have achieved enhancement in momentum diffusion of the atoms under resonance condition [87].

It is to be noted that resonance is a non-generic pure quantum phenomena and no correspondence to it can be seen in the classical system. In the context of a particle in a well, quantum diffusion at the resonance may provide a mechanism to enhance ionization from sufficiently deep finite well systems.

3.5 Results

Having given a sufficient description of the system under investigation, here we analyze the quasienergy states and quasienergies of the generic quantum system (τ is an irrational multiples of 2π) in the relevant classical regimes. On taking a truncated N -dimensional Hilbert space spanned by the first N unperturbed basis states that belong to odd parity, diagonalization of the matrix U_{mn} gives the eigenstates of odd states $\{|\psi\rangle\}$. In the unperturbed basis they can be represented as $|\psi\rangle = \sum_n \psi_n |n\rangle$. Eigenvalues and eigenstates are obtained from numerical diagonalization of the U -matrix. In what follows we consider only states that are “converged” in the sense that they are independent of the truncation size N . Thus the states we are interested in belong to the infinite Hilbert space; they are states of the infinite cylinder and *not* of a truncated cylinder, or torus. The last distinction becomes important as quantum states that belong to the cylinder can have completely different localization features from those that belong to a truncated cylinder.

3.5.1 Localization and length scales

We have shown in the previous Chapter that the dynamical features of the classical system is very much sensitive to the parameter R . In particular, for small classical field strength K (≤ 1) the kick to kick dynamics can be chaotic and as a consequence there is a possibility of classical transport when R is non-integer. The natural and important question to be answered is that how the localization of the generic quantum states is influenced by R in different classical regimes. Localization can be measured using a unified quantity, the Renyi participation ratio ξ_q [88]

$$\xi_q = \left(\sum_n |\psi_n|^{2q} \right)^{1/(q-1)} \quad (3.30)$$

of which the entropy and participation ratio (PR) are special cases. In our analysis we first use a normalized information entropy as a measure of the localization of states, and this is defined as

$$S = \frac{-1}{\ln(N/2)} \sum_{n=1}^N |\psi_n|^2 \ln |\psi_n|^2. \quad (3.31)$$

It is easy to see that $S = \ln \xi_1 / \ln(N/2)$. This measure compares the entropy of the eigenfunctions to that of $N \times N$ matrices belonging to Gaussian orthogonal ensemble (GOE) of random matrix theory (RMT) which is approximately $\ln(N/2)$. The GOE is relevant to time reversal symmetric systems such as the one we are considering.

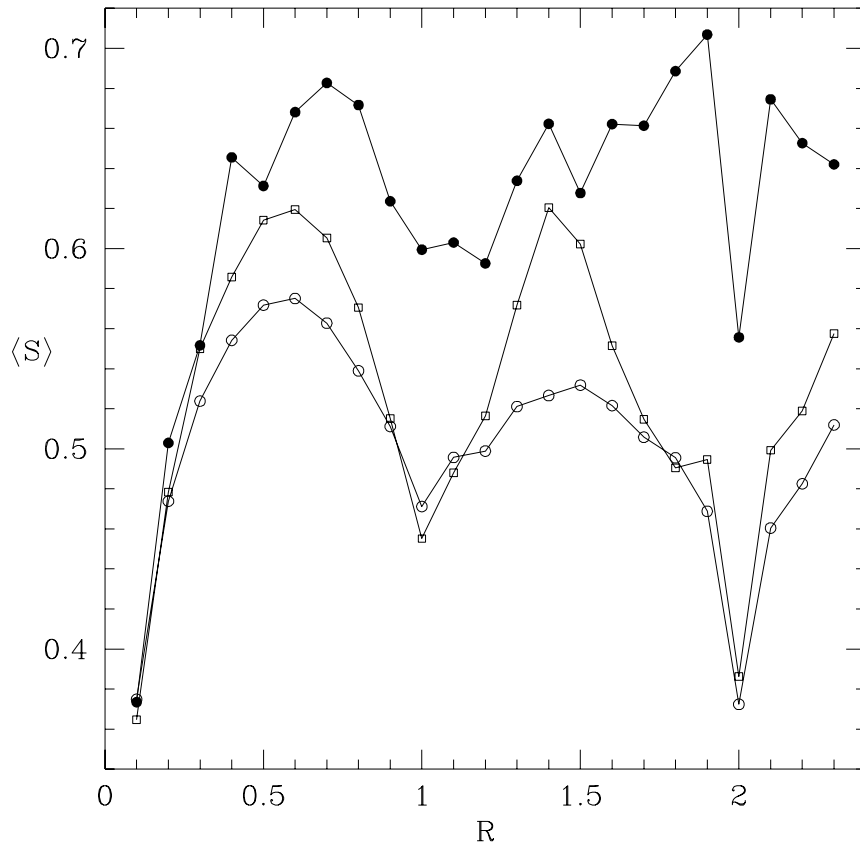


Figure 3.2: Average entropy of 1000 eigenstates for: $K = 0.1, \tau = 0.001$ (\circ); $K = 1, \tau = 0.01$ (\square); $K = 10, \tau = 0.1$ (\bullet). $N = 1200$ in all the cases.

First we calculate a gross measure of localization in a given spectrum by averaging over all converged states. We set criteria for the states to be converged so that the states belong to the cylinder, or are at least very close to states that belong to the cylinder. In all the following cases, the eigenvalues are converged in modulus to unity to within 0.0001 or better. Fig. 3.2 shows the average entropy as a function of R . For small K (≤ 1), the oscillations are qualitatively similar with distinct entropy minima at integer R and maxima at around half-integer R . This

may provide a simple mechanism for experimental control of the extent of localization. The information entropy is, of course, basis dependent; the unperturbed basis we use is a useful one as it has information about localization in the momentum.

The minima in entropy are expected to have strong associations with the presence of stable regions in the classical phase space. Of special significance are KAM tori in phase space, as these structures are complete barriers to classical diffusion in momentum. In spite of the fact that in the classical system all the KAM tori break up in the standard map ($R = 1$) at $K = 1$, we observe a minimum entropy. This is due to the presence of cantori which are partial barriers for chaotic orbits and suppress global diffusion. Maximum entropy around half-integer R is the classical parametric regime where the discontinuity is maximum, corresponding to maximum chaos assisted diffusion.

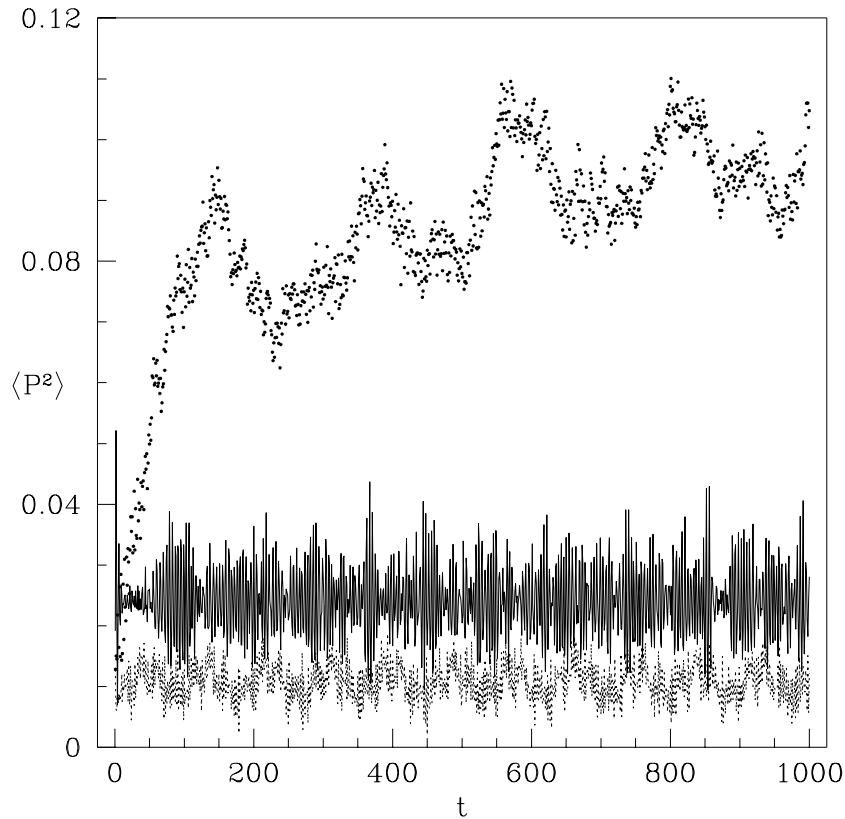


Figure 3.3: Shown is the scaled kinetic energy $\langle P^2 \rangle$ of a state, which is initially the ground state of the unperturbed system, as a function of time. Here the parameters are $K = 1, \tau = 0.01$; $R = 1$ (solid line), $R = 1.5$ (dots) and $R = 2$ (dotted line). The effect of non-integer R is clearly seen in the evolution as the kinetic energy of the quantum particle saturates at a much higher value compared to the integer R cases.

The time evolution of non-stationary states must reflect the properties of the stationary states and is also of importance in the context of experiments. Here we have studied the diffusion in kinetic energy of a state $|\Psi\rangle$ that is initially the ground state of the unperturbed system. We illustrate with one example that for a fixed classical parameter K the effects of non-integer R are seen clearly for a given τ value. Thus tuning R essentially tunes λ since a is fixed through the relation (3.9). In Fig. 3.3 scaled kinetic energy $\langle P^2 \rangle = \langle \Psi(t) | \hat{P}^2 | \Psi(t) \rangle$ is shown as a function of time (number of kicks) for a small value of K corresponding to a small classical field strength ϵ . We note that while the quantum diffusion saturates at a much higher value for $R = 1.5$, than that compared to $R = 1$, the actual classical field strength ϵ (from Eq. (2.4)) is *smaller* by a factor of 1.5. For comparison we show another integer case, $R = 2$, where the classical diffusion is smaller than for $R = 1$.

3.5.2 Localization and classical diffusion

In Fig. 3.2 oscillations in entropy are still present for large K ($= 10$), while there is apparently complete chaos for all relevant R values. We can understand these oscillations as due to the strong correlation between the localization of eigenstates and classical diffusion coefficient. Since K and τ are fixed in our numerical experiments, from the relation (3.16) we see that for $R < 1/2$ the semiclassical parameter k is large. For large k the effective field strength of the quantum particle is large. However, there is increased localization of states as R decreases from $1/2$. This is the quantum reflection of the limited classical diffusion. In this case the diffusion is highly limited presumably due to the presence of cantori. For the kicked rotor the exponential localization length was found to be proportional to the classical diffusion coefficient [52]. This was found by numerical experiments and is supported by certain qualitative arguments. We are now in a position to examine the relationship between quantum localization and classical diffusion in the context of the particle in a well, wherein we have the freedom of another control parameter, namely R , with which to vary the classical diffusion.

Instead of studying localization lengths we study here the measures of localization such as the entropy or the PR. We study the PR more closely rather than the entropy. In chaotic regimes we have numerically ascertained that exponential of the entropy is proportional to the PR, as shown in Fig. 3.4. The relationship between the localization length hitherto calculated for the kicked rotor and the PR calculations we present will need more detailed study, but we expect them to be roughly proportional to each other. In fact, if we assume a fully exponentially localized state with $|\psi_n| \sim \exp(-|n - n_0|/l_\infty)$, then the PR is

$$\xi_2^{-1} = \left(\sum_n |\psi_n|^4 \right)^{-1} = 2l_\infty. \quad (3.32)$$

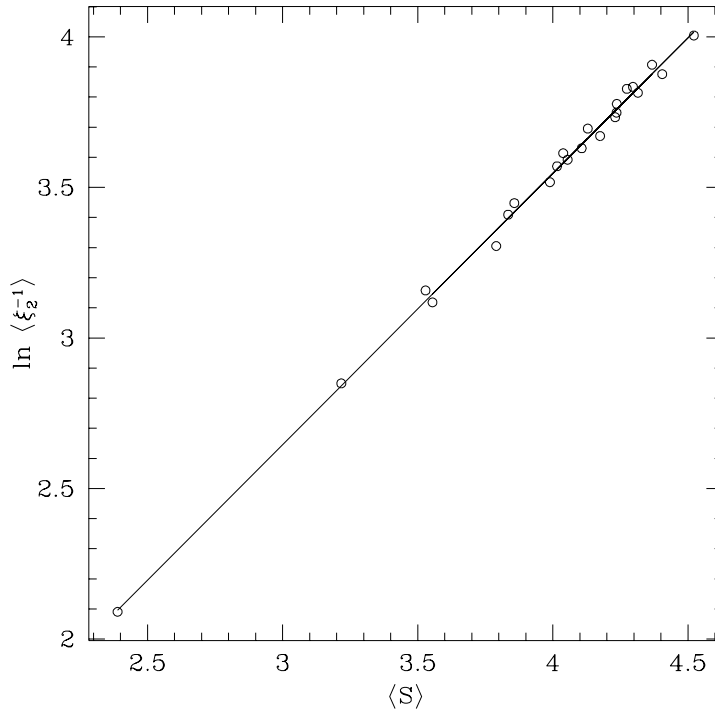


Figure 3.4: Average entropy and the log of the average PR corresponding to the case $K = 10, \tau = 0.1$ of Fig. 3.2. The slope of the fitted straight line is 0.9 ± 0.01 .

We recapitulate the argument connecting classical diffusion and the localization length for the specific system we are considering, as there are difference in factors. Considering time evolution of an initial state, kinetic energy diffuses for a certain time t_c and then attains quasiperiodic saturation. In other words, the number of unperturbed states that are excited during the evolution increases initially and attains a saturation n_c . This implies that n_c is related to the critical time t_c by the diffusion equation

$$\pi^2 \hbar^2 n_c^2 = D_{\text{CL}} t_c \quad ; \quad \langle (p_t - p_0)^2 \rangle = D_{\text{CL}} t \quad (3.33)$$

where D_{CL} is the classical diffusion coefficient in momentum and $\langle \dots \rangle$ represents the ensemble average. Here the momenta and the diffusion coefficient have dimensions and we have taken $a = 1/2$. Since the critical time is the Heisenberg time relevant for n_c equally spaced eigenstates (or quasienergies) such that

$$\Delta E = \Delta \alpha \frac{\hbar}{T} = \left(\frac{2\pi}{n_c} \right) \frac{\hbar}{T} \quad (3.34)$$

then

$$t_c \sim \frac{\hbar}{\Delta E} \sim \frac{n_c T}{2\pi}. \quad (3.35)$$

With the dimensionless diffusion coefficient $D = D_{\text{CL}}/T^3$, if the average localization length $\langle l_\infty \rangle$ is also n_c , we obtain the relation:

$$\langle \xi_2^{-1} \rangle = 2\langle l_\infty \rangle = \frac{\beta\pi}{4\tau^2} D(K, R) \quad (3.36)$$

where τ is the dimensionless effective Planck constant defined in Eq. (3.9) and β is a constant whose value has been numerically determined as $1/2$ for the standard map [89]. The diffusion coefficient $D(K, R)$ may be obtained using the dimensionless maps Eq. (2.5) or Eq. (2.10). Here the dependence of D on *both* K and R is emphasized.

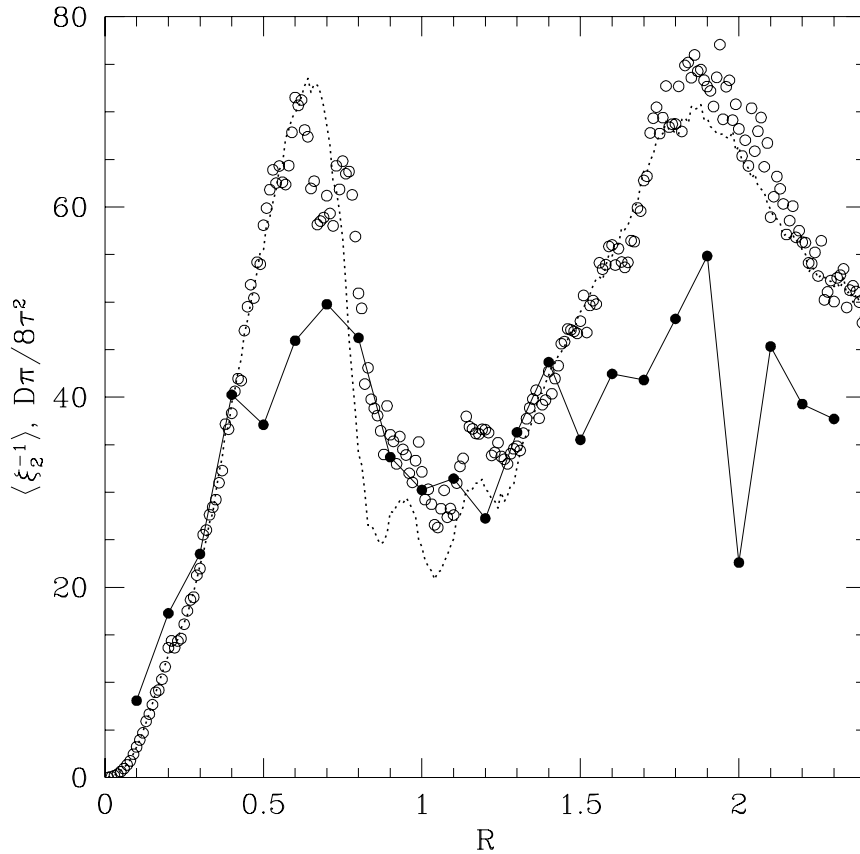


Figure 3.5: The average PR (\bullet) and the scaled classical diffusion coefficient (\circ) are plotted as a function of R for the case $K = 10, \tau = 0.1$. The dotted line is the scaled coefficient calculated using up to the second order time correlation. Higher order time correlations are insignificant since the classical system is highly chaotic.

In Fig. 3.5 we show the average PR and the scaled diffusion coefficient according to the relation Eq. (3.36). We see that the relation derived above holds in some parameter regions while it picks up only qualitative features of the oscillations in others. In particular, the relation seems to hold for $R < 1/2$ when the classical system is hyperbolic as well as around $R = 1$. It is worth reiterating that the above relation assumes that the quasienergy states are exponentially localized. The deviations from the relation (3.36) might be due to fluctuations of the state components in the unperturbed basis (one such case is shown below in Fig. 3.9). These fluctuations may lead to different scaling behaviour between the average PR and the classical diffusion coefficient. More over where there are deviations we notice that the PR is mostly lower than that expected from the diffusion coefficient relationship derived above. Larger the classical diffusion larger is the average PR and consequently the number of states that are averaged over can have significantly lower PR than the average. This happens because on the average energetically lower states below the critical energy determined by the spectrum averaged PR have low PRs. Thus not averaging over sufficient number of states can also lead to different scaling laws. The sharp deviation for $R = 2$ can be accounted for as due to the presence of an extra quantum symmetry discussed above.

3.5.3 Measure of quantum chaos

Following our study on average PR and its scaling with the classical diffusion coefficient, we may then enquire about how the PR itself is distributed in a given spectrum if the average reflects the general behaviour. We find that when the classical system is chaotic, the distribution of the normalized quantity $y = \ln \xi_2^{-1} / \langle \ln \xi_2^{-1} \rangle$ (this is similar to the distribution of the entropy due to the linear relationship exhibited above) is nearly normal as seen in Fig. 3.6. This may be attributed to a realization of the Central Limit Theorem. However the PRs and Inverse Participation Ratios (IPRs) themselves are not normal. Their distributions may be got by assuming that the distribution of y is normal. Thus the PRs are distributed according to the lognormal distribution [90]:

$$\Lambda(\xi_2^{-1}) = \frac{1}{\sqrt{2\pi} \sigma \langle \ln \xi_2^{-1} \rangle \xi_2^{-1}} \exp \left\{ -\frac{1}{2\sigma^2} \left(\frac{\ln \xi_2^{-1}}{\langle \ln \xi_2^{-1} \rangle} - 1 \right)^2 \right\} \quad (3.37)$$

where σ^2 is the variance of y . As an immediate consequence, distribution of IPRs is also lognormal. Distribution of such localization measures is of great significance. Recently the distribution of IPRs has been exploited to show that the distribution of resonance widths in wave-chaotic dielectric cavities is lognormal [91].

When K is small (≤ 1), the classical motion is nearly regular for $R = 1$, while chaotic for $R \leq 0.5$. However the time scales for classical diffusion is large making the observation of

R effects on quantum dynamics hard to discern. For instance, the nearest neighbour spacing distribution may remain very close to the Poisson distribution. In such a situation we find that the distribution of the PRs provides a useful measure. In Fig. 3.7 such an example is shown, wherein even for small field strengths the effect of R is clearly visible as a tendency for y to be normally distributed. This is an indication of the “delocalization” that is taking place in the eigenfunctions. This delocalization is limited in the sense that while the eigenfunctions remain square integrable there is more spreading out in the bulk part of the states. Thus we may conclude that the distribution of the localization measures is a sensitive quantity in chaotic quantum systems.

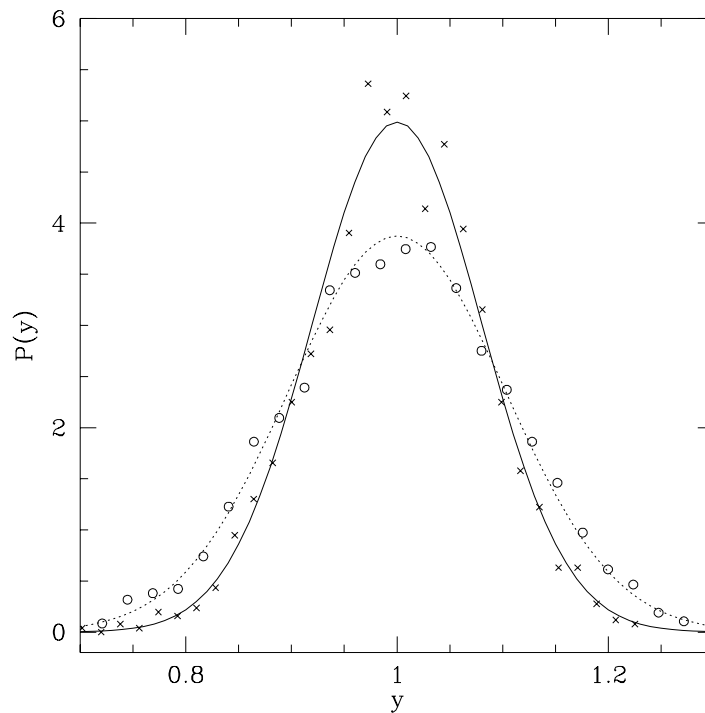


Figure 3.6: Probability distribution of y , the normalized log of the PR, for the kicked rotor case ($R = 1$) in the chaotic regime. Here we have taken $K = 10$ and $\tau = 0.025$ (\times), $\tau = 0.05$ (\circ). Smooth curves are corresponding Gaussian distributions.

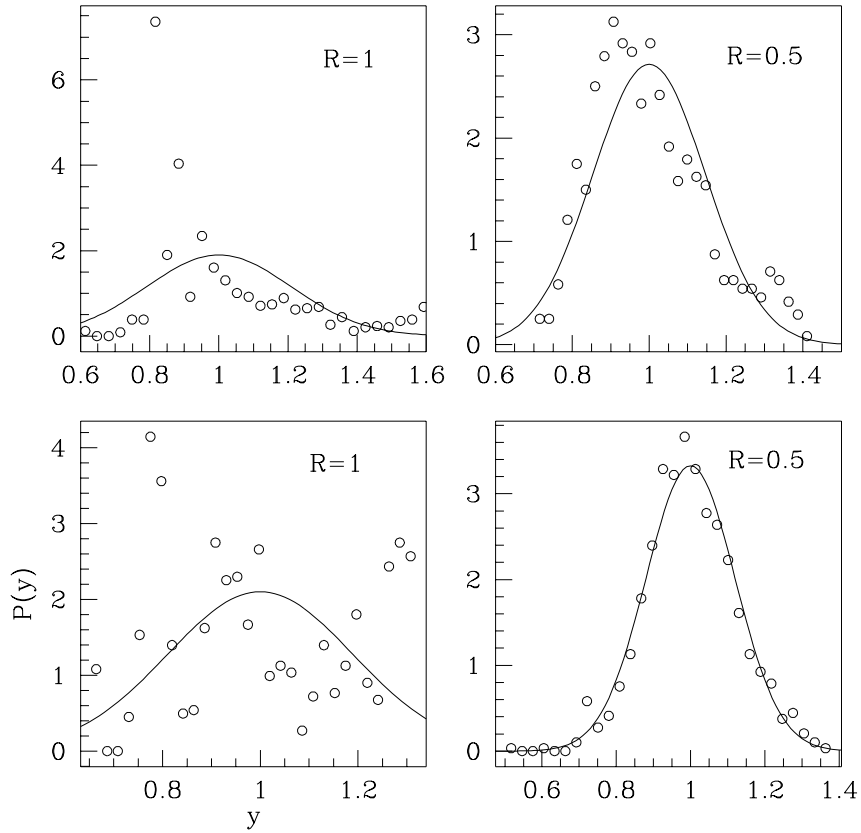


Figure 3.7: *Probability distribution of y , the normalized log of the PR, for the case $K = 0.1, \tau = 0.001$ (first row) and for $K = 1, \tau = 0.01$ (second row). Smooth curves are corresponding Gaussian distributions. Note the sensitivity of these distributions to the classical dynamics.*

3.5.4 Eigenvalues and eigenstates

It is clear from our earlier observations that the states are more localized in the regular or mixed regimes of the classical system while less localized (or delocalized) in the chaotic regimes. The degree of localization is also controlled by the ratio of the length scales and complexity of the classical phase space is reflected in the localization measures. Here we look at the quasienergies and the corresponding states more closely.

In Fig. 3.8 we have shown the nearest neighbour spacing distribution of the quasienergies for various parameters. The first row and the last column of the catalogue correspond to classically chaotic regimes and the rest belong to regular/mixed phase space regimes. In regular/mixed regimes where the states are highly localized, the spacing shows excellent agreement with the Poisson distribution. On the other hand, in chaotic regimes the spacing agrees well with the

Poisson distribution except at small spacings. This is due to the fact that the bulk part of the eigenstates is delocalized and they overlap each other. However, the tail part of the states are exponentially localized and the degree of overlap is not significant enough. We also notice that the spacing distribution is only slightly sensitive to the nature of the classical dynamics in the case of the unbounded kicked rotor or the well, at least in the parameter regimes we have investigated. In such situations, as we have demonstrated earlier, the distribution of PRs is a good measure to distinguish the chaotic quantum systems from the regular systems.

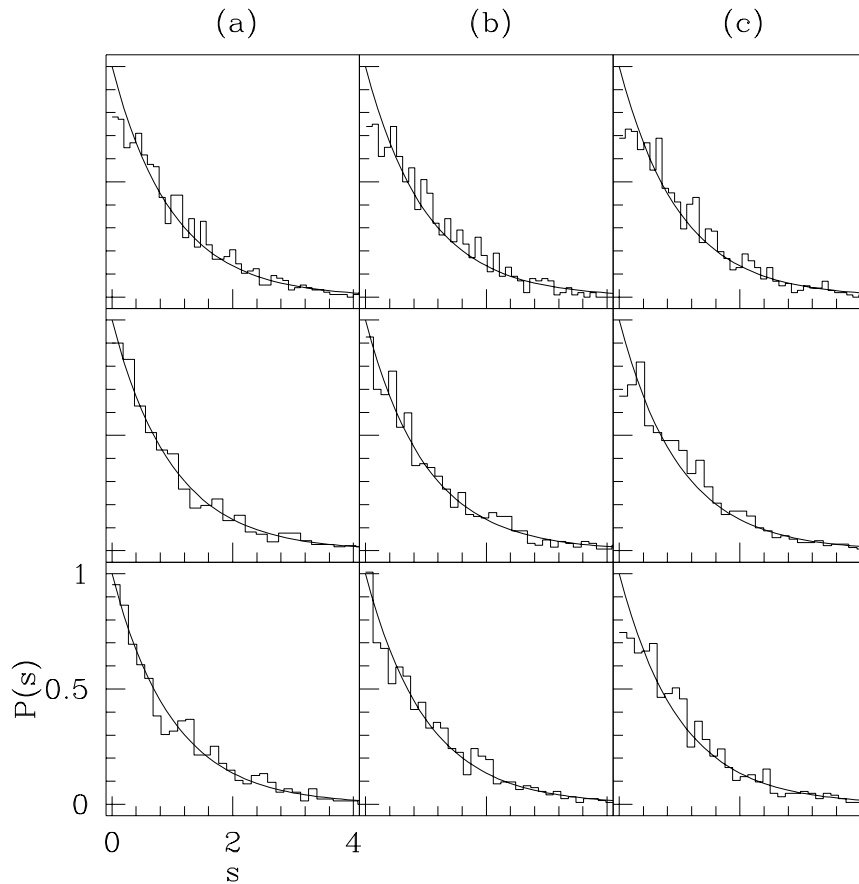


Figure 3.8: *Nearest neighbour spacing distributions of 1000 quasienergies for (a) $K = 0.1, \tau = 0.001$; (b) $K = 1, \tau = 0.01$; (c) $K = 10, \tau = 0.1$ with $R = 0.5, 1, 1.5$ (top to bottom) and $N = 1200$. Smooth curves are Poisson distributions. Note the relative insensitivity of these distributions to the classical dynamics.*

Our extensive calculations of the eigenstates in chaotic regimes show that, in general, it is hard to qualitatively differentiate the states corresponding to non-integer R values from the rotor ($R = 1$) states as far as their localization behaviour is concerned. In particular, it is not easy to distinguish the emergence of non-exponential tails unequivocally. In spite of the fact that the

quantity Q_l falls polynomially, our observations have not revealed any polynomial fall in the eigenfunction components. However, we found that eigenstates corresponding to non-integer R values generally have more fluctuations compared to the rotor states; this is illustrated with some examples in Fig. 3.9. The fluctuations are closer to the RMT predictions in the case of non-integer R values and is shown further below. Although an earlier study [92] shows that the states of one discontinuous version of the standard map are algebraically localized we have not seen any such behaviour throughout our study.

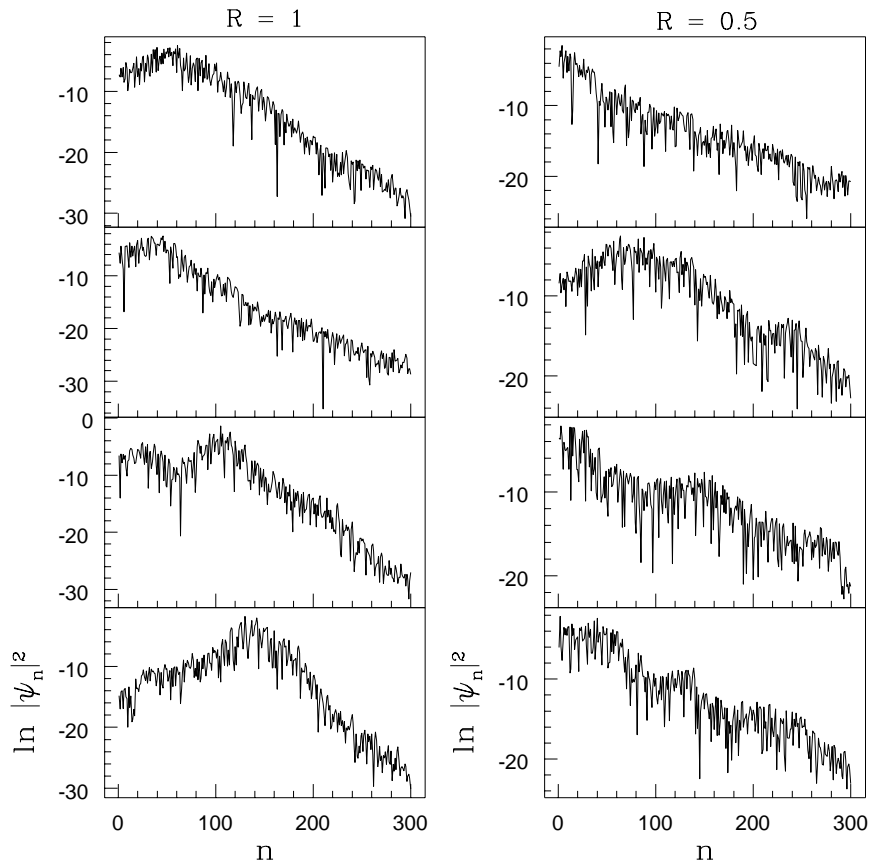


Figure 3.9: *Typical eigenstates for the case $K = 10, \tau = 0.1$. States corresponding to $R = 0.5$ have more fluctuations compared to the rotor ($R = 1$) states.*

Recently there have been studies of the special case ($R = 1/2$) of the system (2.1), with the motivation of revealing quantal behaviour of non-KAM systems [63]. It was observed that the quasienergy states are “extended” in the unperturbed basis and as a result the spacing was shown to be Wigner distributed. At this juncture we would like to compare our results with certain aspects of this work. In [63], the eigenstate shown in the highly chaotic regime ($K = 50, N = 1024$; we have been unable to ascertain the value of τ used in this work) does

not appear to belong to the unbounded phase space as it spreads all over the basis. Thus while states such as these may belong to some truncated dynamical system, they do not belong to the infinite Hilbert space of the well system. Increasing the dimensionality of the matrix used will modify such states; in short, they are not converged. As we demonstrate below, unconverged or poorly converged states may mislead us in understanding the spectrum.

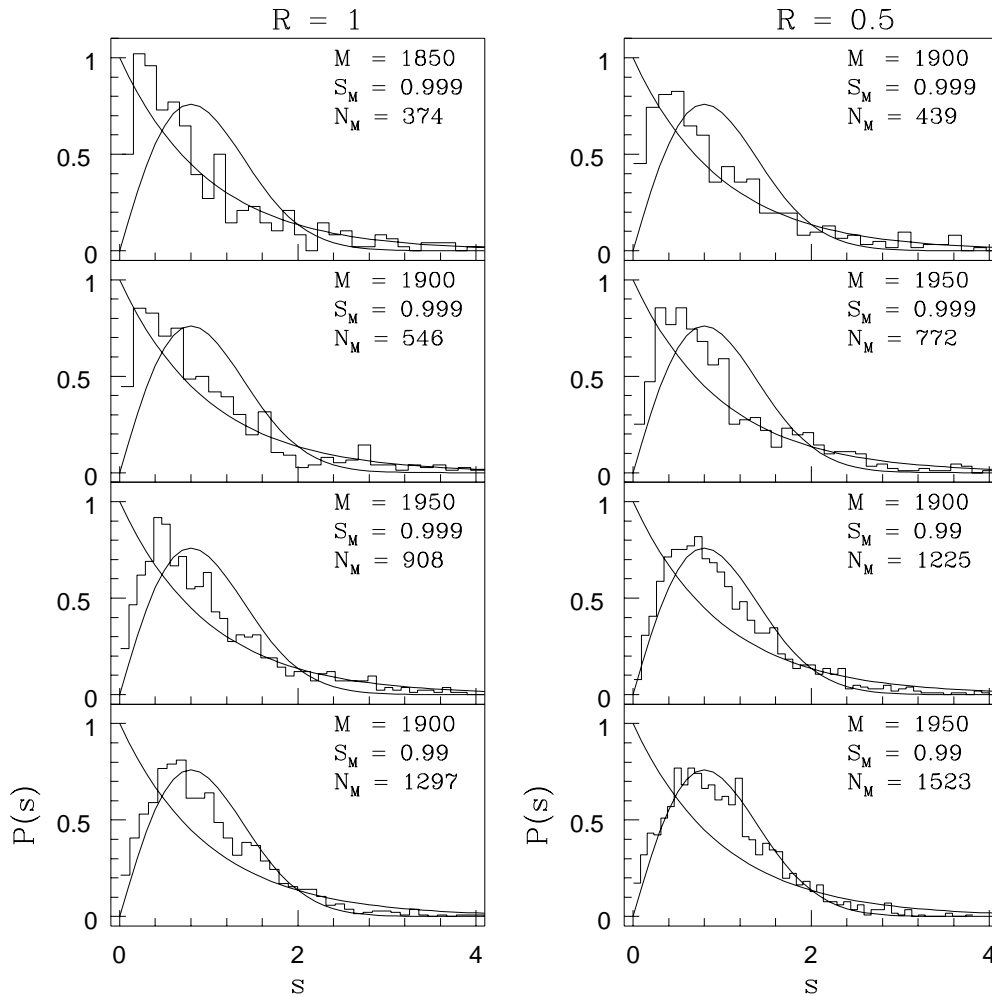


Figure 3.10: The nearest neighbour spacing distributions for the case $K = 50, \tau = 0.1$. Smooth curves are the Poisson and Wigner distributions. The convergence criterion is relaxed as we move from top to bottom. A “spectral transition” is observed.

Large K implies large k for given R and τ , and hence our calculation demands bigger dimensionality N of the truncated Hilbert space, since the PR is roughly increasing as k^2 . Although we take $N = 2000$, getting a good number of converged states is problematic. However, we pursue the spacing distribution with a different convergence criterion for the numerically

obtained states. The convergence criterion uses the partial sum of the state components:

$$\{\text{Sum}\}_M = \sum_{n=1}^M |\psi_n|^2 ; \quad M < N. \quad (3.38)$$

For a well converged state we expect that $\{\text{Sum}\}_M \approx 1$, even for $M \ll N$. We denote by N_M the number of converged eigenstates whose $\{\text{Sum}\}_M$ is greater than S_M (an arbitrary number close to, but less than, unity) for a fixed value of M . Thus the convergence criteria is characterized by M and S_M .

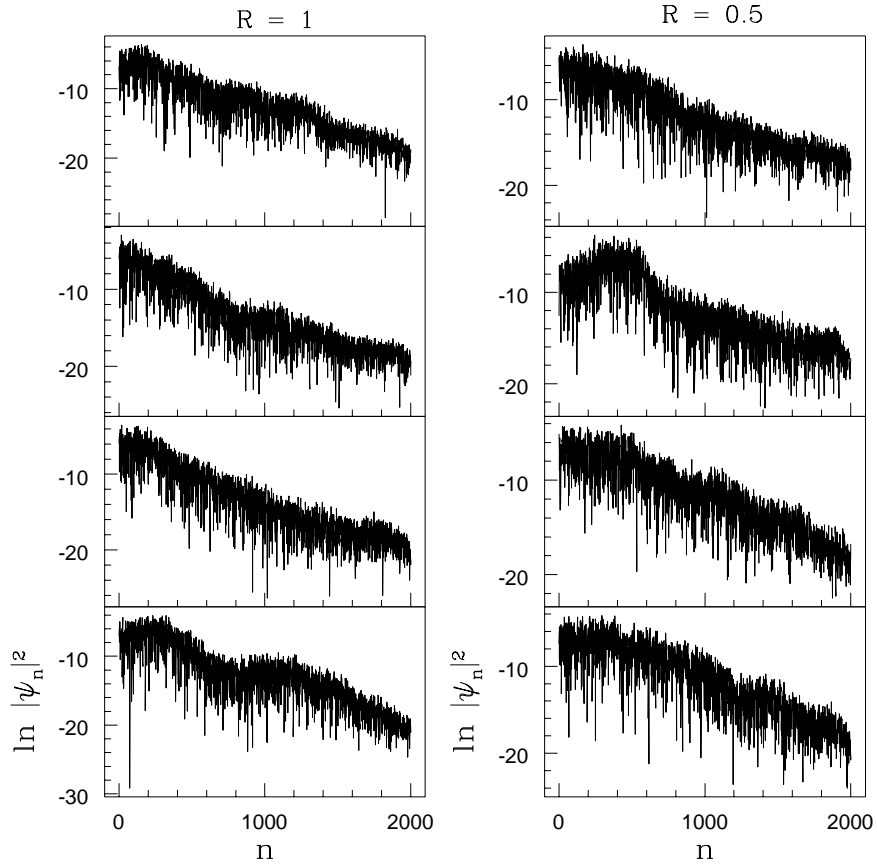


Figure 3.11: Typical well converged eigenstates for the highly chaotic case: $K = 50, \tau = 0.1$ and $N = 2000$.

In Fig. 3.10, we show the spacing distributions with different criterion for two cases. In both the cases transition to Wigner distribution is evident as the convergence criterion is relaxed. The unconverged or poorly converged states do not belong to the physical system of our interest and the corresponding quasienergies follow the RMT prediction. Obviously, reliability of the result is more in the top plots where the spacing shows neither Poisson nor Wigner distributions.

Though the tail part shows the Poisson behaviour there are significant discrepancies in the small spacing. A more correct picture may be closer to the scenario of the chaotic regimes presented in Fig. 3.8.

Shown in Fig. 3.11 are a few “well converged” states, with a more stringent convergence criterion ($M = 1600, S_M = 0.9999$). With this criteria we have only $N_M = 12$ and 4 for $R = 1$ and $1/2$ respectively. The state components exhibit strong fluctuations in the basis. Here again it is hard to differentiate the two cases qualitatively. The states corresponding to $R = 1/2$ also appear to have exponential tails. To see the distribution of the state components, we introduce a variable $\eta_n = |\psi_n|^2 / \overline{|\psi_n|^2}$ where the over bar stands for the average over the state components such that $\overline{\eta} = 1$. As seen from Fig. 3.12, the cumulative distributions of η for both the cases have very similar behaviour. Considerable deviations from the RMT predicted cumulative Porter-Thomas distribution, $I(\eta) = \text{erf}(\sqrt{\eta/2})$, may be attributed to the localization of the states. However, the distribution corresponds to $R = 1/2$ tends to be closer to the RMT predicted behaviour.

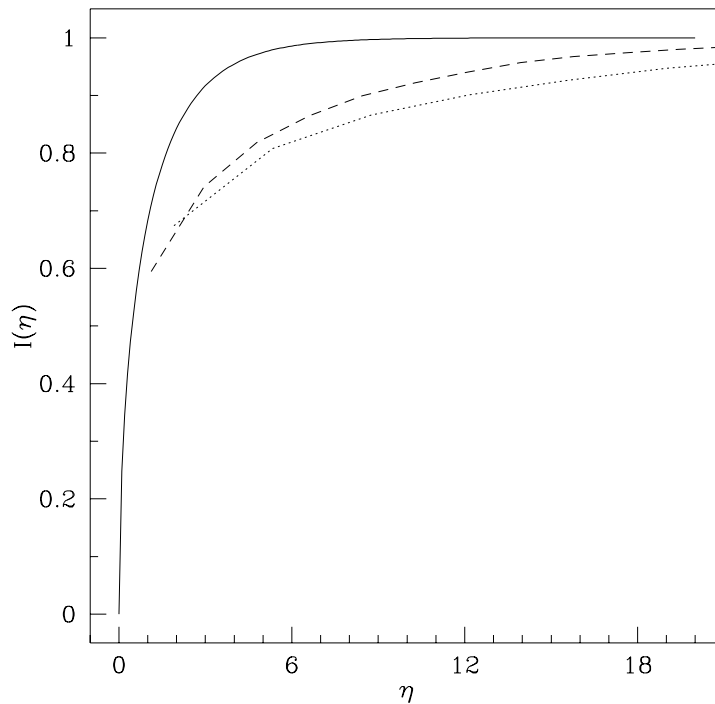


Figure 3.12: *Collective cumulative distribution of the components of the states shown in Fig. 3.11. Dotted curve corresponds to $R = 1$ while dashed curve corresponds to $R = 0.5$. Solid curve is the cumulative Porter-Thomas distribution.*

3.6 Summary

This Chapter dealt with the quantum mechanical features of a particle inside the infinite square well in presence of time periodic impulsive field. Our study was motivated to reveal the role of competing length scales of the system *viz.* well width and wavelength of the field. If their ratio $R = 1$ this system, like the classical version, is the quantum delta kicked rotor. Thus the kicked particle in the well can be thought of as one generalization of the kicked rotor.

In the previous Chapter we showed that when the length scales do not match, even in perturbative regimes the dynamics can be increasingly complex wherein all the KAM tori in phase space break up. As a result the transition to chaos is abrupt, a typical scenario of non-KAM behaviour. Quantum mechanically the imprints of such a transition is seen in the localization properties of the quasienergy states. In particular, the states are more localized for integer R and there is a spread in the bulk part (delocalization) of the states when R assumes half-integer. Thus we realize the length scale ratio R as a control parameter for the localization in the weak field regime. This indeed enhances the quantum diffusion in the generic case if R is half-integer.

On increasing the field strength, chaos assisted diffusion takes place in momentum. From earlier studies on the kicked rotor it is known that the average localization length of the eigenstates is directly proportional to the classical diffusion coefficient. We have shown that in our generalization of the kicked rotor also, this result “grossly” explains the localization behaviour of the eigenstates through the classical transport properties. Thus the kicked rotor continues to serve as a useful model in understanding physical phenomena exhibited by a larger class of systems.

We have observed, as expected, that in the regular case the nearest neighbour spacing distribution of the quasienergies show good agreement with Poisson distribution. Evidences are presented to support that, in highly chaotic regimes the spacings show some deviations from the Poisson distribution though the corresponding eigenstates belong to an unbounded phase space. Limited overlap of the eigenstates results in such deviations. However, spacing does not show the RMT predicted Wigner distribution as was claimed in an earlier study [63]. The earlier result is attributed to lack of converged states in the statistics.

While the spacing is not much sensitive to the classical chaos, the distribution of participation ratios of the eigenstates is shown to be a good measure to distinguish chaotic quantum systems from regular ones. Quantum mechanically, chaotic regimes are characterized by a lognormal distribution of the participation ratios. In addition to the above generic quantum features, we have also studied non-generic phenomena like “quantum resonance”. In the resonance condition, the kinetic energy of the particle grows quadratically with the number of kicks. This unbounded energy growth is not affected by the length scale ratio. The resonance condition may then provide a mechanism to enhance the ionization in the deep finite well system.

As far as experimental realizations of the presented results are concerned, the quantum wells [41] are the possible candidate. We have demonstrated that the length scales effects may be best observed in these experiments for $R > 1$ at small field strengths.

4. Accelerator modes

4.1 Introduction

The phase space of dynamical system is broadly divided into two regions namely regular and chaotic. If there are no regular regions, the deterministic dynamics is more like the Brownian motion. In this case even a single chaotic orbit visits almost all the allowed regions and eventually fills the entire phase space, the dynamics is ergodic and the consequent diffusion process is normal. It is worth remarking that ergodicity is a very restrictive condition, and in general dynamical systems are non-ergodic and the phase space is mixed i.e., regular and chaotic regions coexist. In such situations, a natural concern is the influence of regular regions on chaotic orbits and also on global transport properties of the system in the long time limit. While the long time correlation decays exponentially for fully chaotic systems, in the mixed case regular regions are responsible in slowing the decay and as a result the evolution is no longer governed by diffusion equation [93]. We may recollect from Chapter 2 that, some of the dominant regular regions suppress diffusive nature of chaotic orbits. In contrast, here we will encounter another sort of situation that the regular regions influence in enhancing global diffusion process.

The area-preserving maps which are periodic in both of their conjugate variables have special kind of orbits called *accelerator modes* (AM). They are called so as the particle in the state of these modes is uniformly accelerated in each time step. Among them *stable* AM, which are seen as small regular islands embedded in the chaotic sea (see Fig. 4.1), deserve attention as they alter transport properties quite significantly in the chaotic regimes. Such modes were first identified in standard map of the kicked rotor [48]. They are particular states of the rotor such that the rotor acquires maximum acceleration in each kick (time step). To be precise, momentum of the rotor increases linearly with discrete time n . Or in other words, variance of the momentum is $\sigma^2(n) \sim n^\gamma$ with $\gamma = 2$. As a consequence the diffusion coefficient D diverges (see Eq. 2.25). In phase space the stable AM are separated from the chaotic region by cantori which are partial barriers. The vicinity of the cantori are very sticky in the sense that it retains long time correlations during the evolution. However, the dynamics in region between the cantori and the boundary of the modes are highly complex in nature. If a chaotic orbit enters through the cantori, it sticks to that region for very long time and thus accelerated along the modes. Such long excursions of the chaotic orbits exhibit the Lévy flight type dynamics with $\gamma > 1$. The anomalous diffusion due to the AM have been already studied for the standard map with various motivations [94] and also for the Harper map [95].

In the study of quantum chaos, naturally it is important to know the dynamics and effects of these modes in the corresponding quantum system. A study on quantum kicked rotor has shown that, in the semiclassical regime, momentum distribution of the propagated plane wave has sharp peaks at large momentum as signatures of the AM [96]. Also in the quantum regime, probability of the wave function in an AM decays exponentially with time and the decay rate is $\beta \sim \exp(-1/\hbar)$. It is argued that the loss of probability, interpreted as barrier-penetration, tends to reduce the effects of the modes in the quantum dynamics. Yet another study on the same system illustrates that the AM induced anomalous transport enhances the fluctuations in localization length of the quasienergy states [97]. The fluctuations are due to the non-exponential localization of the states. Recent experimental realization of the quantum kicked rotor has measured the time evolved momentum distribution [98]. It is found that the distribution is no longer exponentially localized, indicating the influence of AM in the quantum system as well. A similar experiment has demonstrated the AM in the quantum kicked rotor through enhanced diffraction of matter waves in the classical path [99]. In this Chapter, we will explore the stable AM and their quantum counterpart in the context of quantum well system.

4.2 Classical modes

We again invoke the GSM (2.10) to understand the dynamical features of AM in phase space of the well map. Since GSM is periodic in J and θ with unit period, the orbit with initial conditions

$$J' = m \quad ; \quad \frac{K}{2\pi} \sin(2\pi R\theta') = l \quad (4.1)$$

with m and l being integers will evolve such that the position θ_n will remain the same and the momentum J_n will increase by l at each step. The orbit will have uniform acceleration at each iteration and hence called the Accelerator Modes. They are also sometime termed as step- $|l|$ AM as the acceleration is $|l|$ at each iteration. Fixed points belong to the family of AM with $l = 0$ (orbits with zero acceleration). The stability condition for the AM is

$$-4 < KR \cos(2\pi R\theta') < 0. \quad (4.2)$$

Using (4.1) the stability condition becomes

$$|l| < \frac{K}{2\pi} < \sqrt{l^2 + \left(\frac{2}{\pi R}\right)^2} \quad (4.3)$$

or

$$0 < R < R_1 \quad (4.4)$$

where $R_1 = (2/\pi) \left\{ (K/2\pi)^2 - l^2 \right\}^{-1/2}$. Stable AM exist in the phase space if the parameters K and R satisfy the above condition. However, the restriction of the dynamics to between the walls of the well or the GSM position co-ordinate to between $-1/2$ and $1/2$ leads to the following considerations.

For stable AM, θ' is such that

$$\frac{1}{R} \left(j + \frac{1}{4} \right) < |\theta'| < \frac{1}{R} \left(j + \frac{1}{2} \right) \quad (4.5)$$

where j is a positive integer. The precise positions of these modes are given by

$$|\theta'| = \frac{1}{2R} \left\{ 2j + 1 - \frac{1}{\pi} \sin^{-1} \left(\frac{2\pi|l|}{K} \right) \right\} \quad (4.6)$$

where arcsin function assumes its minimum value. For a given value of K , as $R \rightarrow \infty$, $|\theta'| \rightarrow 0$ and as $R \rightarrow 0$, $|\theta'| \rightarrow \infty$. Since the GSM is defined on a cylinder such that $|\theta'| \leq 1/2$, zero in the inequality (4.4) can not be the lower limit of R for the stable modes to exist. As R increases $|\theta'|$ decreases resulting the emergence of new stable modes in the phase space with higher values of j ; as R decreases $|\theta'|$ increases and hence stable AM with higher values of j disappear from the phase space when $|\theta'| > 1/2$. The last stable AM that disappear from the phase space are the ones which correspond to $j = 0$. When $j = 0$, $R_0 \leq R$ with $R_0 = 1 - (1/\pi) \sin^{-1}(2\pi|l|/K)$, as $|\theta'| \leq 1/2$. Hence the inequality (4.4) is replaced by

$$R_0 \leq R < R_1. \quad (4.7)$$

Both the inequalities (4.3) and (4.7) are simultaneously required for the stable AM to be present in the dynamics unlike in the case of the standard map where the inequality (4.3) with $R = 1$ is sufficient. Thus the GSM has additional parameter R which also needs to be tuned for a given K for the existence of stable AM. Note that at $K = 2\pi|l|$, lower bound of the inequality (4.3), $R_0 = 1/2$ and this is the minimum possible value of R_0 . Hence as long as $R < 1/2$, for any value of K , stable AM are absent. We may recollect that GSM is hyperbolic for $R < 1/2$. In this regime, there are no stable orbits including the stable AM.

Since the well map and GSM are quantitatively same, the location of the AM are same for both the maps i.e., $(X', P') = (\theta', J')$. All the above arguments hold for the AM of the well map also. Shown in Fig. 4.1 is the phase space of the well map with stable AM. For a given K , the position of the stable mode is such that $|X'| \sim 1/R$. It is also noticeable that the size of the AM islands increases as R decreases. For the well system, when the particle is at the AM modes, n th kick causes the particle to undergo n bounces between the walls. If n is odd,

momentum of the particle changes its sign which in turn flips position of the particle. This can be easily seen by time evolving the well map with the initial condition (X', P') . In phase space, regular regions at the location of AM are separated from the remaining chaotic region by cantori (partial-barriers). If a chaotic orbit happens to pass through the cantori, it can be dragged along the modes ballistically. This mechanism indeed enhances the transport in momentum, leading to anomalous diffusion. This anomalous effect due to the AM can be seen by evolving an ensemble of points for long time.

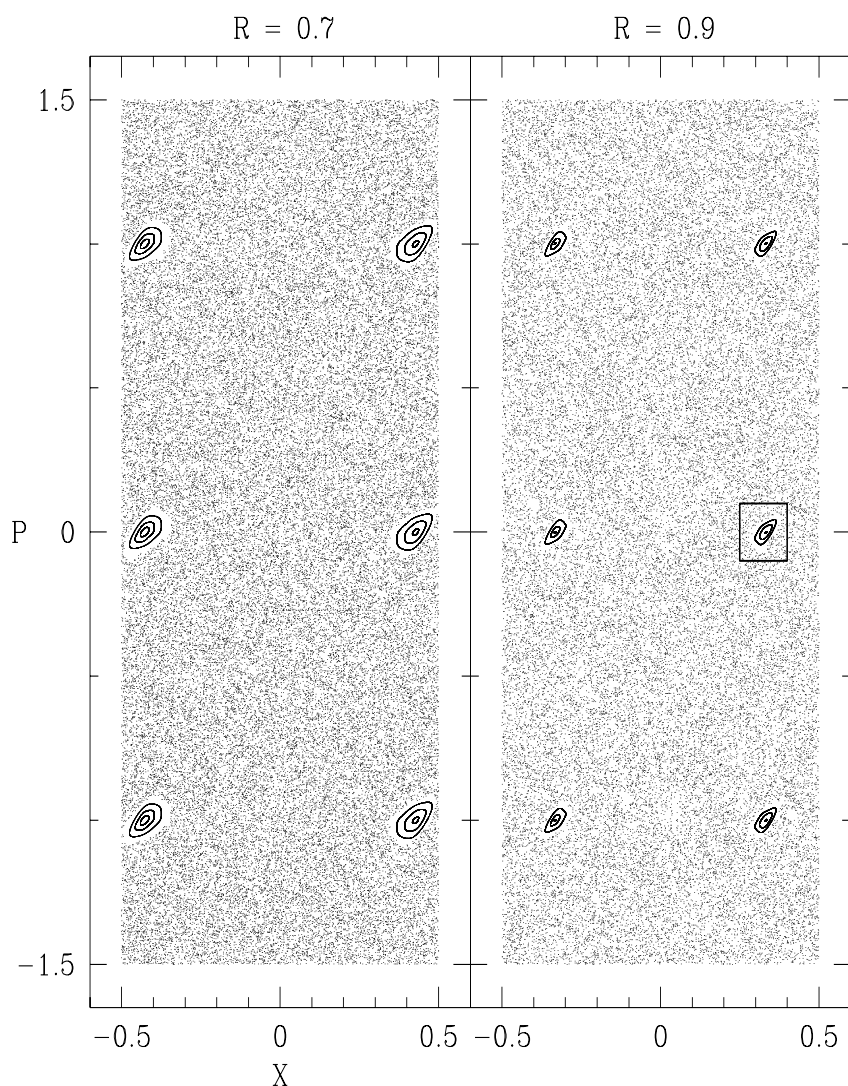


Figure 4.1: Phase space of the well map for $K/2\pi = 1.05$. Islands of regular regions in the chaotic sea are the stable AM. Shown are the step-1 type ($j = 0$) modes. For $R = 0.7$, $|X'| = 0.43$ and for $R = 0.9$, $|X'| = 0.33$. Region marked by the square is enlarged in Fig. 4.2.

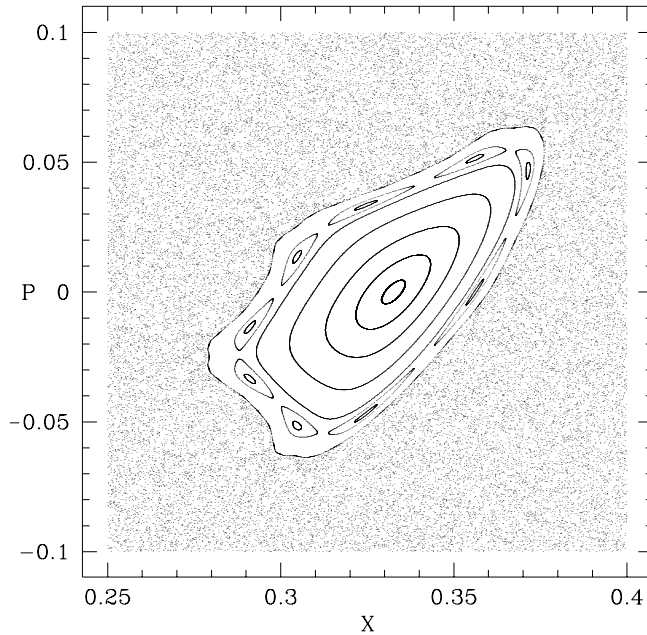


Figure 4.2: A stable mode embedded in the chaotic sea.

Considering $\langle (P_n - P_0)^2 \rangle \sim n^\gamma$, Fig. 4.3 (i) shows the window (4.7) where the second moment of the momentum increases quadratically in time. Notice that the ensemble contains only few points that correspond to the AM. However, in long time limit the evolution is dominated by these points. This is understandable as the rest of the points in the ensemble are chaotic and their diffusion is random walk type (normal, $\gamma = 1$), until they are dragged along the AM islands. Of course, outside the window (4.7), diffusion is quite normal where the AM do not exist in the phase space. On taking the ensemble which does not contain the AM orbits, which is the case of Fig. 4.3 (ii), we observe that $\gamma > 1$ for many values of R within the window (4.7). This could be due to intermittent acceleration of the chaotic orbits when they approach neighbourhood of the stable modes. Thus the ballistic motion of the stable modes and the consequent enhancement in the diffusion are evident from our numerical experiments. Further we will be simulating the quantum dynamics of these modes from the point of view of quantum-classical correspondence.

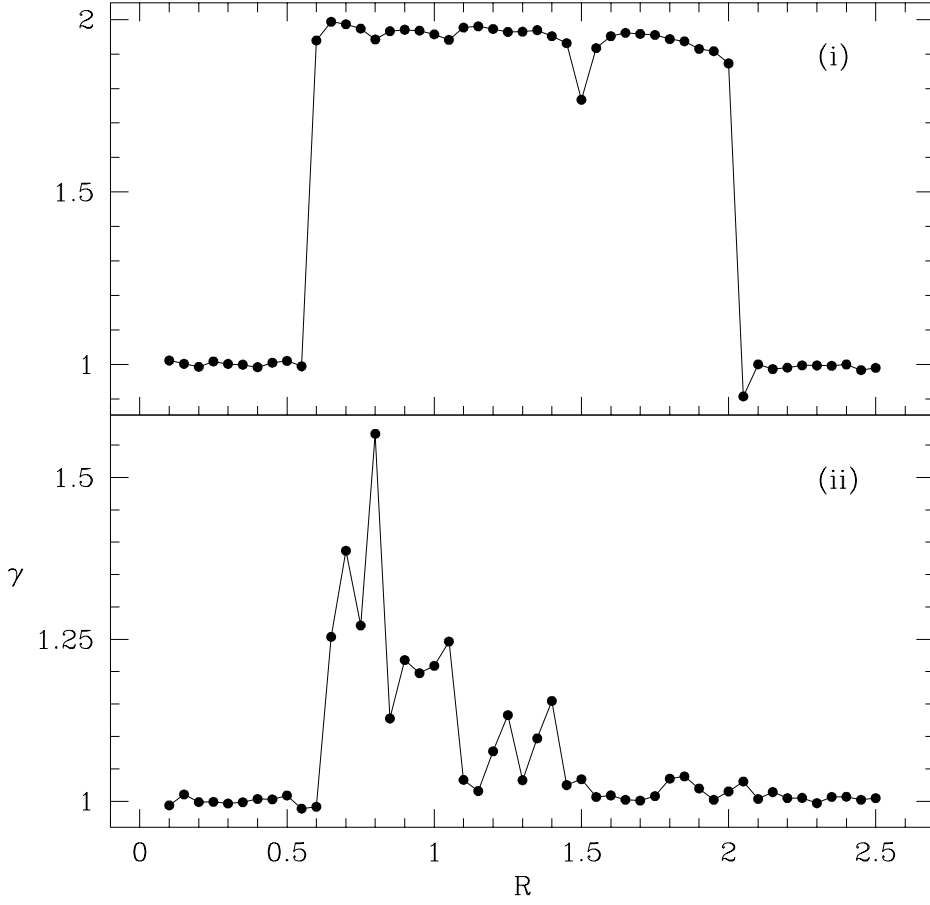


Figure 4.3: Exponent γ is shown for $K/2\pi = 1.05$. For these calculations, classical ensemble contains 5000 phase space points (initial conditions) and each of them is evolved for 10000 time steps. The ensemble has fixed P_0 , and X_0 distributed uniformly between $-1/2$ and $1/2$. For (i) $P_0 = 0$ and for (ii) $P_0 = 0.25$. The window (4.7) with $R_0 = 0.598$ and $R_1 = 1.988$, where stable AM exist, is seen in (i) as $\gamma \approx 2$ due to ballistic evolution of the stable AM orbits contained in the ensemble. In (ii), the anomalous transport ($\gamma > 1$) due to AM is seen.

4.3 Quantum modes

The natural choice to simulate the AM in quantum system is the time evolved Gaussian wave packet which is initially placed on one of the AM. Since the quantum dynamics is represented in unperturbed basis let us recollect the basis, but now in scaled variables as: $H_0|n\rangle = \mathcal{E}_n|n\rangle$ with

$$\langle X|n\rangle = \begin{cases} \sqrt{2} \cos(n\pi X), & \text{for } n \text{ odd} \\ \sqrt{2} \sin(n\pi X), & \text{for } n \text{ even} \end{cases} ; \quad \mathcal{E}_n = \frac{n^2 \pi^2 \hbar^2}{2M}. \quad (4.8)$$

The kick to kick time evolution of the quantum state $|\Psi(t)\rangle = \sum_n \Psi_n(t)|n\rangle$; $\Psi_n(t) = \langle n|\Psi(t)\rangle$, is then given by the quantum map

$$\Psi_m(t+T) = \sum_n U_{mn} \Psi_n(t) ; \quad U_{mn} = e^{-i\tau n^2} \langle m|e^{-ik \cos(2\pi R X)}|n\rangle \quad (4.9)$$

where

$$\tau = \frac{E_n T}{\hbar n^2} = \frac{\pi^2 \hbar T}{2M}.$$

As usual with the relation $K/R = 8k\tau$ the semiclassical limit is $k \rightarrow \infty, \tau \rightarrow 0$ and N is the number of basis states for the calculation.

4.3.1 Gaussian wave packet

As the quantum dynamics is described in $|n\rangle$ basis, and here we need to represent the initial Gaussian wave packet (confined within the well) in this basis. Standard Gaussian wave packet reads

$$\langle X|\Psi(0)\rangle = C \exp \left\{ -\frac{(X - \langle X \rangle)^2}{2\sigma_g^2} + \frac{i\langle P \rangle X}{\hbar_e} \right\} \quad (4.10)$$

where σ_g measures the width of the wave packet, which is centred at $\langle X \rangle$ with momentum $\langle P \rangle$. Here $\hbar_e = 2\tau/\pi^2$ is the effective Planck constant and C is the normalization constant which is obtained from the condition

$$\int_{-1/2}^{1/2} |\langle X|\Psi(0)\rangle|^2 dX = 1$$

as

$$C = \left(\frac{2/\sigma_g \sqrt{\pi}}{\text{erf}(y_+) - \text{erf}(y_-)} \right)^{\frac{1}{2}} ; \quad y_{\pm} = \frac{\pm 1/2 - \langle X \rangle}{\sigma_g}. \quad (4.11)$$

To calculate $\Psi_n(0)$ we consider the following integral

$$G_n = \sqrt{2} \int_{-1/2}^{1/2} e^{in\pi X} \langle X|\Psi(0)\rangle dX. \quad (4.12)$$

With the change of variable $u = (X - \langle X \rangle)/\sqrt{2}\sigma_g$ the integral becomes

$$G_n = 2\sigma_g C e^{iB\langle X \rangle} \int_{u_-}^{u_+} e^{-(u^2 - i\sqrt{2}B\sigma_g u)} du \quad (4.13)$$

where $B = n\pi + \langle P \rangle / \hbar_e$ and $u_{\pm} = y_{\pm} / \sqrt{2}$. Arriving the form of following standard integral [100]

$$\int e^{-(ax^2+2bx+c)} dx = \frac{1}{2} \sqrt{\frac{\pi}{a}} \exp\left(\frac{b^2 - ac}{a}\right) \operatorname{erf}\left(\frac{ax+b}{\sqrt{a}}\right)$$

G_n can be represented as complex error function. Defining the complex error function [101] as

$$w(z) = e^{-z^2} \{1 - \operatorname{erf}(-iz)\} = e^{-z^2} \left(1 + \frac{2i}{\sqrt{\pi}} \int_0^z e^{x^2} dx\right)$$

where z is a complex number, $w(z)$ is computed using the algorithm [102] and hence G_n as well. Now the components of the Gaussian wave packet can easily be represented as

$$\Psi_n(0) = \begin{cases} \frac{1}{2}(G_n + G_{-n}), & \text{for } n \text{ odd} \\ \frac{1}{2i}(G_n - G_{-n}), & \text{for } n \text{ even.} \end{cases} \quad (4.14)$$

With this construction the wave packet dynamics can be studied using the quantum map.

4.3.2 Quantum effects and correspondence

In the context of quantum-classical correspondence, it is necessary to suppress the quantum resonance phenomena which is discussed in Chapter 3. This is possible by taking τ as irrational multiple of 2π . This can be best achieved with $\tau = 2\pi gh'$ where $g = (\sqrt{5} - 1)/2$ is the most irrational number (golden mean) and h' is the scaled Planck constant ($\hbar_e = 0.787h'$). Since our interest is to explore quantum version of the classical modes, the following quantum dynamics corresponds to the classical system with $K/2\pi = 1.05$, $R = 0.9$. The wave packet (4.10) obeys the minimum uncertainty relation $\Delta X \Delta P = \hbar_e/2$ and we take $\Delta X = 0.02$ throughout. The dimensionless kinetic energy of the time evolved state is given by

$$\langle E \rangle_t = \langle \Psi(t) | \hat{P}^2 | \Psi(t) \rangle = \left(\frac{2\tau}{\pi}\right)^2 \sum_{n=1}^N |\Psi_n(t)|^2 n^2 \quad (4.15)$$

which is equivalent to the classical energy $\langle P_t^2 \rangle$. The number of basis taken are as high as $N = 7500$. The time evolution is performed for two cases *viz.* the initial wave packet is placed (a) *on* one of the AM with $(\langle X \rangle, \langle P \rangle) = (X', P') = (0.33, 0)$ and (b) *not on* the AM with $(\langle X \rangle, \langle P \rangle) = (0, 0.5)$. The initial conditions of the wave packet are chosen such that influence of the stable AM can be compared and contrasted with rest of the chaotic motion.

In Fig. 4.4 we have shown the energy with time (kick) for $h' = 0.02$ ($\Delta P = 0.39$). For the case (a), the initial wave packet is confined to the AM in X axis and elongated in P axis. Thus the initial wave packet has both regular and chaotic components as the spread in P direction is more. On the other hand, for the case (b) it has only chaotic components. In both the cases,

energy increases linearly with t for short time, then slows down and finally diffusion is absent as $t \rightarrow \infty$. This is very similar to the suppression of the chaos assisted classical diffusion in the quantum kicked rotor. One does not expect case (a) to show the classical behaviour of the AM even in the short time scale as the initial wave packet has more spread in momentum. More over, no qualitative difference is seen between the two evolutions. This implies that large fraction of chaotic components which make up the initial wave packet dominate the dynamics over the small fraction of regular components.

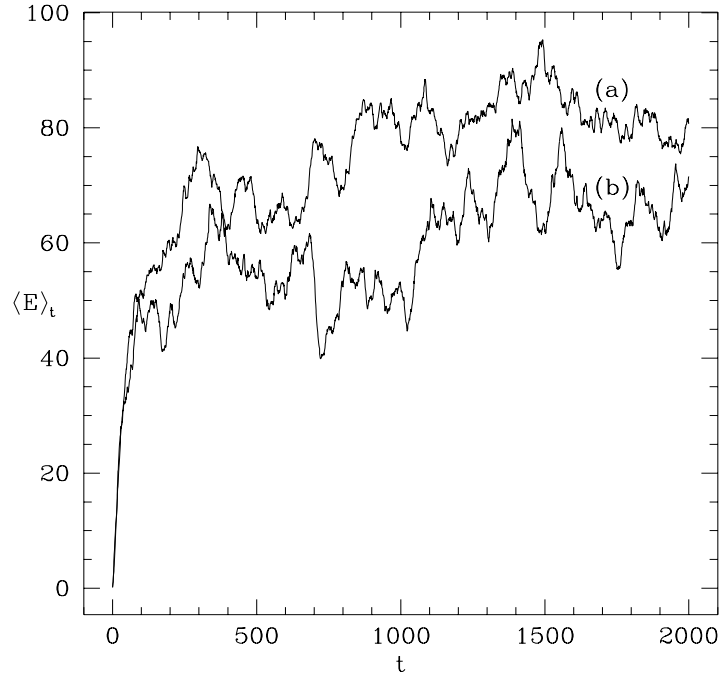


Figure 4.4: *Energy for the cases (a) and (b) with $h' = 0.02$.*

Here we proceed further for the case (a) as $h' \rightarrow 0$. In this semiclassical limit k becomes larger, causing fast spread of the wave packet in unperturbed basis states which in turn demands practically infinite basis states for the long time quantum behaviour. Finite number of basis states thus becomes the numerical constraints to uncover long time quantum features. Keeping the limitations in mind, we focus the attention on short time quantum evolution. Considering the power law behaviour as $\langle E \rangle_t \sim t^\gamma$, Fig. 4.5 shows the exponent γ as a function of scaled Planck constant. As h' decreases from 0.02 to 0.001, ΔP decreases from 0.39 to 0.02. Thus the fraction of chaotic components of the initial wave packet reduces with h' , and consequently the fraction of regular components increases as the wave packet is normalized. We observe that the exponent increases and there is a clear evidence of enhancement in quantum diffusion with $\gamma > 1$ as a signature of the AM. For $h' = 0.001$ or $\Delta P = 0.02$ ($= \Delta X$), the initial Gaussian

wave packet (now circular in $X - P$ space) is confined only within the stable region of the AM (see Fig. 4.2). In other words, the wave packet has only regular components. In this case the energy of the wave packet grows quadratically in time ($\gamma \approx 2$). Thus the quantum dynamics of Gaussian wave packet reproduces ballistic motion of the stable AM in the semiclassical limit.

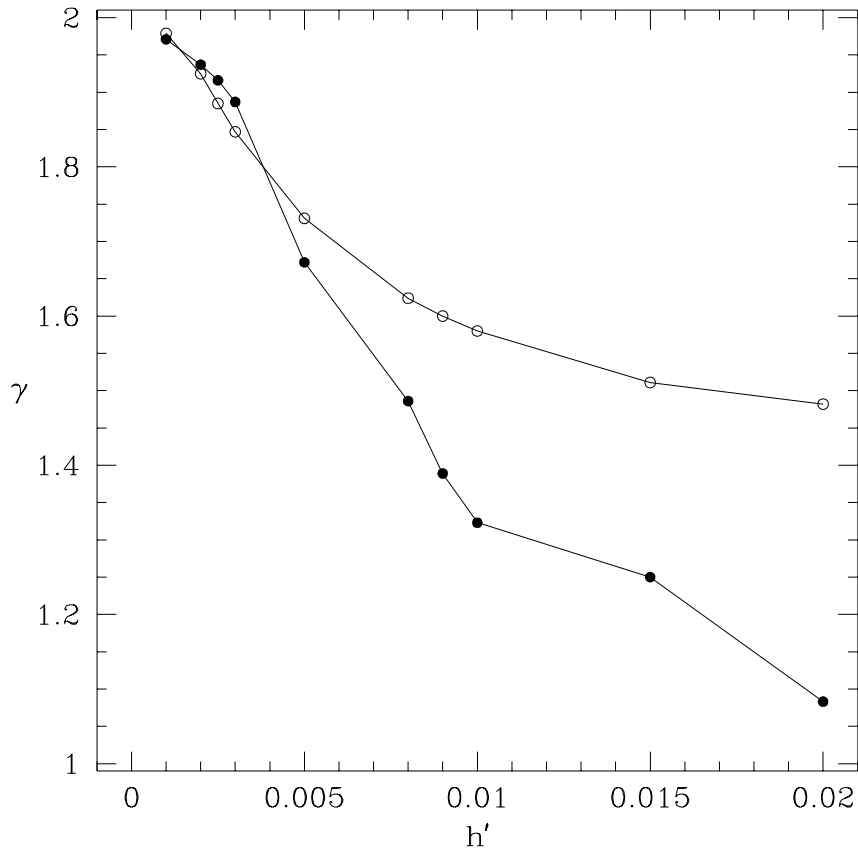


Figure 4.5: Exponent γ of the energy upto $t = 18$ is plotted with h' . Open circle is the exponent of the classical evolution (upto $t = 18$) with the corresponding Gaussian ensemble containing 10000 points.

For comparison we have also shown the classical exponent in Fig. 4.5 which is calculated by time evolving an ensemble of initial conditions whose distribution is the corresponding Gaussian. The deviation of quantum exponent from the classical exponent decreases with h' . That is the quantum-classical deviation is proportional to the fraction of chaotic components of the initial wave packet. If the wave packet has any chaotic components it loses its shape exponentially faster in time and hence it fails to show the classical behaviour. In the case of $h' = 0.001$, due to the absence of chaotic components, the time evolved wave packet shows good quantum-classical correspondence without losing its shape (see below).

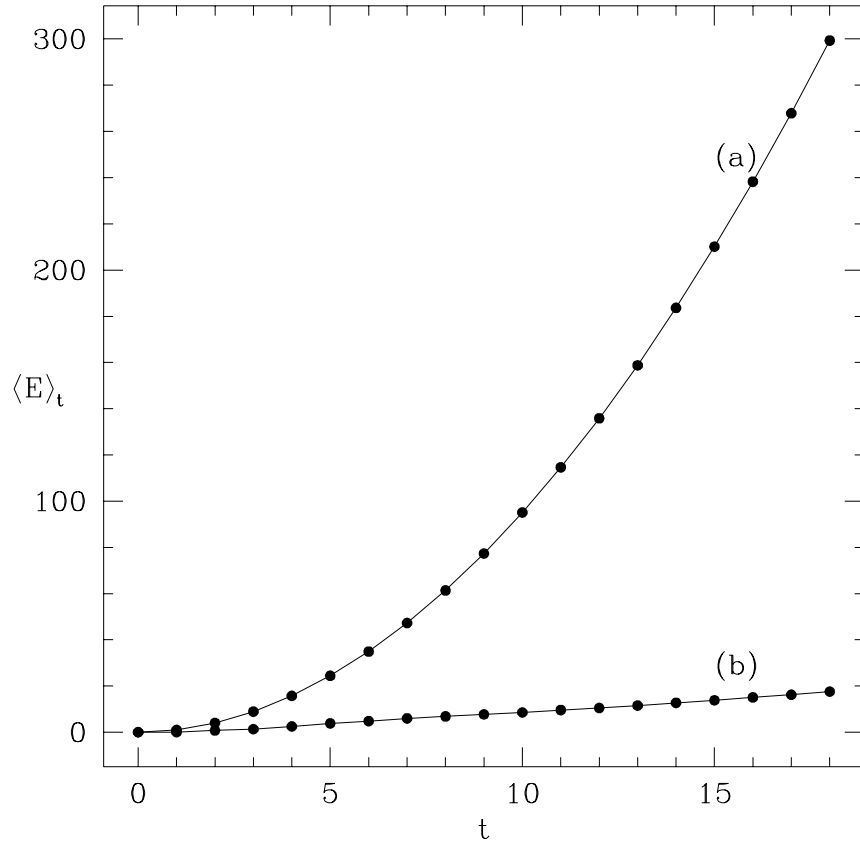


Figure 4.6: Energy for the cases (a) and (b) with $\hbar' = 0.001$.

Shown in Fig. 4.6 is the short time behaviour of the cases (a) and (b) in semiclassical limit. While the energy growth is quadratic in the former, it is linear in the latter. Corresponding wave packet dynamics is shown in Fig. 4.7. We may recollect that the time evolved position of the particle with the initial condition (X', P') flips its position i.e., X' becomes $-X'$ after odd kicks. In (a) the time evolved wave packet, without losing its initial shape, exhibits all the classical behaviour satisfactorily. On the other hand, wave packet of case (b) loses its shape and spreads over the square well very quickly. This is indeed a typical behaviour of initially localized wave function which corresponds to chaotic region of phase space. Suppose if we associate two localized wave function to each of two neighbourhood orbits in a chaotic region, general quantum solution (superposition of the two wave functions) delocalizes very quickly in course of time. Once the wave packet delocalizes, in the long time limit chaotic and diffusive nature may not be seen. Instead, phenomena like quantum interferences govern the dynamics.

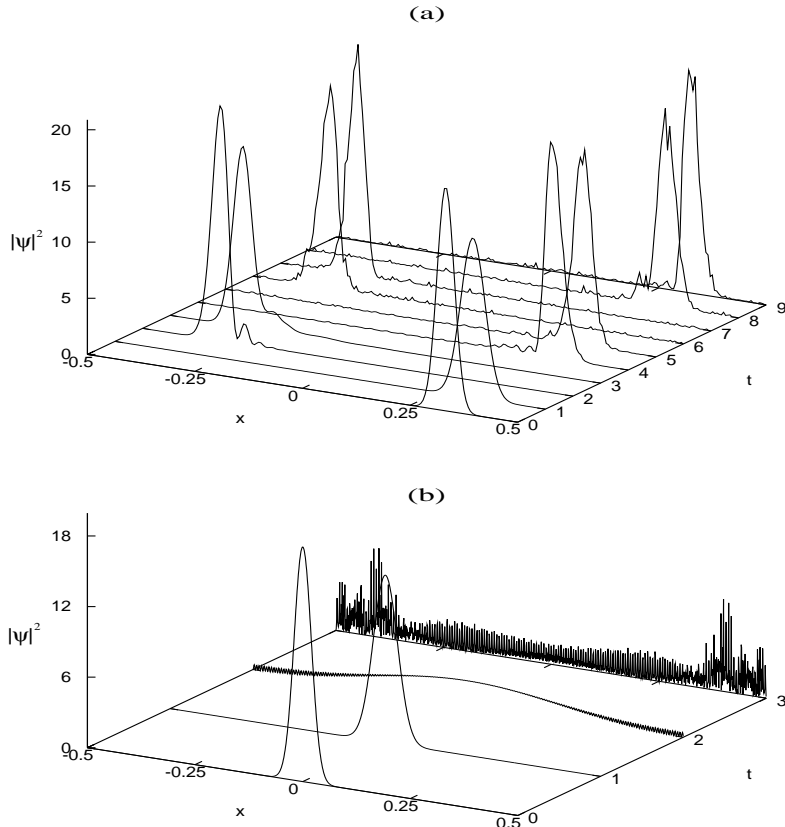


Figure 4.7: Evolution of the wave packet for the cases (a) and (b) with $\hbar' = 0.001$.

4.4 Summary

We have analyzed stable accelerator modes, which are small regular regions embedded in chaotic phase space, for the kicked particle inside an infinite square well potential. Parametric regimes for the existence of these modes are obtained. Ballistic behaviour of the modes are shown to enhance the global transport in the chaotic regime. Quantum dynamics of these modes are studied by time evolving Gaussian wave packet. It is shown that the chaotic components of the wave packet are dominant in the time evolution and are also responsible for the quantum-classical deviations. In appropriate semiclassical limit, the wave packet reproduces classical behaviour of the accelerator modes in full correspondence.

5. Quantized torus

5.1 Introduction

Area-preserving maps that are periodic in their conjugate variables can be restricted to unit square with identified edges or equivalently to 2-torus. The periodic boundary conditions also facilitate the quantization procedure wherein quantum dynamics is described in a finite N dimensional Hilbert space. Resultant quantized maps on the torus are the simplest semiclassical models that reflect generic features of chaotic quantum systems. The maps which are studied in this line of approach are the baker map [103, 104], the saw-tooth map [105] and the standard map [106]. Since the GSM is periodic in its conjugate variables with unit period (see Eqn. (2.10)), it is sufficient to confine the mapping onto the torus. In this Chapter, we explore quantized version of the GSM on torus as a model of quantum chaos. Before quantizing the GSM, a brief account on certain basic ingredients will be in order.

The compact toral phase space can be quantized by introducing boundary conditions in q and p [107] such that

$$\hat{q}|n\rangle = \left(\frac{n+\beta}{N}\right)|n\rangle \quad ; \quad \hat{p}|m\rangle = \left(\frac{m+\alpha}{N}\right)|m\rangle \quad (5.1)$$

where $n, m = -N/2, -N/2 + 1, \dots, N/2 - 1$ and N is an integer. Here n and m are the discrete eigenvalues of position and momentum operators respectively; $|n\rangle$ and $|m\rangle$ are the corresponding eigenstates; α, β are the real numbers between 0 and 1. Note that $N = (2\pi\hbar)^{-1}$ is the dimensionality of the Hilbert space. The semiclassical limit is $N \rightarrow \infty$. In this quantization, the eigenstates satisfy the relation

$$\langle n+N| = \langle n|e^{i2\pi\alpha} \quad ; \quad |m+N\rangle = e^{i2\pi\beta}|m\rangle. \quad (5.2)$$

The discretized eigenstates are periodic with period N except the quantum phases α and β . Then the corresponding transformation function is

$$\langle n|m\rangle = \frac{1}{\sqrt{N}} \exp \left[\frac{i2\pi}{N}(m+\alpha)(n+\beta) \right]. \quad (5.3)$$

It would be useful to define unitary operators A and B which shift the eigenstates as

$$\begin{aligned} \langle n|A &= \langle n+1| \quad ; \quad A^N = e^{i2\pi\alpha} \\ B|m\rangle &= |m+1\rangle \quad ; \quad B^N = e^{i2\pi\beta}. \end{aligned} \quad (5.4)$$

These operators satisfy the relation

$$\begin{aligned}\langle m|A|m'\rangle &= \delta_{mm'} e^{i2\pi(m'+\alpha)/N} \\ \langle n|B|n'\rangle &= \delta_{nn'} e^{i2\pi(n+\beta)/N}.\end{aligned}\tag{5.5}$$

That is the momentum states $|m\rangle$ are the eigenvectors of A and similarly the position states $|n\rangle$ are the eigenvectors of B . Thus we may realize that the operators A and B are analogous to the translation operators $\exp(iq\hat{p}/\hbar)$ and $\exp(ip\hat{q}/\hbar)$ in the continuous case. An analogue of the uncertainty relation is then given by the commutation relation

$$AB = BA \exp\left[i\frac{2\pi}{N}(1 + \alpha - \beta)\right].\tag{5.6}$$

It is to be noted that the momentum and position eigenstates are orthonormal sets and individually they form basis for the N -dimensional space. An arbitrary quantum state can be represented either in $|n\rangle$ basis or in $|m\rangle$ basis i.e.,

$$|\psi\rangle = \sum_n |n\rangle \langle n|\psi\rangle = \sum_m |m\rangle \langle m|\psi\rangle.\tag{5.7}$$

Both the basis are complimentary to each other and the state components in one representation is related to that of the other through the discrete Fourier transformation

$$\langle n|\psi\rangle = \sum_m \langle n|m\rangle \langle m|\psi\rangle.\tag{5.8}$$

Thus both the representations together form “quantum” phase space.

5.2 Quantized GSM

Considering a particle which trapped in a one dimensional infinite square well potential $V_0(q)$ of unit width (hard walls at $q = \pm 1/2$) and experiences periodic kicks from the external pulse. The Hamiltonian is

$$\tilde{H} = \frac{p^2}{2} + V_0(q) + \frac{k\lambda}{4\pi^2} \cos\left(\frac{2\pi q}{\lambda}\right) \sum_j \delta(j - t)\tag{5.9}$$

As shown in Chapter 2, the underlying kick to kick dynamics is *essentially* governed by a dimensionless area-preserving mapping:

$$\begin{aligned}p_{j+1} &= p_j + (k/2\pi) \sin(2\pi r q_j) \\ q_{j+1} &= q_j + p_{j+1}\end{aligned}\tag{5.10}$$

which is defined on 2-torus i.e., a unit square $[-1/2, 1/2) \times [-1/2, 1/2)$ with periodic boundaries. Here $r = 1/\lambda$ is the ratio of the two length scales of the system namely, the well width and wavelength of the pulse field; k is the effective strength of the kick. The above map arises from the equations of motion of free particle in presence of a field $V(q)$ which is applied as time periodic impulse. The field is defined as: $V(q) = k \cos(2\pi r q)/(4\pi^2 r)$; $V(q) = V(q + 1)$ and the corresponding Hamiltonian is

$$H = \frac{p^2}{2} + V(q) \sum_j \delta(j - t). \quad (5.11)$$

As in the case of classical map, it is easy to describe the kick to kick quantum dynamics using the propagator

$$\hat{U} = e^{-i\hat{p}^2/2\hbar} e^{-iV(\hat{q})/\hbar} \quad (5.12)$$

which is obtained by integrating the Shrödinger equation $-i\hbar\partial|\psi(t)\rangle/\partial t = \hat{H}|\psi(t)\rangle$ over unit time. Thus, we have $|\psi(t+1)\rangle = \hat{U}|\psi(t)\rangle$ as the quantum map. The Schrödinger equation with the Hamiltonian (5.11) in N -dimensional space has N solutions which satisfy the eigenvalue equation $\hat{U}|\phi_j\rangle = e^{-i\phi_j}|\phi_j\rangle$ where $j = 1, 2, \dots, N$. Here ϕ_j and $|\phi_j\rangle$ are the quasienergies and quasienergy states and they may be obtained by diagonalizing the propagator matrix.

We note from the Eqn. (5.1) that for $\alpha \neq 0$ the time reversal symmetry of the system is broken. On the other hand, the phase β can be used to avoid any spatial symmetry. In what follows we do not break the time reversal symmetry (i.e., $\alpha = 0$). Choosing the position representation we may write down the propagator matrix as

$$\begin{aligned} U_{nn'} &= \langle n|\hat{U}|n'\rangle = \langle n|e^{-i\hat{p}^2/2\hbar} e^{-iV(\hat{q})/\hbar}|n'\rangle \\ &= \exp\left[-\frac{i}{\hbar}V\left(\frac{n'+\beta}{N}\right)\right] \langle n|e^{-i\hat{p}^2/2\hbar}|n'\rangle \\ &= \exp\left[-\frac{i}{\hbar}V\left(\frac{n'+\beta}{N}\right)\right] \sum_m \langle n|e^{-i\hat{p}^2/2\hbar}|m\rangle \langle m|n'\rangle \\ &= \frac{1}{N} \exp\left[-\frac{i}{\hbar}V\left(\frac{n'+\beta}{N}\right)\right] \sum_m \exp\left[\frac{i\pi}{N}\{-m^2 + 2m(n-n')\}\right]. \end{aligned} \quad (5.13)$$

We may notice that if N is even the term which is inside the sum is periodic with period N . Recognizing the summation as Gauss sum [108, 109], with N as even, the matrix becomes

$$U_{nn'} = \frac{1}{\sqrt{N}} \exp\left[-i\pi\left\{\frac{1}{4} - \frac{(n-n')^2}{N} + 2NV\left(\frac{n'+\beta}{N}\right)\right\}\right]. \quad (5.14)$$

The resultant propagator matrix for the Hamiltonian (5.11) is then

$$U_{nn'} = \frac{e^{-i\pi/4}}{\sqrt{N}} e^{i\pi(n-n')^2/N} \exp \left\{ \frac{-ikN}{2\pi r} \cos \left[\frac{2\pi r}{N} (n' + \beta) \right] \right\}. \quad (5.15)$$

The parity symmetry of the Hamiltonian is reflected in the quantum propagator as the commutation relation $[\hat{U}, \hat{R}] = 0$ where the hermitian operator \hat{R} is defined as

$$\begin{aligned} \hat{R}|n\rangle &= | -n \rangle & \text{for } \beta = 0 \\ &= | -n - 1 \rangle & \text{for } \beta = 0.5. \end{aligned} \quad (5.16)$$

Since $\hat{R}^2 = 1$ we may label the eigenstates of \hat{U} with the eigenvalues ± 1 of \hat{R} i.e., the states are $|\phi_{\pm}\rangle$. Taking $\beta = 0.5$ the symmetry matrix of order N is

$$R_N = \langle n | \hat{R} | n' \rangle = \delta(n + n' + 1) \pmod{N} \quad (5.17)$$

which has ones along secondary diagonal and zeros elsewhere. The components of quasienergy states are such that $\langle -n - 1 | \phi \rangle = \pm \langle n | \phi \rangle$, i.e., the states are of the form

$$|\phi_{\pm}\rangle = \begin{pmatrix} |z\rangle \\ \pm R_{N/2} |z\rangle \end{pmatrix}. \quad (5.18)$$

The eigenstates are obtained by diagonalizing the matrix $U_{nn'}$ of order N . Since N is even integer, due to the R -symmetry we have $N/2$ even parity states $\{|\phi_{+}\rangle\}$ and $N/2$ odd parity states $\{|\phi_{-}\rangle\}$. On exploiting R -symmetry in the quantum system, we can reduce the diagonalization to matrix of order $N/2$ by standard procedure [104]. The reduced matrix is

$$\begin{aligned} \mathcal{U}_{nn'} &= \frac{e^{-i\pi/4}}{\sqrt{N}} \exp \left\{ \frac{-ikN}{2\pi r} \cos \left[\frac{2\pi r}{N} \left(n + \frac{1}{2} - \frac{N}{2} \right) \right] \right\} \\ &\quad \times \left\{ e^{i\pi(n-n')^2/N} \pm e^{i\pi(n+n'+1)^2/N} \right\} \end{aligned} \quad (5.19)$$

where $n, n' = 0, 1, 2, \dots, N/2 - 1$. Now the separation of the parity states is obvious.

5.3 Quasienergies

We may recollect that the GSM exhibits abrupt non-KAM transition to chaos for non-integer r even small perturbation strength ($k \leq 1$). On the other hand, for integer r the transition is smooth with the gradual increase of perturbation strength k . In semiclassical limit, it is natural to expect that complexity of the classical dynamics arises due the parameter r would be reflected

in the quasienergy spectrum. Here we study the nearest neighbour spacing distribution of the quasienergies.

In Fig. 5.1 we show typical behaviour of the spacing distribution for the standard map ($r = 1$). For small k the spacings follow Poisson distribution. This is a generic spectral behaviour of an integrable system. For integrable/nearly integrable system the quantum states are localized along the classical local invariants in phase space subject to the uncertainty condition. The localized states avoid overlapping among themselves such that the quasienergies are independent and uncorrelated. This results in Poisson distribution of the quasienergy level spacings.

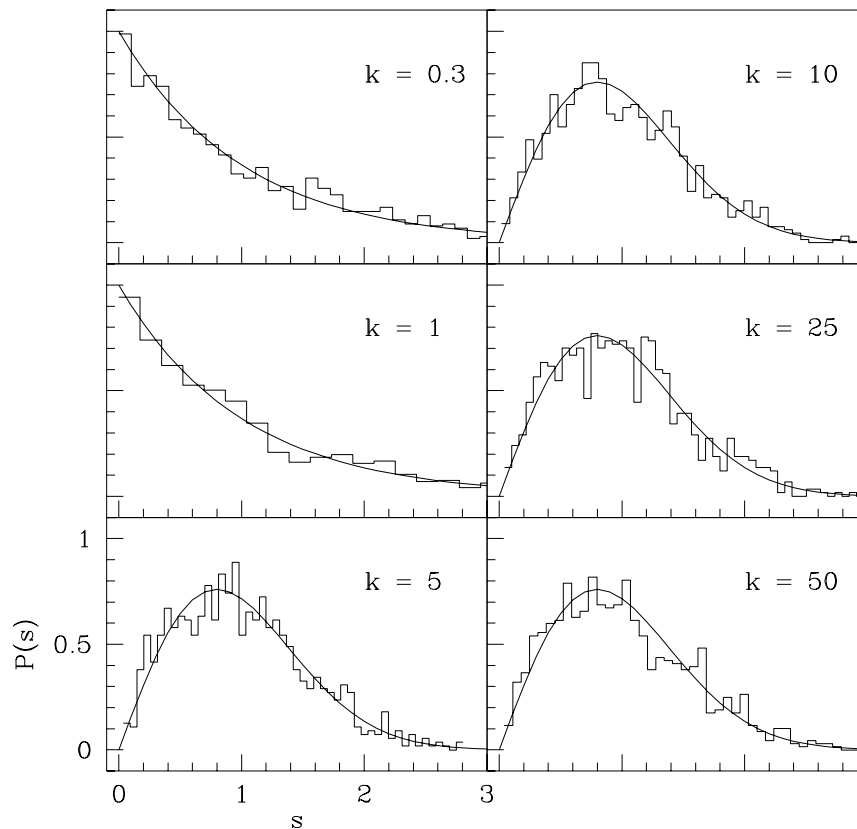


Figure 5.1: *Nearest neighbour spacing distributions of 1000 quasienergies that correspond to even parity states i.e., $N = 2000$, for the standard map ($r = 1$). Smooth curve drawn for $k = 0.3, 1$ is the Poisson distribution. The smooth curve drawn for other cases is the Wigner distribution.*

On increasing k beyond unity, transition to chaos is smooth and for $k = 5$ the classical system becomes highly chaotic. We observe that the spacings agree with the RMT predicted

Wigner distribution as a signature of quantum chaos. In the chaotic regime, classical dynamics lacks invariants and the phase space is filled with unstable orbits. Correspondingly, generic quantum states are delocalized (ergodic) in the phase space. Strong overlapping of the states causing the quasienergies to be correlated such that the spacings follow Wigner distribution. For further increase of k , classically the degree of complexity increases. That is, the time scale in attaining ergodic nature reduces. However, the spacing measure of quantum spectrum remains unchanged and follows the RMT prediction.

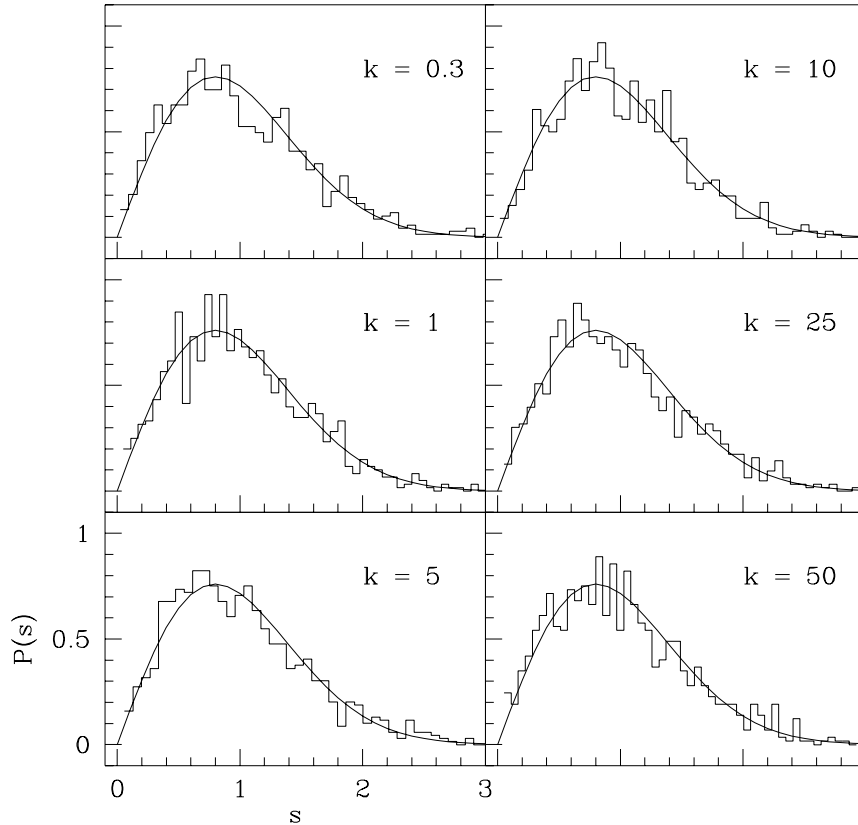


Figure 5.2: *Spacing distributions for $r = 0.5$. Other parameters are same as Fig. 5.1. Smooth curve is the Wigner distribution.*

On the other hand, for $r = 0.5$ the spacings follow Wigner distribution irrespective of k values (see Fig. 5.2). We recollect that for $r = 0.5$ the underlying classical system is completely chaotic. This shows that the spacings are sensitive to the classical dynamics. It is instructive to compare these results with those that are obtained for the unbounded chaotic case discussed in Chapter 3. In the latter, states generally deviate from the RMT prediction due to their localization in momentum space and as a consequence the spacing distribution is close to Poisson. In

other words, spacings are insensitive to the classical dynamics.

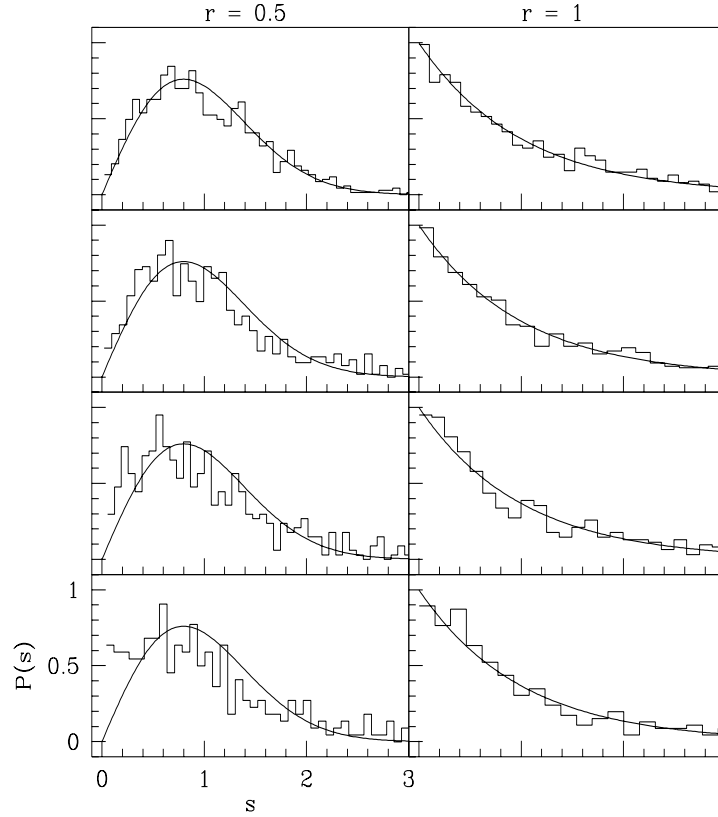


Figure 5.3: *Spacing distributions of quasienergies that correspond to even parity states for $k = 0.3$. (Top to bottom: $N = 2000, 1400, 1000, 600$). Smooth curve drawn in left column is the Wigner distribution and in right column the curve is Poisson distribution.*

In Fig. 5.3 we show the spacing distribution with different N for regular and chaotic cases. In the regular case ($r = 1$), the Poisson behaviour of spacings is independent of N . On contrary, the spacings for $r = 0.5$ are significantly deviated from Wigner distribution for small N . Such deviations of chaotic spectrum from the RMT predicted universality need detailed investigations in future.

5.4 Quasienergy states and phase space

5.4.1 Information entropy

In this section we study the behaviour of the quasienergy states in different parametric regimes. We quantify the states using information entropies both in position and momentum

basis. Entropies in both the basis together are appropriate measures to understand how the eigenstates are influenced by the phase space transitions. Let us define entropies of the eigenstate

$$S_q^j = - \sum_n |\langle n | \phi_j \rangle|^2 \ln |\langle n | \phi_j \rangle|^2 \quad ; \quad S_p^j = - \sum_m |\langle m | \phi_j \rangle|^2 \ln |\langle m | \phi_j \rangle|^2 \quad (5.20)$$

and the normalized average entropy

$$\langle S \rangle_q = \frac{1}{N \ln(N/2)} \sum_j S_q^j \quad ; \quad \langle S \rangle_p = \frac{1}{N \ln(N/2)} \sum_j S_p^j. \quad (5.21)$$

Notice that the average is normalized with the RMT value, which is approximately $\ln(N/2)$ for GOE. Shown in Fig. 5.4 are typical behaviour of the entropies for two cases: $r = 0.5, 1$. For $r = 1$, the momentum entropy initially increases with k until it reaches the maximum which is slightly above the RMT predicted value at $k \approx 5$. For any further increase of k the entropy remains almost constant. On the other hand, entropy in position basis is larger than the RMT value for small k and it decreases with the increase of k . Interestingly, it attains the RMT value at $k \approx 1$. The entropy is minimum at $k \approx 2$ and it settles to the RMT value for $k > 5$.

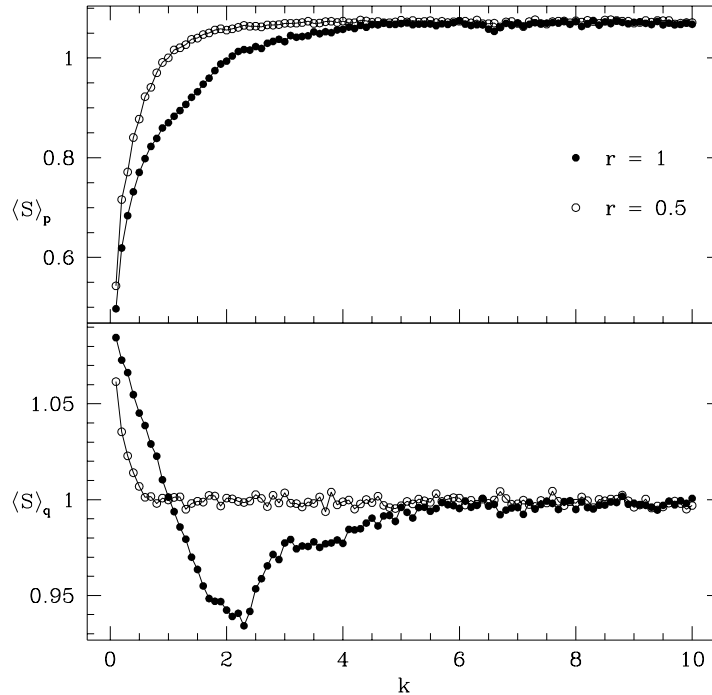


Figure 5.4: Normalized average entropies of the eigenstates for two cases. For this calculation $N = 100$ and β is chosen to be 0.35 to avoid parity symmetry.

As we will see below, quantum spectrum for the regular case is such that many states are associated to the phase space region where there are KAM tori, while only very few states are associated to the resonance region. In this case, average entropy is dominated by the KAM tori states. For small k , lower momentum entropy is due to the KAM states which are highly localized in momentum. However, these states are maximally spread in position resulting the $\langle S \rangle_x$ to be higher than the RMT prediction. As k increases, KAM tori are slowly destroyed and the diffusion in momentum begins. Parallely, more nonlinear resonances emerge in the phase space. This transition causes the increase in $\langle S \rangle_p$ and decrease in $\langle S \rangle_x$ as k increases. For $k > 5$, the phase space is almost completely chaotic and in this regime both the entropies do not show any variations with the parameter. Presence of accelerator modes for $6.28 < k < 7.45$ is not prominently reflected in the average entropies because of the fact that the modes are very small regular regions embedded in the chaotic phase space and also the states corresponding to the modes are very few.

Entropies of the other shown case ($r = 0.5$) also reflect all the complexities of the phase space. In this case the phase space is completely chaotic. For small k the diffusion in momentum is highly limited, presumable due to the cantori; increasing k increases the diffusion. Here we observe that the momentum entropy increases much faster with k and the saturation is reached much earlier than the previous case. On the other hand, for small k , position entropy is higher than the RMT value for which cantori are the responsible classical structures. The position entropy falls to RMT value very rapidly and remains unchanged for any increase of k value.

5.4.2 Coherent-state representation

We now have a close look at some of the eigenstates for different parameters. It is convenient to adopt coherent-state representation for the eigenstates. This gives useful semiclassical description of the quantum states in phase space [110, 111]. The coherent state $|q, p\rangle$ can be constructed using shift operators A and B as

$$|q, p\rangle = A^{-q} B^p |0, 0\rangle \quad (5.22)$$

where q, p are integers and $|0, 0\rangle$ is the minimum uncertainty wave packet located at the origin of the phase space. The above unitary translation provides a coherent-state that is placed at the desired location in the quantized phase space. We follow the method devised in [104] to construct $|0, 0\rangle$ as the ground state of Harper operator:

$$\left[2 - \frac{1}{2}(A + A^\dagger) - \frac{1}{2}(B + B^\dagger) \right] |0, 0\rangle = E_0 |0, 0\rangle. \quad (5.23)$$

Thus any quantum state can be represented in the phase space using the normalized positive definite quantity

$$\mathcal{H}_\phi = \frac{1}{N} |\langle q, p | \phi \rangle|^2 \quad (5.24)$$

which is a discrete equivalence of the Husimi distribution [112].

In the near integrable regime, the spectrum has many doublet states with nearly degenerate eigenvalues. In a given pair, each state corresponds to different parity. All the doublet states belong to the region of phase space where there are KAM tori. Two such states for the standard map are shown in Fig. 5.5. Notice that the quantum states have non-zero intensities both on positive *and* negative p -axis. This is forbidden in the classical system since the standard map has periodic boundary condition in position unlike the well map where the boundary condition is reflective (see Chapter 2). Fig. 5.5 also shows the superpositions of the nearly degenerate states

$$|\psi_\pm\rangle = |\phi_1\rangle \pm i|\phi_2\rangle \quad (5.25)$$

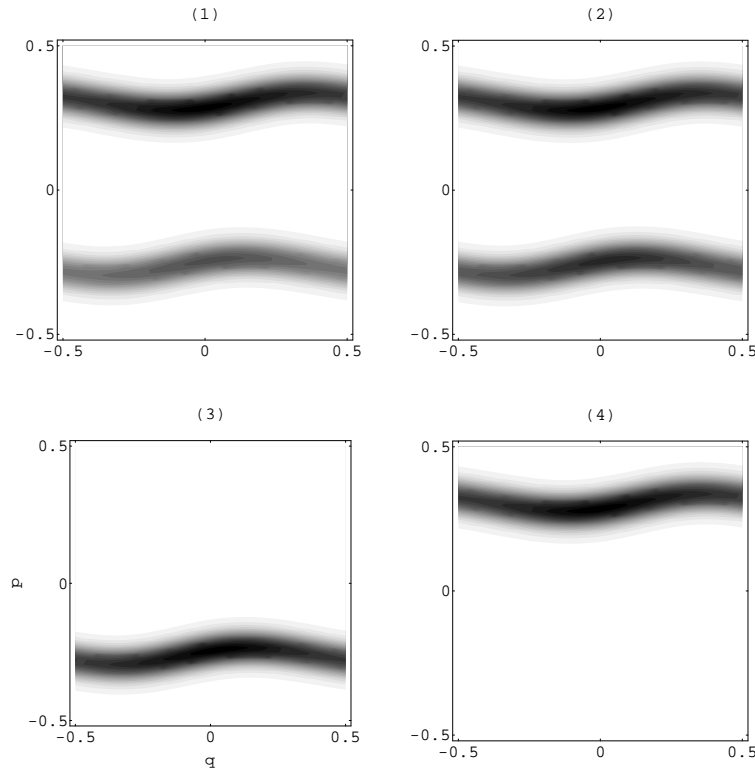


Figure 5.5: Husimi distribution of the quantum states. Intensity of the state is maximum in black shaded region and zero in white background. (1) and (2) correspond to the nearly degenerate states $|\phi_1\rangle$ and $|\phi_2\rangle$ with difference in their quasienergies $\Delta\phi \sim 10^{-12}$. (3) and (4) correspond to the states $|\psi_+\rangle$ and $|\psi_-\rangle$. Here $\beta = 0.5$ and $N = 50$.

that correspond to symmetry related classical KAM tori. This pure quantum behaviour is analogous to the text book problem of barrier tunnelling in symmetric double well system [113]. The analogy is that the states $|\phi_{1,2}\rangle$ are the nearly degenerate energy eigenstates of the double well and the states $|\psi_{\pm}\rangle$ are the non-stationary states localized in one of the wells. With this, the separatrix which demarcates the pair of KAM tori can be thought of as the classical potential barrier. The observed quantum tunnelling between two distinct regular regions of the phase space is called the “dynamical tunnelling” [114]. The tunnelling event in our case is presumably due to coupling of nearly degenerate states which is correlated to the classical resonances [115, 116]. This demonstration emphasizes that the nontrivial tunnelling phenomena can be explored with a simple quantum model like the one we have considered. Very recently, quantized kicked Harper model has been used to study \hbar dependence of the tunnelling splitting in near integrable regimes [117].

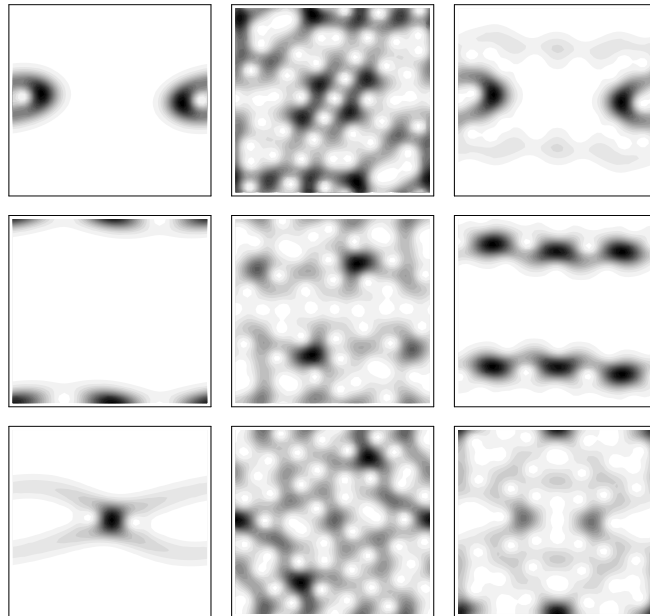


Figure 5.6: *Quasienergy states in different classical regimes. First column: $k = 0.3, r = 1$; second column: $k = 25, r = 1$ and third column: $k = 0.3, r = 0.5$. In all the cases we have taken $\beta = 0.5$ and $N = 50$.*

In Fig. 5.6 we show few of the eigenstates that correspond to different classical regimes. In the nearly integrable regime (first column), one state is localized on the primary resonance; the other on the secondary resonance; the third one is highly localized at the origin which is the unstable fixed point. In the highly chaotic regime (second column), the states have more complicated structures. In the hyperbolic regime (third column), one of the state is very complex while the two other are more localized. This may be due to small values of k .

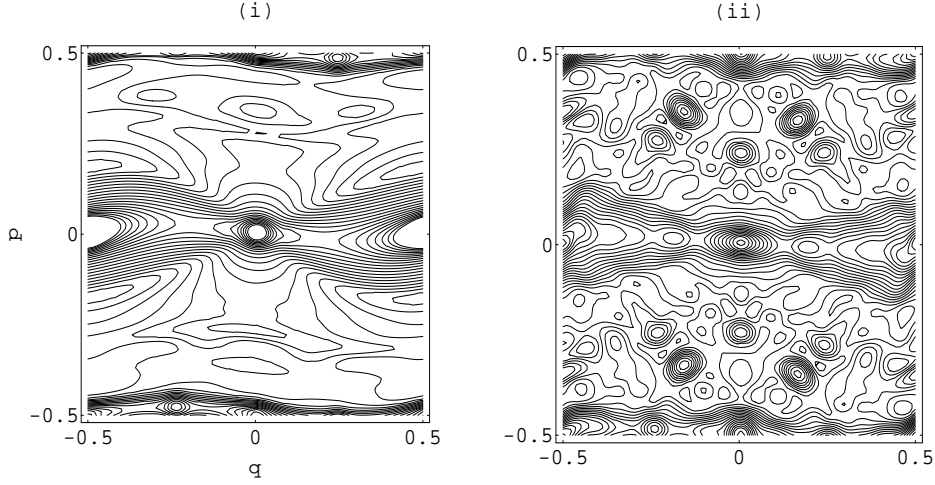


Figure 5.7: Contours of $f(q, p)$ for two cases: (i) $r = 1$ and (ii) $r = 0.5$ with $k = 0.3$. Here $\beta = 0.5$ and $N = 100$.

Further we illustrate the influence of r in the quantized phase space for small k using inverse participation ratio (IPR) which is defined as

$$f(q, p) = \sum_j |\langle q, p | \phi_j \rangle|^4. \quad (5.26)$$

The function $f(q, p)$ is the inverse of number of eigenstates associated with a given phase space region. In Fig. 5.7, number of contours is proportional to the intensity of IPR in a given region. We observe that IPR has very different behaviour for the two classically distinct cases. For nearly regular case (i), very few eigenstates are associated to the primary resonance region and many states are associated to the region where there are KAM tori. In (ii) IPR exhibits more complicated structures as the quantum signature of underlying chaotic dynamics.

5.5 Level dynamics

In the studies on chaotic quantum systems, dynamics of quantum levels in parameter space reflects many of the classical complexities. In particular, the levels do cross each other if the system is regular while they avoid such crossings if the system is chaotic in the classical limit. The level dynamics is mainly characterized by level velocity wherein the system parameter plays the role of pseudo-time. The notion of curvature i.e., second derivative of the levels with respect to the parameter, is introduced in [118] to quantify the avoided crossing. It is shown that the curvature distribution of the chaotic system exhibits universal behaviour [119].

This universality has been tested for various complex quantum systems [120]. Recently it is shown that the variance of the level velocity is equivalent to diffusion coefficient of the action velocity that corresponds to long periodic orbits [121]. In the same work it is also observed that, even in highly chaotic regime RMT fails to capture detail behaviour of the velocity variance in parametric space. These details are found to be important for semiclassical analysis. In this section some statistical properties of the level velocities are exploited to characterize chaotic quantum system.

5.5.1 Level velocities and RMT predictions

In what follows we take $\beta = 0.35$ so that R -symmetry is broken in the quantum system. For convenience we ignore the factor β in the following expressions. The quasienergies $\phi_j \equiv \phi_j(k, r)$ have the scaled velocities:

$$\begin{aligned}
x_j &= \left(\frac{2\pi^2 r^2}{N} \right) \frac{\partial \phi_j}{\partial k} \\
&= \left(\frac{2\pi^2 r^2}{N} \right) \left[\frac{1}{\hbar} \langle \phi_j | \partial V / \partial k | \phi_j \rangle \right] \\
&= \pi r \sum_n \cos(2\pi r n / N) |\langle n | \phi_j \rangle|^2
\end{aligned} \tag{5.27}$$

and

$$\begin{aligned}
y_j &= \left(\frac{2\pi r^2}{Nk} \right) \frac{\partial \phi_j}{\partial r} \\
&= \left(\frac{2\pi r^2}{Nk} \right) \left[\frac{1}{\hbar} \langle \phi_j | \partial V / \partial r | \phi_j \rangle \right] \\
&= -2\pi r \sum_n (n/N) \sin(2\pi r n / N) |\langle n | \phi_j \rangle|^2 - \sum_n \cos(2\pi r n / N) |\langle n | \phi_j \rangle|^2.
\end{aligned} \tag{5.28}$$

The average velocities in the semiclassical limit are

$$\begin{aligned}
\langle x \rangle &= \frac{1}{N} \sum_j x_j = \sin(\pi r) \\
\langle y \rangle &= \frac{1}{N} \sum_j y_j = \cos(\pi r) - \frac{2 \sin(\pi r)}{\pi r}.
\end{aligned} \tag{5.29}$$

The second moment of x is given by

$$\begin{aligned}
\langle x^2 \rangle &= \frac{1}{N} \sum_j x_j^2 \\
&= (\pi r)^2 \left\{ \sum_n \cos^2(2\pi r n/N) \langle |\langle n | \phi_j \rangle|^4 \rangle \right. \\
&\quad \left. + \sum_{n \neq n'} \cos(2\pi r n/N) \cos(2\pi r n'/N) \langle |\langle n | \phi_j \rangle|^2 |\langle n' | \phi_j \rangle|^2 \rangle \right\} \quad (5.30)
\end{aligned}$$

where the relation

$$\sum_n f_n \sum_n g_n = \sum_n f_n g_n + \sum_{n \neq n'} f_n g_{n'} \quad (5.31)$$

has been used in the derivation. Assuming that the average behaviour of the eigenfunction components are independent of the specific position eigenvalues, the term within the angle bracket can be taken out of the sum. The application of the relation (5.31) to the cross terms gives

$$\begin{aligned}
\langle x^2 \rangle &= (\pi r)^2 \left\{ \left[\langle |\langle n | \phi_j \rangle|^4 \rangle - \langle |\langle n | \phi_j \rangle|^2 |\langle n' | \phi_j \rangle|^2 \rangle \right] \sum_n \cos^2(2\pi r n/N) \right. \\
&\quad \left. + \langle |\langle n | \phi_j \rangle|^2 |\langle n' | \phi_j \rangle|^2 \rangle \left[\sum_n \cos(2\pi r n/N) \right]^2 \right\}. \quad (5.32)
\end{aligned}$$

Note that, in chaotic regimes the standard RMT results [122]

$$\begin{aligned}
\langle |\langle n | \phi_j \rangle|^4 \rangle &= 3[N(N+2)]^{-1} \simeq 3N^{-2} \\
\langle |\langle n | \phi_j \rangle|^2 |\langle n' | \phi_j \rangle|^2 \rangle &= [N(N+2)]^{-1} \simeq N^{-2}
\end{aligned} \quad (5.33)$$

which correspond to Gaussian orthogonal ensemble are applicable here as well. We may notice that applying these RMT results essentially adopt the assumption made above. On replacing the sum by integration in semiclassical limit we arrive to

$$\langle x^2 \rangle_{\text{RMT}} = \frac{(\pi r)^2}{N} \left[1 + \frac{\sin(2\pi r)}{2\pi r} \right] + \langle x \rangle^2. \quad (5.34)$$

Similarly the second moment of y is

$$\begin{aligned}
\langle y^2 \rangle &= \frac{1}{N} \sum_j y_j^2 \\
&= \sum_n \{ [2\pi r(n/N) \sin(2\pi r n/N)]^2 + \cos^2(2\pi r n/N) \\
&\quad + 4\pi r(n/N) \sin(2\pi r n/N) \cos(2\pi r n/N) \} \langle |\langle n | \phi_j \rangle|^4 \rangle \\
&\quad + \sum_{n \neq n'} \{ (2\pi r/N)^2 n n' \sin(2\pi r n/N) \sin(2\pi r n'/N) + \cos(2\pi r n/N) \cos(2\pi r n'/N) \\
&\quad + 4\pi r(n/N) \sin(2\pi r n/N) \cos(2\pi r n'/N) \} \langle |\langle n | \phi_j \rangle|^2 |\langle n' | \phi_j \rangle|^2 \rangle . \tag{5.35}
\end{aligned}$$

As before we can write down the RMT approximated second moment of y as

$$\langle y^2 \rangle_{\text{RMT}} = \frac{1}{N} \left\{ 1 + \frac{(\pi r)^2}{3} + \frac{\sin(2\pi r)}{2\pi r} \left[\frac{5}{2} - (\pi r)^2 \right] - \frac{3}{2} \cos(2\pi r) \right\} + \langle y \rangle^2 . \tag{5.36}$$

We also have

$$\begin{aligned}
\langle xy \rangle &= \frac{1}{N} \sum_j x_j y_j \\
&= - \sum_n f(n) \cos(2\pi r n/N) \langle |\langle n | \phi_j \rangle|^4 \rangle \\
&\quad - \sum_{n \neq n'} f(n) \cos(2\pi r n'/N) \langle |\langle n | \phi_j \rangle|^2 |\langle n' | \phi_j \rangle|^2 \rangle \tag{5.37}
\end{aligned}$$

where

$$f(n) = \pi r \{ (2\pi r n/N) \sin(2\pi r n/N) + \cos(2\pi r n/N) \} .$$

Repeating the above procedure we get

$$\langle xy \rangle_{\text{RMT}} = \frac{\pi r}{2N} \left[\cos(2\pi r) - \frac{3 \sin(2\pi r)}{2\pi r} - 2 \right] + \langle x \rangle \langle y \rangle . \tag{5.38}$$

In general, quantum eigenfunctions in the chaotic regimes are such that the quantities in (5.33) fluctuate about the respective RMT values. It is worth noting that the RMT values ignore basis dependent fluctuations. These fluctuations are in fact crucial for the quantities like second

moments of the level velocities. Here we may enquire whether the fluctuations that are ignored by the RMT are significant or not. To answer this, let us first write down the equations:

$$\langle x^2 \rangle_{\text{RMT}} = \langle x^2 \rangle + \delta_x ; \quad \langle y^2 \rangle_{\text{RMT}} = \langle y^2 \rangle + \delta_y ; \quad \langle xy \rangle_{\text{RMT}} = \langle xy \rangle + \delta_{xy} \quad (5.39)$$

where δ_i are deviations of the RMT approximated quantities from the corresponding actual values. Defining absolute normalized deviations as

$$\Delta_x = \left| \frac{\delta_x}{\langle x^2 \rangle} \right| ; \quad \Delta_y = \left| \frac{\delta_y}{\langle y^2 \rangle} \right| ; \quad \Delta_{xy} = \left| \frac{\delta_{xy}}{\langle xy \rangle} \right| \quad (5.40)$$

we average all the three positive quantities as

$$\Delta = \frac{\Delta_x + \Delta_y + \Delta_{xy}}{3} . \quad (5.41)$$

Here the single quantity Δ would validate the RMT approximations (5.33). One would expect the above quantity be large for regular/mixed regimes, where the RMT is not applicable, and nearly zero for highly chaotic regimes. The above quantity is calculated for various parameters and plotted in Fig. 5.8. We observe that Δ is nearly zero *only* for $r \leq 1/2$ in all the cases. On the other hand, Δ is large even for some parametric values that correspond to non-hyperbolic chaotic regimes.

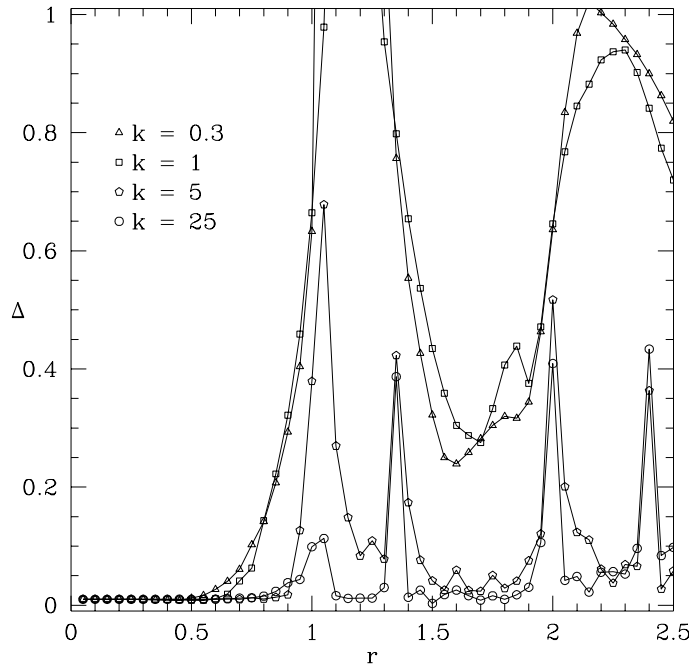


Figure 5.8: Deviation Δ for different parameters with $N = 200$.

In Fig. 5.9, the deviations are plotted for two distinct cases. For $r = 1$, the deviation exhibits many oscillations with k . It is noticeable that the first two prominent peaks appear around $r = 2\pi, 4\pi$ respectively and for which there are accelerator modes in the phase space. These deviations are even larger than those which occur in the mixed regime ($k < 5$). On contrary, for $r = 0.5$, where the classically system is hyperbolic, the deviation is almost independent of k and remains close to zero.

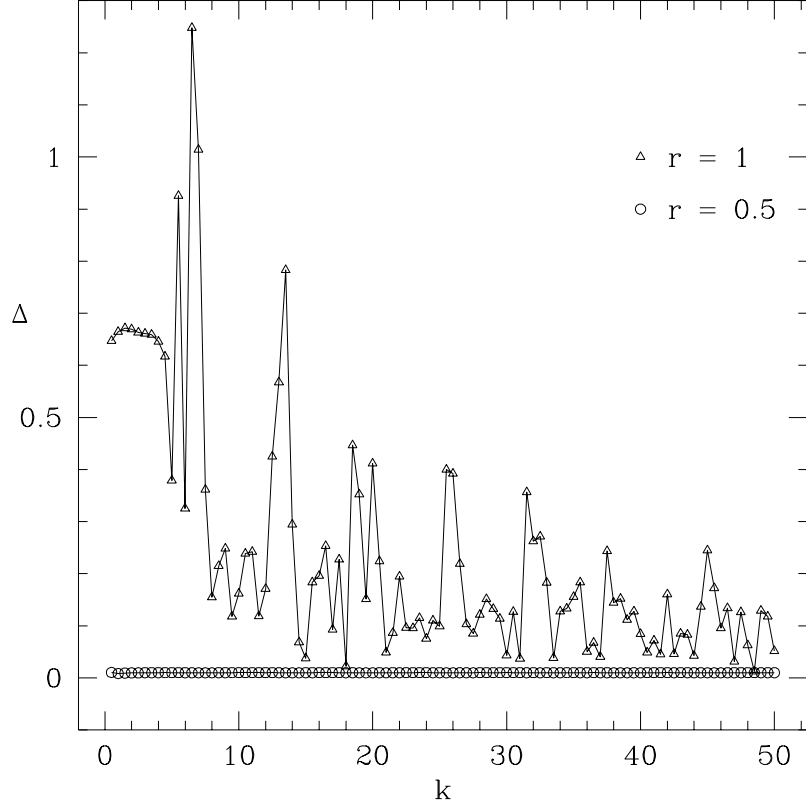


Figure 5.9: *Deviation in the RMT approximated second moments of the level velocities for two cases with $N = 200$.*

These results indicate that even in highly chaotic regimes, basis dependent fluctuations of the spectrum averaged eigenfunction properties are significant. These fluctuations may reflect many finer details of the chaotic quantum states. On the other hand, in the hyperbolic regime ($r \leq 1/2$), the approximations in (5.33) are quite satisfactory. However, we have not observed any qualitative difference between fluctuations that correspond to hyperbolic regimes and those of other highly chaotic regimes. These observations collectively support that, basis dependent fluctuations of some of the spectrum averaged eigenstate properties about their RMT predictions are significant for non-hyperbolic chaotic regimes but *not* for the hyperbolic regimes.

5.5.2 Correlation of level velocities

Now we enquire the correlation between two level velocities x and y . The correlation coefficient between them is

$$\gamma = \frac{\sigma_{xy}}{\sigma_x \sigma_y} \quad (5.42)$$

where

$$\sigma_x^2 = \langle x^2 \rangle - \langle x \rangle^2 ; \quad \sigma_y^2 = \langle y^2 \rangle - \langle y \rangle^2 ; \quad \sigma_{xy} = \langle xy \rangle - \langle x \rangle \langle y \rangle .$$

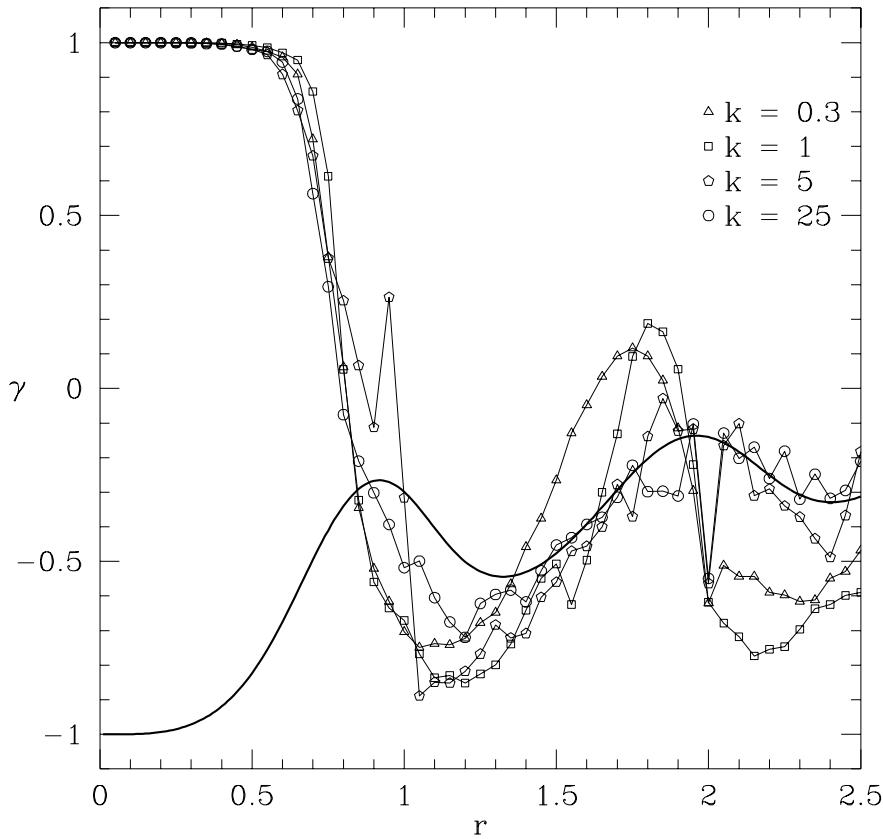


Figure 5.10: *Correlation coefficient between the two level velocities with $N = 200$. Thick smooth curve is the RMT predicted correlation.*

The level velocity correlation has been calculated for various parameters and the results are shown in Fig. 5.10. We find that only in the hyperbolic regime ($r \leq 1/2$), the two level velocities are perfectly correlated, i.e., $\gamma = 1$. We have already shown that the RMT approximations

are valid in this regime, and the RMT predicted velocity correlation can be calculated by applying the equations (5.34), (5.36) and (5.38) in (5.42). As we see from Fig. 5.10, the RMT predicted correlation completely fails to agree with the observed correlation. At first sight this disagreement may look strange. However, the following analysis reveals the reason for this discrepancy. Let us now define three quantities

$$\Delta'_x = \left| \frac{\delta_x}{\sigma_x^2} \right| ; \quad \Delta'_y = \left| \frac{\delta_y}{\sigma_y^2} \right| ; \quad \Delta'_{xy} = \left| \frac{\delta_{xy}}{\sigma_{xy}} \right| \quad (5.43)$$

and the average of them is

$$\Delta' = \frac{\Delta'_x + \Delta'_y + \Delta'_{xy}}{3} . \quad (5.44)$$

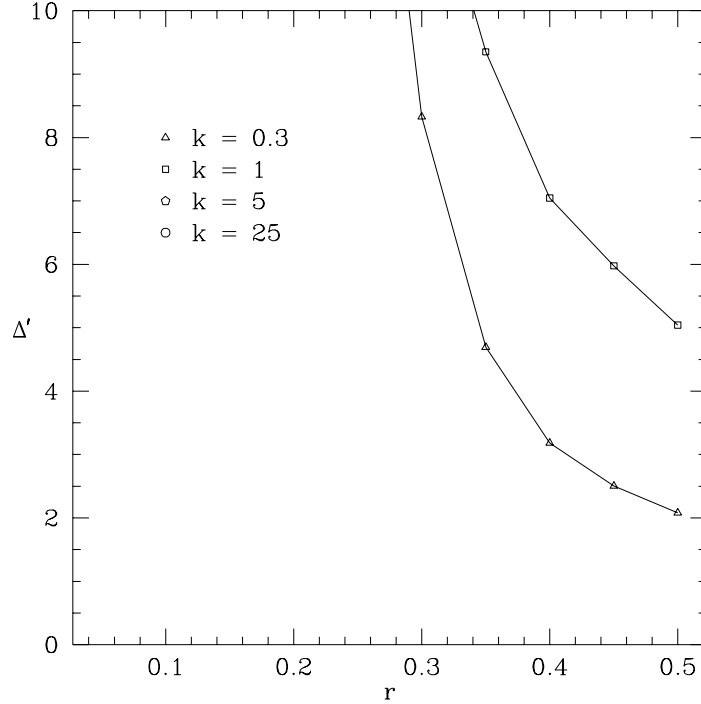


Figure 5.11: The quantity Δ' is plotted for $r \leq 1/2$ with $N = 200$. Notice that two sets of data are beyond the range shown here.

Fig. 5.11 shows that Δ' diverges. That is, the quantities in Eqn. (5.43) diverge for $r \leq 1/2$ while the quantities in Eqn. (5.40) are close to zero. This implies that the denominators in Eqn. (5.43) are very small. In other words, $\langle x^2 \rangle \approx \langle x \rangle^2$, $\langle y^2 \rangle \approx \langle y \rangle^2$ and $\langle xy \rangle \approx \langle x \rangle \langle y \rangle$ for $r \leq 1/2$. This can also be seen from the RMT approximations (5.34), (5.36) and (5.38) in the limit $N \rightarrow \infty$. In fact, convergence of the approximations to the actual values of the second

moments in the limit $N \rightarrow \infty$ is not fast enough to resolve very small variances. Here the finiteness of N plays crucial role. Thus, although the RMT predictions for the second moments are valid for $r \leq 1/2$, this approximation is not applicable for the variance and hence for the correlation of level velocities.

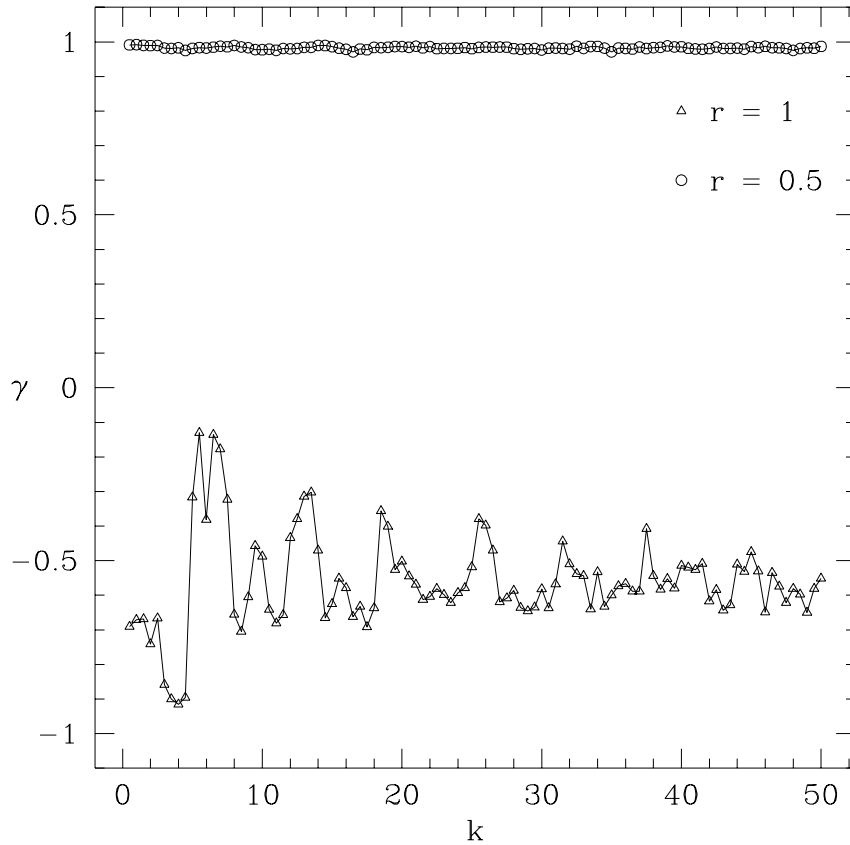


Figure 5.12: Correlation coefficient, with $N = 200$, between the two velocities x and y for two cases.

Shown in Fig. 5.12 are the correlation coefficient for two cases. For $r = 0.5$ the coefficient remains unity as k varies and thus showing that perfect correlation is independent of strength of the nonlinear perturbation. On the other hand, for $r = 1$ the coefficient oscillates with k but never becomes unity. These results confirm that, *only* in hyperbolic regime ($r \leq 1/2$) the velocities are *fully* correlated.

5.6 Summary

In this Chapter we have quantized GSM on 2-torus as a model system of a chaotic quantum system and presented detailed numerical analysis on the quantum spectrum. Unlike the diffusive system, nearest neighbour spacing distribution of quantum levels are sensitive to the underlying classical dynamics. In semiclassical limit, RMT predicted spacing distribution is found to be an unequivocal signature of quantum chaos. We have also studied quantum phase space transitions as the classical system undergo transition to chaos in different regimes.

The GSM is a rare class of dynamical systems which has both hyperbolic and non-hyperbolic chaotic regimes. This provided an opportunity to investigate these two regimes in the corresponding quantum system. It is found that basis dependent fluctuations in some of the spectral averaged properties of the quantum states are significant in non-hyperbolic chaotic regimes. On contrary, the fluctuations are insignificant in hyperbolic regimes. This new characterization of the chaotic quantum system is achieved using level dynamics statistics. More over, the level velocities are found to be perfectly correlated *only* in the hyperbolic regimes.

Epilogue

This thesis is an attempt to uncover transition to chaos and the corresponding quantum signatures for externally driven particle in square well potential. The external driving force could be an electromagnetic field. It is worth remarking that presence of reflective boundary walls of the well causes the particle to experience discontinuous or at least non-smooth force. Hence classical dynamics of the particle and the underlying transition to chaos could be beyond the purview of the celebrated theorems on dynamical systems *viz.* KAM theorem and Poincaré-Birkhoff (PB) theorem. Naturally the emerging scenario is important from dynamical point of view. Implications of this scenario in the quantum system are also of great significance as semiconductor quantum wells have opened up new avenues for the experimental study of quantum chaos. As our results have been summarized at the end of each chapter, here we delineate some of the salient aspects of the problems addressed in the thesis with future prospects indicated.

In this thesis we have introduced a simple model which consists of a particle within an one-dimensional infinite square well potential in presence of time periodic impulsive external field. This system is exhaustively studied with the corresponding kick-to-kick dynamics. Albeit simple, the model emerges as an instructive one as it shares variety of dynamical features with the above mentioned class of systems. Classically and quantum mechanically this model is one generalization of the delta kicked rotor. To be specific, it is equivalent to the kicked rotor when the length scales of the system *viz.* width of the well and wavelength of the external field, match. If the length scales do *not* match, the classical system displays non-KAM scenario of transition to chaos. A simple stability theory is found to be sufficient to have fair understanding of ostensibly non-trivial scenario. With an illustration we have also shown an alternative to the PB scenario. This deserves a qualitative study in future. We would like to emphasize that the classical system is a rare family of dynamical systems as it possesses both hyperbolic *and* non-hyperbolic chaotic regimes.

When the length scales do *not* match, even for weak field strength there are possibilities of chaos assisted diffusion in momentum of the particle. Quantum mechanically this is manifested as delocalization of eigenstates in momentum space. Thus we realize the competing length scales as control parameters for the localization in the weak field regime. We have also demonstrated the possibility of observing such effects in the quantum system. We believe that these *new* effects can also be observed in finite quantum well system, and it is highly desirable if they are experimentally tested. One of the promising extensions of the present work is to unfold the role of length scales in tunnelling and ionization phenomena of the finite well system. We have shown that the distribution of localization measure of the eigenstates is sensitive to

the underlying classical dynamics. To be specific, in chaotic regime participation ratios of the eigenstates in unperturbed basis are lognormally distributed - a *new* measure of quantum chaos. This empirical observation requires an appropriate theoretical support.

In this thesis we have also introduced a new quantum map as a simple model of quantum chaos. Although the field of quantum chaos is populated with many models, one of the main advantages of this model over other models is that it provides an *unique* opportunity to distinguish hyperbolic and non-hyperbolic chaotic regimes in the quantum domain. Some of our results indicate that spectral averaged behaviour of quantum states are different in both the regimes. In particular, basis dependent fluctuations of the states are insignificant *only* in the hyperbolic chaotic regimes but not in the non-hyperbolic chaotic regimes. This new characterization of chaotic quantum system demands detailed study using semiclassical theory.

Bibliography

- [1] Pierre Simon de Laplace, *A Philosophical Essay on Probabilities*, Dover, New York, 1951.
- [2] James Gleick, *Chaos - making a new science*, p. 321, Vintage, 1998.
- [3] Edward N. Lorenz, *J. Atmos. Sci.* **20**, 130 (1963).
- [4] Robert M. May, *Nature* **261**, 459 (1976).
- [5] T-Y. Li and James A. Yorke, *Amer. Math. Monthly*, **82**, 985 (1975).
- [6] Robert L. Devaney, *An Introduction to Chaotic Dynamical Systems*, Addison-Wesley, 1987.
- [7] J. Banks, J. Brooks, G. Cairns, G. Davis and P. Stacey, *Amer. Math. Monthly*, p. 332, April 1992.
- [8] V.I. Arnold, *Mathematical Methods of Classical Mechanics*, Springer-Verlag, New York, 1989.
- [9] M. Hénon and C. Heiles, *Astron. J.* **69**, 73 (1964).
- [10] M. Toda, *Suppl. Prog. Theor. Phys. No. 45*, 174 (1970).
- [11] A.C. Scott, F.Y.F. Chu and D.W. Mclaughlin, *Proc. IEEE* **61**, 1443 (1973).
- [12] J. Ford, S.D. Stoddard and J.S. Turner, *Prog. Theor. Phys.* **50**, 1547 (1973).
- [13] G. Casati and J. Ford, *Phys. Rev. A* **12**, 1702 (1975).
- [14] H.D. Meyer, *J. Chem. Phys.* **84**, 3147 (1986).
- [15] D. Wintgen and H. Friedrich, *Phys. Rev. A* **36**, 131 (1987).
- [16] H. Friedrich and D. Wintgen, *Phys. Rep.* **183**, 37 (1989).
- [17] M.V. Berry, *Eur. J. Phys.* **2**, 91 (1981).
- [18] Ya. G. Sinai. *Russ. Math. Surv.* **25**, 137 (1970).
- [19] L.A. Bunimovich, *Funct. Anal. Appl.* **8**, 254 (1974); *Commun. Math. Phys.* **65**, 295 (1979).

- [20] A. Einstein, Verh. Deut. Phys. Ges. **19**, 82 (1917); L. Brillouin, J. Phys. Radium **7**, 353 (1926); J.B. Keller, Ann. Phys. **4**, 180 (1958).
- [21] M.C. Gutzwiller, J. Math. Phys. **8**, 1979 (1967); **10**, 1004 (1969); **11**, 1791 (1970); **12**, 343 (1971).
- [22] R. Balian and C. Bloch, Ann. Phys. **60**, 401 (1970); **64**, 271 (1971); **69**, 76 (1972); **85**, 514 (1974).
- [23] M.V. Berry, in *Chaotic Behaviour of Deterministic Systems (Les Houches Lectures 36)*, G. Iooss, R.H.G. Hellman and R. Stora (eds.), p. 171, North-Holland Publishing Company, 1983.
- [24] Ya.G. Sinai, *Introduction to Ergodic Theory*, Princeton University Press, Princeton, 1976.
- [25] D. Wintgen, Phys. Rev. Lett. **58**, 1589 (1987).
- [26] A. Holle, J. Main, G. Wiebusch, H. Rottke and K.H. Welge, Phys. Rev. Lett. **61**, 161 (1988).
- [27] H.-J. Stöckmann, J. Stein and M. Kollmann in *Quantum Chaos: Between order and disorder*, G. Casati and B. Chirikov (eds.) p. 661, Cambridge University Press, Cambridge, 1995.
- [28] T.M. Fromhold, P.B. Wilkinson, F.W. Sheard, L. Eaves, J. Miao and G. Edwards, Phys. Rev. Lett. **75**, 1142 (1995).
- [29] I.C. Percival, J. Phys. B **6**, L229 (1973).
- [30] E. Wigner, Phys. Rev. **40**, 749 (1932).
- [31] M.V. Berry, Phil. Trans. R. Soc. A **287**, 237 (1977).
- [32] A. Voros, Ann. Inst. Henri Poincaré A **24**, 31 (1976); **26**, 343 (1977); in *Stochastic Behaviour in Classical and Hamiltonian Systems*, G. Casati and J. Ford (eds.), Lecture Notes in Physics Vol. 93, p. 326, Springer-Verlag, Berlin, 1979.
- [33] M.V. Berry, J. Phys. A **10**, 2083 (1977).
- [34] A.I. Shnirelman, Usp. Mat. Nauk. **29**, 181 (1974).
- [35] E.J. Heller, Phys. Rev. Lett. **53**, 1515 (1984).
- [36] E.B. Bogomolny, Physical D **31**, 169 (1988).

- [37] M.V. Berry, Proc. R. Soc. Lond. A **423**, 219 (1989).
- [38] R.L. Waterland, J.M. Yuan, C.C. Martens, R.E. Gillilan and W.P. Reinhardt, Phys. Rev. Lett. **61**, 2733 (1988).
- [39] D. Wintgen and A. Hönig, Phys. Rev. Lett. **63**, 1467 (1989).
- [40] S. Sridhar, Phys. Rev. Lett. **67**, 785 (1991).
- [41] P.B. Wilkinson, T.M. Fromhold, L. Eaves, F.W. Sheard, N. Miura and T. Takamasu, Nature **380**, 608 (1996).
- [42] M.V. Berry and M. Tabor, Proc. R. Soc. Lond. A **356**, 375 (1977).
- [43] O. Bohigas, M.J. Giannoni and C. Schmit, Phys. Rev. Lett. **52**, 1 (1984); J. Phys. Lett. **45**, L1015 (1984).
- [44] C.E. Porter (ed.), *Statistical Theories of Spectra: Fluctuations*, Academic Press, New York, 1965; M.L. Mehta, *Random Matrices and Statistical Theory of Energy Levels*, Academic Press, New York, 1967.
- [45] D. Delande and J.C. Gay, Phys. Rev. Lett. **57**, 2006 (1986).
- [46] H.-J. Stockmann and J. Stein, Phys. Rev. Lett. **64**, 2215 (1990).
- [47] G. Casati, B.V. Chirikov, F.M. Izrailev and J. Ford in *Stochastic Behaviour in Classical and Hamiltonian Systems*, G. Casati and J. Ford (eds.), Lecture Notes in Physics Vol. 93, p. 334, Springer-Verlag, Berlin, 1979.
- [48] B.V. Chirikov, Phys. Rep. **52**, 263 (1979).
- [49] B.V. Chirikov, Rev. Plasma Phys. **13**, 1 (1987).
- [50] R.V. Jensen, J.G. Leopold and D. Richards, J. Phys. B **21**, L527 (1988).
- [51] B.V. Chirikov in *Chaos and Quantum Physics*, M.-J. Giannoni, A. Voros and J. Zinn-Justin (eds.), Les Houches, North-Holland, 1989; F.M. Izrailev, Phys. Rep. **196**, 299 (1990).
- [52] B.V. Chirikov, F.M. Izrailev and D.L. Shepelyansky, Sov. Sci. Rev. C **2**, 209 (1981).
- [53] P.W. Anderson, Phys. Rev. **109**, 1492 (1958).
- [54] S. Fishman, D.R. Grempel and R.E. Prange, Phys. Rev. Lett. **49**, 509 (1982); D.R. Grempel, R.E. Prange and S. Fishman, Phys. Rev. A **29**, 1639 (1984).

- [55] F.L. Moore, J.C. Robinson, C.F. Bharucha, Bala Sundaram and M.G. Raizen, Phys. Rev. Lett. **75**, 4598 (1995).
- [56] S. Chu, Science **253**, 861 (1991).
- [57] J.E. Bayfield and P.M. Koch, Phys. Rev. Lett. **33**, 258 (1974); J.E. Bayfield, L.D. Gardner and P.M. Koch, Phys. Rev. Lett. **39**, 76 (1977).
- [58] J.E. Bayfield, G. Casati, I. Guarneri and D.W. Sokol, Phys. Rev. Lett. **63**, 364 (1989).
- [59] R. Graham, M. Schlautmann and P. Zoller, Phys. Rev. A **45**, R19 (1992).
- [60] J.C. Robinson, C. Bharucha, F.L. Moore, R. Jahnke, G.A. Georgakis, Q. Niu and M.G. Raizen, Phys. Rev. Lett. **74**, 3963 (1995).
- [61] W.A. Lin and L.E. Reichl, Physica D **19**, 145 (1986)
- [62] T. Hogg and B.A. Huberman, Phys. Rev. Lett. **48**, 711 (1982); Phys. Rev. A **28**, 22 (1983); Physica Scripta **30**, 225 (1984).
- [63] B. Hu, B. Li, J. Liu and Y. Gu, Phys. Rev. Lett. **82**, 4224 (1999).
- [64] J.D. Meiss., Rev. Mod. Phys. **64**, 795 (1992).
- [65] L.E. Reichl, *The Transition to Chaos, In Conservative Classical Systems: Quantum Manifestations*, Springer-Verlag, New York, 1992.
- [66] S.J. Shenker and L.P. Kadanoff, J. Stat. Phys. **27** (4), 631 (1982).
- [67] J.M. Greene, J. Math. Phys. **20**, 1183 (1979).
- [68] M.-J. Giannoni, A. Voros, and J. Zinn-Justin (eds.), *Chaos and Quantum Physics*, Les Houches LII, North-Holland, 1991.
- [69] Edward Ott, *Chaos in Dynamical Systems*, Cambridge University Press, 1997.
- [70] John R. Cary and James D. Meiss, Phys. Rev. A **24**, 2664 (1981).
- [71] Q. Chen, I. Dana, J. D. Meiss, and I. C. Percival, Physica D **46**, 217 (1990).
- [72] V.I. Arnold and A. Avez, *Ergodic Problems of Classical Mechanics*, 1968.
- [73] P. Gaspard, M.E. Briggs, M.K. Francis, J.V. Sengers, R.W. Gammon, J.R. Dorfman and R.V. Calabrese, Nature **394**, 865 (1998).

- [74] P. Gaspard in *Nonlinear Dynamics and Computational Physics*, V.B. Sheorey (ed.), Narosa Publishing House, New Delhi, 1999.
- [75] F. Reif, *Fundamentals of Statistical and Thermal Physics*, McGraw-Hill, 1985.
- [76] M.F. Shlesinger, G.M. Zaslavsky and J. Klafter, *Nature* **363**, 31 (1993).
- [77] J. Klafter, M.F. Shlesinger and G. Zumofen, *Phys. Today* **49** (2), 33 (1996).
- [78] M.F. Shlesinger, G.M. Zaslavsky and U. Frish (eds.), *Lévy Flights and Related Topics in Physics*, Springer-Verlag, 1995.
- [79] G.M. Zaslavsky and B.A. Niyazov, *Phys. Rep.* **283**, 73 (1997).
- [80] S. Benkadda, Y. Elskens and B. Ragot, *Phys. Rev. Lett.* **72**, 2859 (1994).
- [81] A.B. Rechester and R.B. White, *Phys. Rev. Lett.* **44**, 1586 (1980); A.B. Rechester, M.N. Rosenbluth and R.B. White, *Phys. Rev. A* **23**, 2664 (1981).
- [82] D.W. Jordon and P. Smith, *Nonlinear Ordinary Differential Equations*, Oxford, 1977.
- [83] Ya.B. Zel'dovich, *Zh. Eksp. Teor. Fiz.* **51**, 1492 (1966) [*Sov. Phys. JETP* **24**, 1006 (1967)].
- [84] H. Sambe, *Phys. Rev. A* **7**, 2203 (1973).
- [85] M. Abramowitz and I.A. Stegun (eds.), *Handbook of Mathematical Functions*, p. 360, Dover Publications, New York, 1965.
- [86] F.M. Izrailev and D.L. Shepelyanskii, *Sov. Phys. Dokl.* **24** (12), 996 (1979); *Teor. Mat. Fiz.* **43**, 417 (1980) [*Theor. Math. Phys.* **43**, 553 (1980)].
- [87] W.H. Oskay, D.A. Steck, V. Milner, B.G. Klappauf and M.G. Raizen, *Opt. Commun.* **179**, 137 (2000); M.B. d'Arcy, R.M. Godun, M.K. Oberthaler, D. Cassettari and G.S. Summy, *Phys. Rev. Lett.* **87**, 074102 (2001).
- [88] G. Casati and B. Chirikov in *Quantum Chaos: Between order and disorder*, Eds. G. Casati and B. Chirikov, Cambridge University Press, 1995. For Renyi information refer: A. Renyi, *Probability Theory*, North Holland, Amsterdam, 1970.
- [89] D.L. Shepelyansky, *Phys. Rev. Lett.* **56**, 677 (1986); *Physica D* **28**, 103 (1987).
- [90] J. Aitchison and J.A.C Brown, *Lognormal Distribution: With special reference to its uses in Economics*, Cambridge University Press, 1957.

- [91] O.A. Starykh, P.R.J. Jacquod, E. Narimanov and A.D. Stone, *Phys. Rev. E* **62**, 2078 (2000).
- [92] F. Borgonovi, *Phys. Rev. Lett.* **80**, 4653 (1998).
- [93] C.F.F. Karney, *Physica D* **8**, 360 (1983).
- [94] R. Ishizaki, T. Horita, T. Kobayashi and H. Mori, *Prog. Theor. Phys.* **85** (5), 1013 (1991); Y.H. Ichikawa, T. Kamimura and T. Hatori, *Physica* **29 D**, 247 (1987); G. Zumofen and J. Klafter, *Europhys. Lett.* **25** (8), 565 (1994).
- [95] P. Lebœuf, *Physica D* **116**, 8 (1998).
- [96] J.D. Hanson, E. Ott and T.M. Antonsen Jr., *Phys. Rev. A* **29**, 819 (1984).
- [97] Bala Sundaram and G.M. Zaslavsky, *Phys. Rev. E* **59**, 7231 (1999).
- [98] B.G. Klappauf, W.H. Oskay, D.A. Steck and M.G. Raizen, *Phys. Rev. Lett.* **81**, 4044 (1999).
- [99] M.K. Oberthaler, R.M. Godum, M.B. d'Arcy, G.S. Summy and K. Burnett, *Phys. Rev. Lett.* **83**, 4447 (1999).
- [100] M. Abramowitz and I.A. Stegun (eds.), *Handbook of Mathematical Functions*, p. 303, Dover Publications, New York, 1965.
- [101] M. Abramowitz and I.A. Stegun (eds.), *Handbook of Mathematical Functions*, p. 297, Dover Publications, New York, 1965.
- [102] W. Gautschi, *SIAM J. Numer. Anal.* **7** (1), 187 (1970).
- [103] N.L. Balazs and A. Voros, *Ann. Phys.* **190**, 1 (1989); A. Lakshminarayan, *Ann. Phys.* **239**, 272 (1995).
- [104] M. Saraceno, *Ann. Phys.* **199**, 37 (1990).
- [105] A. Lakshminarayan, *Phys. Lett. A* **192**, 345 (1994); A. Lakshminarayan and N.L. Balazs, *Chaos, Fractals and Solitons*, Vol. 5, No. 7, p. 1169 (1995).
- [106] A. Lakshminarayan, *Pramana - J. Phys.* **48**, 517 (1997).
- [107] J. Ford, G. Mantica and G.H. Ristow, *Physica D* **50**, 493 (1991).
- [108] S. Lang, *Algebraic Number Theory*, Addison-Wesley, New York, 1970.

- [109] J.H. Hannay and M.V. Berry, *Physica D* **1**, 267 (1980).
- [110] J. Kurchan, P. Lebœuf and M. Saraceno, *Phys. Rev. A* **40**, 6800 (1989).
- [111] A. Voros, *Phys. Rev. A* **40**, 6814 (1989).
- [112] K. Husimi, *Proc. Phys. Math. Soc. Jpn.* **22**, 264 (1940); K. Takahashi, *Prog. Theor. Phys. Suppl. No. 98*, 109 (1989).
- [113] D. ter Haar (ed.), *Problems in Quantum Mechanics*, p. 13, Pion, London, 1975; J.J. Sakurai, *Modern Quantum Mechanics*, p. 256, Addison-Wesley, 1994.
- [114] M.J. Davis and E.J. Heller, *J. Chem. Phys.* **75**, 246 (1981).
- [115] T. Uzer, D.W. Noid and R.A. Marcus, *J. Chem. Phys.* **79**, 4412 (1983).
- [116] A.M. Ozario de Almeida, *J. Phys. Chem.* **88**, 6139 (1984).
- [117] O. Brodier, P. Schlagheck and D. Ullmo, *Phys. Rev. Lett.* **87**, 064101 (2001).
- [118] P. Gaspard, S.A. Rice, and K. Nakamura, *Phys. Rev. Lett.* **63**, 930 (1989).
- [119] P. Gaspard, S.A. Rice, H.J. Mikeska and K. Nakamura, *Phys. Rev. A* **42**, 4015 (1990).
- [120] D. Saher and F. Haake, *Phys. Rev. A* **44**, 7481 (1991); T. Takami and H. Hasegawa, *Phys. Rev. Lett.* **68**, 419 (1992); J. Zakrzewski and D. Delande, *Phys. Rev. E* **47**, 1650 (1993).
- [121] A. Lakshminarayan, N.R. Cerruti and S. Tomsovic, *Phys. Rev. E* **60**, 3992 (1999).
- [122] T.A. Brody, J. Flores, J.B. French, P.A. Mello, A. Pandey, and S.S.M. Wong, *Rev. Mod. Phys.* **53**, 385 (1981).
-

List of Publications

1. Chaos in a well: effects of competing length scales, *R. Sankaranarayanan*, A. Lakshminarayan and V.B. Sheorey, Phys. Lett. A **279**, 313 (2001).
 2. Quantum chaos of a particle in a square well: Competing length scales and dynamical localization, *R. Sankaranarayanan*, A. Lakshminarayan and V.B. Sheorey, Phys. Rev. E **64**, 046210 (2001).
-